

Moisés Santillán

Mathematical Modeling for Life Sciences: A Primer

February 26, 2025

Springer

Contents

1	On the Use of Models in Science	1
1.1	Introduction	1
1.2	Categories of scientific models	2
1.2.1	Living Organisms as Models	2
1.2.2	Physical Models	3
1.2.3	Conceptual Models	3
1.2.4	Mathematical Models	3
1.3	Philosophy of Scientific Modeling	4
1.3.1	Models as Idealizations	4
1.3.2	The Art of Productive Simplification	5
1.3.3	Models as Epistemic Tools	5
1.4	Discussion	6
2	Why don't Clouds Fall?	7
2.1	Introduction	7
2.2	The method of separation of variables: a technique for solving certain differential equations	8
2.3	Modeling the fall of cloud droplets	9
2.4	Expanding the model to include ambient air currents	13
2.5	Discussion	14
3	From Ancient Math to Modern Science: The Fantastic Journey of the Exponential Function	19
3.1	Introduction	19
3.2	The Invention of Logarithms	20
3.3	From Logarithms to the Exponential Function	21
3.4	Transcendence of the Exponential Function	22
3.5	Discussion	23

4	Exponential Decay	25
4.1	Introduction	25
4.2	Dynamics of Aging	26
4.3	Age-Independent Death Rate	27
4.4	Stochastic Description	27
4.5	Individual Lifetime Distribution	29
4.6	Discussion	30
4.7	Epilogue	30
5	Exponential Growth	33
5.1	Introduction	33
5.2	Explosiveness of Exponential Growth	34
5.3	Geometric Sequences and the Exponential Function	35
5.4	Discussion	36
6	Local Stability Analysis	37
6.1	Introduction	37
6.2	Steady States	38
6.3	Assessment of Fixed Point Stability via Graphical Analysis	38
6.4	Local Stability Analysis	40
6.5	Discussion	41
7	On the Interconnected Origins of Statistics, Probability Theory and Population Dynamics	43
7.1	Introduction	43
7.2	Background	44
7.3	Cardano's Work	45
7.4	Pascal and Fermat	45
7.5	Huygens' Treatise	46
7.6	Graunt's Bills of Mortality	47
7.7	Probabilistic Life Tables and Early Insurance Mathematics	47
7.8	Discussion	48
8	Logistic Model	49
8.1	Introduction	49
8.2	A Brief Historical Review	50
8.3	The Logistic Model	50
8.4	Local Stability of Steady States	52
8.5	Discussion	54
9	Extending the logistic model	57
9.1	Introduction	57
9.2	Increased mortality	57
9.3	Allee Effect	59
9.4	Discussion	61

10 A Brief History of Nonlinear Dynamics	63
10.1 Introduction	63
10.2 The Origins of a Field	64
10.2.1 The Genius of Henri Poincaré	64
10.2.2 Formalizing Stability	65
10.2.3 Additional Pioneers	65
10.3 Advancing the Foundations	66
10.3.1 Birkhoff's Contributions	66
10.3.2 The Rise of Soviet Dynamical Thought	66
10.3.3 The emergence of Bifurcations	67
10.4 The Emergence of Chaos and Beyond	67
10.4.1 The Discovery of Deterministic Chaos	67
10.4.2 Illuminating Complexity Across Scales	68
10.5 Discussion	69
11 Local Stability Analysis in 2D Systems	71
11.1 Introduction	71
11.2 Steady States in 2D Systems	72
11.3 Local Linearization and Stability Analysis	73
11.4 Steady-State Classification	74
11.5 Discussion	77
12 Historical Origin of Population Ecology	79
12.1 Introduction	79
12.2 Early Foundations of Population Ecology	80
12.3 Formative Years of the Discipline	81
12.4 Lotka's Interdisciplinary Approach and Influence from Adams	82
12.5 Lotka-Volterra Equations	82
12.6 Discussion	83
13 Competitive Lotka-Volterra Model	85
13.1 Introduction	85
13.2 The Competitive Lotka-Volterra Model	86
13.3 Analysis of the Non-Dimensional Model	87
13.4 Discussion	91
14 SIR Model	93
14.1 Introduction	93
14.2 Model Formulation	94
14.3 Normalizing the Model	95
14.4 Fixed Points and Stability Analysis	96
14.5 Discussion	99

15	A Matter of Scales	101
15.1	Introduction	101
15.2	Structural scaling	102
15.3	Metabolic Scaling	103
15.4	Evolutionary Scaling Constraints and Lessons Learned	103
15.5	Discussion	104
16	Simplified SIR Model	105
16.1	Introduction	105
16.2	Model development	106
16.3	Analysis of Disease-Free Equilibria	107
16.4	Characterizing Outbreak Dynamics	107
16.5	Discussion	108
17	The Interdisciplinary Journey of Oscillators: From Transatlantic Navigation to Neurophysiology	111
17.1	Introduction	111
17.2	The Longitude Problem and the Development of Clocks	112
17.3	Harnessing Oscillators for Wireless Communication	114
17.4	Modelling Neural Excitation with Oscillators	115
17.5	Conclusion	117
18	The Damped Harmonic Oscillator	119
18.1	Introduction	119
18.2	Spring-mass system	120
18.3	Pendulum	121
18.4	RLC Circuit	122
18.5	Steady State Analysis	123
18.6	Application to Biological Systems	124
18.7	Discussion	125
19	The van der Pol Oscillator	127
19.1	Introduction	127
19.2	The van der Pol model	128
19.3	Steady State and Stability Analysis	129
19.4	Existence of a limit cycle	130
19.5	Relaxation Oscillations	131
19.6	Discussion	132
20	The FitzHugh-Nagumo Model	135
20.1	Introduction	135
20.2	The Hodgkin-Huxley Model	136
20.3	Motivation for Simplification	138
20.4	Derivation of the FitzHugh-Nagumo Equations	138
20.5	Analysis of Steady States	139
20.6	Phase Plane Analysis	141

20.7	Relaxation oscillator behavior	142
20.8	Applications to Excitable Systems	142
20.9	Discussion	143
21	Quasisteady State Approximation	145
21.1	Introduction	145
21.2	RC Low-Pass Filter Circuit	146
21.3	A Generalized Response Equation	147
21.4	Solution Forms for Specific Input Cases	148
21.4.1	Constant Input	148
21.4.2	Sinusoidal input	148
21.4.3	General Time-Varying Input	149
21.5	Timescale Separation	150
21.6	Comparing Steady States and Stability of the Full and Reduced Systems	150
21.7	Conclusions	152
22	Hematopoiesis Regulation	153
22.1	Introduction	153
22.2	Hematopoiesis Physiology	154
22.3	Mathematical modeling of erythropoiesis	155
22.4	Quasi-steady state approximation	156
22.5	Steady State Analysis	156
22.6	Stability Analysis	157
22.7	Discussion	158
23	A.V. Hill and the Origins of Modern Biophysics	161
23.1	Education and Early Career	161
23.2	Studies on Muscle Physiology	162
23.3	Hemoglobin saturation and the Hill equation	163
23.4	Discussion	163
24	Ligand-Receptor Dynamics	165
24.1	Introduction	165
24.2	Chemical Reactions	166
24.3	Chemical Kinetics Approach	166
24.4	Modeling Ligand Binding to a Receptor with Single Binding Site	167
24.5	Modeling Ligand Binding to Receptors with Multiple Independent Binding Sites	168
24.6	Extension to Cooperatively Binding Ligands	169
24.7	Saturation Fraction, Cooperativity and the Hill Function	171
24.8	Discussion	173

25	The Interdisciplinary Origins of Molecular Biology	175
25.1	Introduction	175
25.2	Early Steps Towards a Physical and Molecular View of Genes	176
25.3	The Structural School in Molecular Biology	177
25.4	The Informational School and its Origins in Quantum Physics	178
25.5	The Emergence of Molecular Biology in France	178
25.6	The Discovery of the Double Helix	179
25.7	Discussion	180
26	Gene Regulation	181
26.1	Introduction	181
26.2	The Central Dogma of Molecular Biology	182
26.3	Gene Regulatory Networks	183
26.4	The Amino Acid Tryptophan	183
26.5	The Tryptophan Operon	184
26.6	The Tryptophanase Operon	185
26.7	Discussion	186
27	Mathematical Modelling of Simple Bacterial Gene Regulatory Networks	189
27.1	Introduction	189
27.2	General Model Development	189
27.3	The Tryptophan Operon	190
27.4	The Tryptophanase Operon	193
27.5	Discussion	195
	References	196

Chapter 1

On the Use of Models in Science

Abstract This chapter discusses the conceptual foundations and roles of scientific modeling. It categorizes models from living organisms to mathematical equations, analyzing their purposes and limitations as simplified representations that distill complexity. Key principles are explored, establishing that models are strategic idealizations rather than perfect replicas, requiring skill in productive simplification. Models are framed as epistemic tools that generate hypotheses and organize empirical research to iteratively refine theories over time through explanatory or predictive functions. By synthesizing these philosophical underpinnings, the chapter conveys modeling as a balance between art and science that sustains open-ended scientific progress through provisional frameworks and evolving abstraction informed by empirical evidence.

1.1 Introduction

Science seeks to understand the natural systems that make up our world. Whether it is cells, climate or evolution of life, the phenomena investigated involve countless interacting components operating across multiple scales. To address such complexity, scientists employ models that are simplified representations aimed at distilling the key features of the system under study, while ignoring less important details. Models take diverse forms, ranging from living organisms and physical constructions to mathematical equations and conceptual diagrams. Despite their different representations, all models seek to condense complexity into forms comprehensible to the human mind.

The development of models is fundamental in several scientific disciplines. Among other applications, models facilitate hypothesis testing and theoretical development when direct experimentation is difficult. It could even be argued that

scientific theories themselves are models that provide simplified frameworks for explaining and predicting natural phenomena.

This chapter explores the conceptual foundations and functions of modeling in science. It details the various types of model and investigates their philosophical foundations. The ideas presented synthesize information extracted from these sources (Rosenblueth and Wiener, 1945; Borges, 1982; Box, 1976).

1.2 Categories of scientific models

Scientific models simplify the complexity of natural systems through various forms of representation designed to serve specific purposes. In general, models may be classified into four categories ordered from less to more abstract:

1.2.1 *Living Organisms as Models*

Some living organisms such as rodents, zebrafish, fruit flies, bacteria and other species are used as models to simulate key aspects of human biology, or biology of other species of interest, and the underlying mechanisms of disease. Since they involve living organisms, these models capture the inherent systemic complexity of life that cannot be replicated through other types of models.

Living models offer benefits such as allowing the study, under controlled conditions and in a longitudinal way, of dynamic and complex biological processes such as development, physiology and the progression of diseases. This allows understanding such processes in the functional multisystemic context of the living organism. Likewise, animal testing enables pre-clinical evaluation of drug efficacy, safety and optimal dosing regimens before clinical trials with human subjects. This ensures, as far as possible, the protection of health and well-being of participants in human research.

However, they also have certain limitations. The inherent complexity of living organisms makes it difficult to isolate and study individual molecular or physiological variables, making it difficult to establish direct cause-effect links. In addition, biological differences between species require extrapolating animal data to humans, as not all disease mechanisms can be directly comparable due to evolutionary divergence.

In summary, while offering a more holistic approximation of human biology, or biology of species of commercial interest, than other models, they must be evaluated according to intrinsic limitations and ethical factors, to ensure they continue to significantly contribute to advances in biomedicine.

1.2.2 Physical Models

Physical models are concrete material representations of biological structural elements. Some historically relevant examples are physical prototypes of the DNA double helix and various protein complexes. These models describe key attributes such as molecular geometry and conformational changes in a tangible and visualizable way.

Physical models offer certain advantages for research and education. Their practical nature facilitates visualization and conceptualization of abstract biomolecular organizations. This interactive characteristic inspires new hypotheses and experiments as researchers manipulate the replicas. They also effectively convey structural concepts to students and broad audiences.

However, they also have inherent limitations due to their nature. The replicas necessarily simplify and omit small-scale features. Consequently, they provide a simplified representation that can obscure subtle but biologically relevant interactions.

1.2.3 Conceptual Models

Conceptual models use diagrams, analogies and other visual and verbal frameworks to represent systems qualitatively. They include descriptions of biological structures such as the circulatory system or the atomic system. Conceptualizations also encompass descriptive illustrations of dynamic processes and networks.

The main advantages of conceptual models lie in their ability to distill abstract relationships and emergent properties into mentally comprehensible forms. Visual diagrams and verbal abbreviations communicate general functional principles accessibly. This ability makes them highly effective tools for interdisciplinary exchange and building conceptual foundations.

However, qualitative abstraction also involves limitations. These models omit specific mechanisms and numerical data, which can limit their applicability to answering quantitative questions. Their generality facilitates communication but risks oversimplification or spreading unelaborated concepts. Overall, their explanatory power depends on the nature of the research problem and the availability of complementary approaches.

1.2.4 Mathematical Models

Mathematical models express relationships through symbolic equations and formulas that quantify natural phenomena. Some examples are equations describing population growth, disease spread and kinetics of biochemical reactions.

A key advantage is their ability to rigorously characterize systems through numerical parameters and functions. When parameterized with experimental data, they enable predictive and testable forecasting. Their quantitative nature also facilitates hypothesis testing through numerical simulations. They also allow integrating diverse data sets and implementing hierarchical modeling across multiple scales.

However, quantitative precision depends on establishing appropriate functional forms and empirically estimating parameters. Gaps or uncertainties in available data can reduce predictive power or require simplifying assumptions. The quantitative approach also requires scoping the focus to avoid analytically or numerically intractable complexities. As a result, they work best when focused on well-defined subsystems.

When constructed and applied correctly, mathematical models constitute a powerful tool. But their ability to represent reality depends on empirical knowledge of the system under study and incorporating idealizations that make them analytically or numerically tractable.

Together, the model categories outlined here, from animal models to mathematical formalisms, capture the diverse yet complementary ways in which scientific abstraction seeks to understand intricate natural phenomena. Each paradigm offers benefits while possessing inherent limitations that delimit its applicability.

1.3 Philosophy of Scientific Modeling

While models take diverse forms, they share a common philosophical perspective regarding the simplification of reality. The following analyzes some key principles underpinning scientific modeling.

1.3.1 Models as Idealizations

Developing models entails an abstraction process aimed at distilling the essence of complexity through simplification and interpretation. As Rosenblueth and Wiener expressed, perfectly replicating a system would require the model to be identical to the object, losing its usefulness.

This is comically illustrated in Borges' story of a fictional empire in which the science of cartography becomes so exact that it ultimately elaborates a single map at the empire's own scale. These ideas emphasize that models avoid being perfect replicas to become manageable representations of the systems under study.

The goal is thus abstraction through which the essential is condensed in simplified constructions cognizable. Modeling seeks to reveal the essence beneath through idealization, not mere imitation of details. This could be summarized in George Box's following statement: "Although all models are wrong, some prove useful."

The standard is not strict precision but the ability to shed light on scientific questions through strategic abstraction and simplification.

1.3.2 The Art of Productive Simplification

Developing a useful model requires discerning which details can be omitted and which must be included to answer specific scientific questions. Too much abstraction can generate non-informative models, while insufficient abstraction hinders analysis.

There is an “art” to selective idealization. According to Rob Phillips, incorporating simplifications that preserve core behaviors and mechanisms, reducing ancillary details, can inspire new perspectives. Phillips distinguishes between errors of idealization, by omitting non-essential factors, and objective errors, by mischaracterizing the phenomenon. The former may be acceptable if they do not affect the model’s functions; the latter are less permissible.

The test of simplifications lies in whether they support models’ understanding and predictive capacity more than strict similarity to reality. There is no precise methodology to determine which simplifications are acceptable and which are not, as this judgment depends on the modeler’s experience and intuition.

1.3.3 Models as Epistemic Tools

Due to their simplified and abstract nature, scientific models serve as epistemic tools rather than definitive representations of reality. It is better to understand them as operational frameworks that drive scientific inquiry.

By condensing complexity, models configure empirical research and point to novel scientific lines of work. Their value lies more in stimulating novel scientific questions than in definitively closing projects. In this sense, they catalyze iterative refinement of knowledge over time.

In the context of mathematical models, these can be explanatory or predictive. The former formalize causal relationships, representing and testing dynamics to deepen understanding through predictions that can be experimentally tested. The latter focus on providing accurate forecasts by integrating patterns and trends.

Both types of models advance knowledge in different yet complementary ways. Explanatory models provide mechanistic perspectives. When their predictions are substantiated with experimental outcomes, they help consolidate theoretical frameworks. Predictive models provide reliable forecasts. Together, these approaches advance understanding through hypotheses, theoretical synthesis, questions and evidence-based decisions.

1.4 Discussion

This chapter has examined the foundations and roles of scientific modeling. In summary, developing models requires expertise in creating productive simplifications that preserve explanatory or predictive functionality. This implies a balance between art and science: data substantiate but abstraction remains an interpretive process.

Looking ahead, modeling will become even more important as technologies reveal greater details of systems. Progress will depend on interaction between simplification, experimentation and iterative theoretical refinement.

Models ensure that scientific inquiry remains an empirical, mentally open process. By establishing provisional understandings, they invite dialogue and extension of theories in the face of emergent realities. This sustains the central role of modeling in science.

While natural mysteries surpass human comprehension, modeling guarantees perpetual advancement through abstraction levels. Gradually revealing the intricate designs of nature, it propels both discovery and a deeper understanding of natural complexity across diverse spatiotemporal scales.

Chapter 2

Why don't Clouds Fall?

Abstract In this chapter we introduce differential equations as a tool to study change. We describe a way to classify them, and the nature of its solutions when they exist. We also introduce the concept of initial value problems to narrow down a family of solutions to a particular one, and provide a method to solve a very specific set of easily solvable differential equations. We later study a phenomenon using mathematical modeling, and show step by step the path to do so: beginning with understanding the phenomenon, to writing a mathematical expression to describe it, to solving it using the method introduced earlier in this chapter and finally to discussing the obtained results.

2.1 Introduction

The natural world around us is constantly changing. To adequately study and understand changing phenomena, appropriate mathematical tools are needed that can describe systems and their evolution over time. Differential equations provide just such a framework, allowing representation of natural processes in terms of rates of change.

Specifically, differential equations relate the derivative of an unknown variable to functions of that variable and/or independent variables. For instance:

$$\frac{dy}{dx} = f(x), \quad (2.1)$$

$$\frac{dy}{dx} = f(x, y), \quad (2.2)$$

$$\frac{\partial y}{\partial x_1} + \frac{\partial y}{\partial x_2} = f(y, x_1, x_2). \quad (2.3)$$

Eqs. (2.1) and (2.2) involve a single unknown variable and are called ordinary differential equations (ODEs). Eq. (2.3) contains partial derivatives with respect to multiple independent variables and is thus a partial differential equation (PDE). Differential equations provide a mathematical language for quantitatively describing natural systems and how they evolve over space and time.

A solution to a differential equation refers to any function that satisfies the equation. Often, differential equations admit multiple solution functions, collectively called a family of solutions. However, real-world systems are uniquely defined by their initial state. By specifying an initial condition, the problem becomes an initial value problem. This additional information allows narrowing down the family of solutions to a single, unique solution corresponding to the system's behavior over time. Some basic differential equations can be solved analytically through explicit mathematical techniques. But for most equations, numerical methods are necessary to approximate solutions since exact closed-form solutions are intractable.

2.2 The method of separation of variables: a technique for solving certain differential equations

Differential equations of the form $dy/dx = F(x, y)$ admit closed-form solutions via the method of separation of variables when $F(x, y)$ can be expressed as the product of a function solely of x , $g(x)$, and a function solely of y , $h(y)$:

$$\frac{dy}{dx} = F(x, y) = g(x)h(y). \quad (2.4)$$

Letting $h(y) = 1/f(y)$, Eq. (2.4) can be rearranged such that the variables x and y are isolated on opposite sides:

$$f(y) \frac{dy}{dx} = g(x).$$

This separable equation is then solved by integrating both sides with respect to x :

$$\begin{aligned} \int f(y) \frac{dy}{dx} dx &= \int g(x) dx, \\ \int f(y) dy &= \int g(x) dx, \end{aligned}$$

provided the integrals exist.

2.3 Modeling the fall of cloud droplets

Mathematical modeling utilizing differential equations has increasingly become a valuable complement to experimental research in understanding natural phenomena. Modeling involves more than just solving equations—it is a complete process. The first step is to develop a mathematical model through formulation of governing equations that describe the key aspects of the system or problem. Crafting an appropriate model requires balance, as models need to be sufficiently simple to analyze while still accurately representing the phenomenon. Once established, models are used to gain insights through mathematical and analytical techniques rather than just obtaining numeric solutions. Critically, the results must then be interpreted by relating the mathematical abstractions back to the real system. This contextualization provides enhanced understanding and conclusions. Moreover, answering questions through modeling often leads to new questions, thereby driving development of improved or new models in an iterative process. The overarching goal of mathematical modeling is to complement empirical studies by mechanistically linking mathematics to observed natural phenomena.

As an example of the mathematical modeling process, consider the observable phenomenon of clouds remaining suspended in the sky despite being composed of water/ice; materials denser than air. Why do clouds not simply fall to the earth under the force of gravity given the density of their constituents?

To construct an initial model to investigate this question, we begin by abstracting the intricate, large-scale cloud system into its fundamental building blocks. Clouds are formed from innumerable minuscule droplets and particulates. Therefore, modeling the dynamics of a single representative component isolates the key issue while reducing overall complexity. This abstraction enables formulation of a simplified framework to theoretically explore the forces governing a single constituent's behavior, providing insights into the large-scale behavior of clouds as aggregates of many such parts.

At the level of the individual droplet, the key elements governing its dynamics are the downward pulling force of gravity and the counteracting upward pushing force of air resistance opposing the droplet's movement. Other complex cloud-scale phenomena are negligible for this preliminary model. Fig. 2.1 provides a conceptual illustration of this abstracted perspective, visually depicting the isolated droplet subject to only two delineated forces via a diagrammatic force representation.

Consider the positive axis directed along the weight vector. Then by Newton's second law, we can write:

$$ma = mg - F_r, \quad (2.5)$$

where a is droplet acceleration, m its mass, g gravity, and F_r frictional air force. Assuming a spherical droplet, Stokes' law for a sphere in a fluid gives $F_r = 6\pi\mu r v$, with μ the air viscosity, r the droplet radius, and v velocity. We can thus write $F_r = \eta v$, where $\eta = 6\pi\mu r$. Substituting into (2.5) and solving for \dot{v} yields:



Fig. 2.1 Diagrammatic force representation of a solitary descending water droplet (or ice particle), with the downward pointing weight and upward pointing air resistance delineated.

$$\dot{v} = \frac{\eta}{m} \left(\frac{mg}{\eta} - v \right). \quad (2.6)$$

Defining $\tau = m/\eta$ and $v_T = mg/\eta$ allows us to rewrite Eq. (2.6) as:

$$\dot{v} = \frac{1}{\tau} (v_T - v). \quad (2.7)$$

Applying the method of separation of variables to Eq. (2.7) yields:

$$\int \frac{1}{v - v_T} dv = \int \frac{-1}{\tau} dt.$$

Integrating both sides gives:

$$\ln(v - v_T) = \frac{-t}{\tau} + C.$$

Solving this for the velocity v produces:

$$v = v_T + C e^{\frac{-t}{\tau}}.$$

The initial condition $v(0) = v_0$ gives:

$$C = v_0 - v_T.$$

Substituting this result provides the expression:

$$v = v_T + (v_0 - v_T) e^{\frac{-t}{\tau}}. \quad (2.8)$$

Which describes the time evolution of the droplet's velocity.

To understand the droplet's velocity behavior over very long time periods, we calculate:

$$\lim_{t \rightarrow \infty} v = \lim_{t \rightarrow \infty} \left[v_T + (v_0 - v_T) e^{-\frac{t}{\tau}} \right] = v_T.$$

This indicates that the droplets will eventually reach a terminal constant velocity of v_T . Fig. 2.2 displays plots of Eq. (2.8) for differing initial velocities v_0 while holding τ fixed. Notice that all solutions converge to the common value of v_T , regardless of the initial conditions. This illustrates that droplets decelerate over time, eventually matching the characteristic falling speed v_T defined by fluid properties and gravitational acceleration.

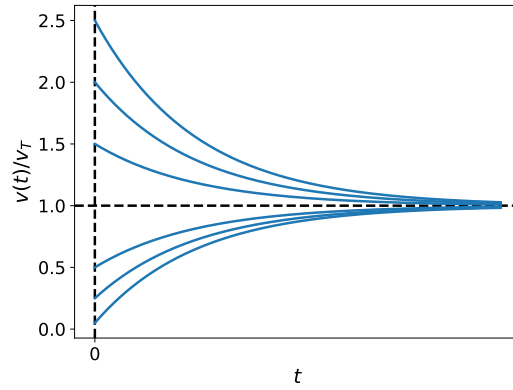


Fig. 2.2 Plots of Eq. (2.8) with varying initial velocities v_0 (blue curves), holding τ fixed. The dashed line denotes the terminal velocity v_T . Note that all blue asymptotically approach v_T .

Let us further analyze the terminal velocity. Recall that $v_T = mg/\eta$. However, we can express mass as $m = V\rho$, where V is droplet volume and ρ its density. Since the droplet is assumed spherical, substituting gives:

$$v_T = \frac{V\rho g}{\eta} = \frac{\frac{4}{3}\pi r^3 \rho g}{6\pi\mu r} = \frac{2\rho g}{9\mu} r^2, \quad (2.9)$$

which reveals the final velocity is proportional to the square of the droplet radius. That is, larger droplets reach a higher terminal speed.

Let us now explore the behavior of Eq. (2.8) for varying values of τ . Fig. 2.3 displays plots of normalized particle velocity versus time for cases where $\tau/2$, τ , and 2τ are considered, while holding v_0/v_T fixed. Notably, as τ increases, it takes longer for the droplet velocity to approach v_T . This observation leads us to identify τ as the relaxation time of the system, representing the duration required to reach equilibrium.

To investigate the rate at which the droplet velocity approaches v_T , let us examine $\tau = m/\eta$:

$$\tau = \frac{m}{\eta} = \frac{V\rho}{\eta} = \frac{\frac{4}{3}\pi r^3 \rho}{6\pi\mu r} = \frac{2}{9} \frac{\rho}{\mu} r^2, \quad (2.10)$$

Once again, we find that τ is directly proportional to the square of the droplet radius. Therefore, larger droplets have longer relaxation times to attain their terminal velocity.

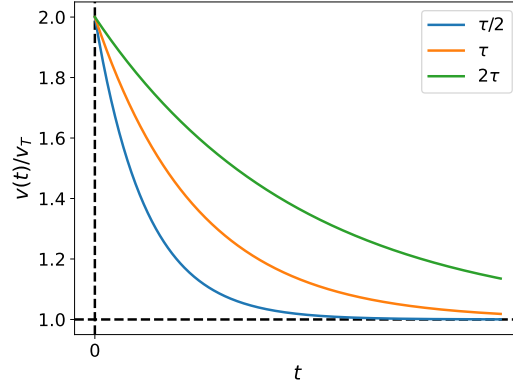


Fig. 2.3 Plots of the normalized particle velocity $v(t)/v_T$, obtained from Eq. (2.8), for different values of τ . The orange curve represents $\tau/2$, the purple curve represents τ , and the blue curve represents 2τ . A fixed value of v_0/v_T was considered in all plots.

The above analysis provides insight into why microscopic droplets present in clouds do not readily fall under the force of gravity. Eq. (2.10) demonstrates that the relaxation time τ is directly proportional to the square of the droplet radius. Given typical cloud droplet sizes on the order of $10 \mu\text{m}$, this results in relaxation times that are exceedingly short; on the order of milliseconds based on standard fluid properties.

According to Eq. (2.8), these microscopic droplets would reach 99% of their terminal velocity v_T within a fraction of a second due to the ultra-fast relaxation timescale. However, for cloud droplet sizes, the associated terminal velocity v_T itself as given by Eq. (2.9) is minuscule, on the order of centimeters per second.

Therefore, over observational timescales relevant to the human eye, micrometer-sized cloud droplets do not perceptibly change in velocity. This is a result of both the very small terminal velocities and exceedingly rapid approach to equilibrium velocity. Their behavior appears static, even though they are slowly descending owing to gravity.

Only larger droplets within clouds have observable terminal velocities and thus visibly fall. Coincidentally, this analysis helps explain the triggering of rain from clouds. Precipitation occurs through coalescence of multiple microscopic droplets

into larger falling raindrops, encouraged by processes like droplet collisions, up-drafts/downdrafts, cooling temperatures, and presence of foreign particles.

2.4 Expanding the model to include ambient air currents

Thus far, our analysis has focused on the simplified scenario where air currents are neglected and droplets fall under the isolated actions of gravity and drag forces. However, clouds exist within a dynamic atmospheric environment subjected to fluctuating air movements. To gain a more realistic perspective, let us now expand our model to include the effects of ambient wind forces.

Fig. 2.4 displays a revised free body diagram depicting a single droplet experiencing an additional time-varying force $f(t)$ imposed by surrounding air motions. Previously, the droplet equilibrium was determined by a balance between the constant downward pull of gravity and upwards drag resistance. With inclusion of $f(t)$, the force budget acting on each droplet becomes more complex as transient lift/drag disturbances alter the net downward acceleration at any given instant. Modeling this third force offers opportunity to deepen understanding of cloud-scale behaviors emerging from interactions between falling constituent droplets and turbulent airflow fluctuations.

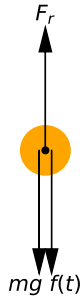


Fig. 2.4 Free body diagram of a single falling droplet of water (or particle of ice). Pointing downwards the weight of the droplet and the force produced by an air current, and pointing upwards the resistance of the air.

Choosing the vertical axis positive in the direction of gravitational acceleration, the equation of motion is:

$$m\dot{v} = mg + f(t) - \eta v, \quad (2.11)$$

where $f(t)$ denotes the time-varying lift or drag imposed by surrounding winds. Let us define the total force acting on the droplet as $F(t) = mg + f(t)$. Isolating the drag

term in Eq. (2.11) yields:

$$\dot{v} = \frac{\eta}{m} \left(\frac{F(t)}{\eta} - v \right). \quad (2.12)$$

Consistent with our prior analysis, we identify the relaxation time as $\tau = m/\eta$ and the instantaneous terminal velocity as $v_T(t) = F(t)/\eta$. Substituting these into Eq. (2.12) gives:

$$\dot{v} = \frac{1}{\tau} (v_T(t) - v), \quad (2.13)$$

which has the same form when time-varying wind effects were not included on the droplet motion.

Our previous analysis of the equation of motion without time-varying winds showed that the droplet velocity asymptotically approaches the constant terminal velocity v_T , independent of initial conditions. Additionally, we determined the relaxation time τ governs how rapidly this approach occurs.

When extending our model to include time-varying winds inducing a transient terminal velocity $v_T(t)$, similar behavior is expected for the droplet velocity $v(t)$. Specifically, $v(t)$ will tend towards the instantaneous value of $v_T(t)$ at each moment in time. The rate at which $v(t)$ adjusts to changes in the fluctuating $v_T(t)$ is determined by the relaxation time τ .

For droplets experiencing fluctuations in $v_T(t)$ due to winds, our prior analysis indicates that those with smaller τ will track variations in $v_T(t)$ most closely over time. Within clouds, where droplet sizes yield relaxation times on the order of milliseconds, this property allows for rapid synchronization between $v(t)$ and microscale variations in airflow velocity induced by turbulence.

On observable human timescales, this near-perfect tracking imposed by minute τ obscures individual droplet motions. Instead, clouds appear nebulous and suspended motionless despite droplets smoothly adjusting their velocities downward while also following transient atmospheric currents. Therefore, the small droplet sizes characteristic of clouds effectively couple velocities to instantaneous air movements, contributing significantly to their visual appearance.

2.5 Discussion

In this chapter, we introduced differential equations and discussed using them to develop mathematical models of physical phenomena. We applied this approach to investigate the behavior of cloud droplets and why they do not visibly fall under gravity.

Through analytical modeling of a cloud droplet experiencing gravity, drag, and wind forces, we derived equations of motion and solved them to determine droplet velocity over time. This revealed that each droplet reaches a constant terminal settling velocity, v_T , irrespective of initial conditions.

Analysis of the model showed the scaling relationships of both v_T and relaxation time constant τ with droplet radius r . Specifically, we found v_T and τ are directly proportional to r^2 . Given cloud droplet radii are on the micron scale, this results in two key properties:

1. Droplets attain v_T extremely rapidly due to exceedingly short τ .
2. The actual magnitude of v_T is minuscule due to the r^2 scaling.

Therefore, while droplets gradually descend at their slow terminal velocities, this imperceptible motion occurs below human observational resolution scales.

Additionally, ambient winds disrupting continuous descent contribute further to clouds' static visual appearance. Overall, the mathematical modeling elucidated the underlying reasons clouds evade falling visibly despite gravitational forces acting on constituent droplets.

Even simple mathematical models of natural phenomena, like the linear drag model developed here for cloud droplets, can provide deep insights into observable behaviors that may otherwise be taken for granted. By distilling relationships down to their essential mathematical elements, qualitative and quantitative predictions emerge regarding how underlying physical factors control system-level properties.

The rest of this book is dedicated to expanding on such modeling techniques, specifically through nonlinear dynamics approaches. Subsequent chapters will introduce nonlinear methods and apply them to study the time-evolving behavior of various biological systems. The overarching goal is to utilize analytical and computational nonlinear dynamics tools to elucidate the unexpectedly complex and sometimes counterintuitive dynamics that often arise in living systems due to nonlinear interactions between components.

Exercises

1. Consider an object with an initial temperature T_0 , a specific heat capacity C , and a thermal conductance α . This object is placed in an oven that maintains a constant temperature T_H . The rate of heat influx into the object is proportional to the difference between the oven temperature and the object's current temperature. This relationship can be expressed mathematically as:

$$J_Q = \alpha(T_H - T),$$

where T represents the temperature of the object at any given time. Additionally, the heat influx is related to the rate of change of the object's temperature through the specific heat capacity C :

$$J_Q = C \frac{dT}{dt}.$$

By combining these two equations, derive the differential equation that describes the evolution of the object's temperature T over time. After formulating the differential equation, discuss its solution in detail, focusing particularly on the concept of relaxation time, which characterizes how quickly the object approaches thermal equilibrium with the oven.

2. Consider an electrical circuit in which a capacitor, with capacitance C , is connected to a voltage source V_S through a resistor R . Initially, the capacitor is uncharged, and the circuit is open. Since the resistor and capacitor are in series, the sum of the voltage drops across each component equals the source voltage:

$$V_S = V_R + V_C$$

Here, the current I flowing through both the resistor and the capacitor is the same. According to Ohm's Law, the voltage drop across the resistor is given by:

$$V_R = IR$$

Additionally, the relationship for the capacitor is described by:

$$I = C \frac{dV_C}{dt}$$

Taking all of this into account, derive the differential equation for the voltage across the capacitor, V_C , once the circuit is closed. Identify the factors that determine the relaxation time of the circuit. Is the result intuitive?

3. Consider a chemical reaction in which a protein A shifts forth and back between conformational states A_1 and A_2 . The forward and backward reaction velocities are:

$$\begin{aligned} v_f &= k_f[A_1], \\ v_b &= k_b[A_2], \end{aligned}$$

with k_f and k_b denote the forward and backward reaction rate constants and $[X]$ represents the concentration of substance X . The rates of change of $[A_1]$ and $[A_2]$ are given by:

$$\frac{d[A_1]}{dt} = -\frac{d[A_2]}{dt} = -v_f + v_b.$$

From these considerations and the assumption that the total concentration of A molecules is constant ($[A_1] + [A_2] = [A_T]$) derive a differential equation for $[A_2]$. Study the solution and discuss how the equilibrium value and the relaxation time depend of k_f and k_b .

4. Numerically solve the differential equation

$$\frac{dx}{dt} = \gamma(f(t) - x)$$

for various forms of the function $f(t)$. Specifically, consider:

- A sinusoidal function.
- A square-wave function.
- A sawtooth wave function.

Explore different values for the parameter γ , ranging from very small to very large relative to the period of the function $f(t)$. Plot your results and provide a discussion on the outcomes. Consider the implications of your findings for the systems analyzed in the previous exercises.

Chapter 3

From Ancient Math to Modern Science: The Fantastic Journey of the Exponential Function

Abstract For centuries, the exponential function has been a cornerstone of mathematics, and its influence has extended far beyond the confines of this discipline. This chapter will delve into the rich history of the exponential function, tracing its origins back to ancient civilizations and exploring its evolution over time. The chapter will also highlight some of the key mathematical breakthroughs that led to the exponential function. Finally, we will present a brief survey of how the exponential function is used in fields such as physics, engineering and biology.

3.1 Introduction

A story goes that once God Krishna took the form of a wise man and went to the king's court. He challenged the king to a game of chess because he loved playing it. Before the game started, they had to decide what the prize would be if the sage won. The sage said that he only wanted a small amount of rice, but the amount had to be calculated using the chessboard. A grain of rice would be placed in the first square and the number of rice grains would double for each successive square on the board. The king lost the game and had to give the sage the rice. But as he started putting the rice grains on the board, the king realized that he wouldn't have enough rice to pay his debt. Krishna then showed himself in his true form and told the king that he didn't have to pay all the rice right away, but he could do it gradually. Every day, the king would serve free rice pudding to people who came to the temple until the debt was paid off.

This story has different versions. In some versions, God Krishna is replaced by a servant, the inventor of chess, or a craftsman who makes the best chessboards. In others, rice is substituted by wheat. The ending is also different. In some versions, the ruler has the person who should get the reward killed, while in others, the reward

is given only if each grain is counted individually. But the message stays the same: the explosive increase in a pattern where each step is multiplied by the same number (geometric progression) instead of just being added by the same amount (arithmetic progression).

With a history dating back to the Greeks and possibly even the Sumerians, geometric progressions—a discrete form of the exponential function—boasts a rich legacy. Despite this, it wasn't until the 18th century, with the contribution of some of the world's most renowned mathematicians, that the exponential function was finally uncovered. Nevertheless, its influence has been tremendous and spans across numerous scientific domains. A key milestone in this history is the creation of logarithms, which was a seminal event.

In this chapter we briefly review their history. For those seeking a deeper understanding of the history of logarithmic and exponential functions, the *History of the Exponential and Logarithmic Concepts* series of articles, published in 1913 in the *American Mathematical Monthly* (Cajori, 1913b,c,d,e,a,f,g).

3.2 The Invention of Logarithms

Logarithms were independently developed by the mathematicians John Napier, from Scotland, and Jost Bürgi, from Switzerland, to simplify computations in spherical trigonometry, which is used in astronomy and celestial navigation. Despite Bürgi's probable creation of his system around 1600, Napier's discovery was published first in 1614 in the book *Mirifici Logarithmorum Canonis Descriptio* (*Description of the Wonderful Canon of Logarithms*), making him widely known as the inventor of logarithms and greatly influencing its subsequent evolution.

Logarithms establish a connection between the operation of multiplication on the positive real numbers and addition on the real number line. Napier, in particular, viewed logarithms as the relationship between two particles moving along a line—one at a constant speed, the other at a speed proportional to its distance from a fixed endpoint. In current terms, Napier's logarithm (NapLog) can be related to the natural logarithm (\ln) in this way:

$$\text{NapLog}(x) = -10^7 \ln(x/10^7).$$

English mathematician Henry Briggs made two visits to Edinburgh to collaborate with John Napier in 1616 and 1617. During their conversations, they reached an agreement on Briggs' proposed modification to Napier's logarithms. After his second trip, Briggs released the first table of his improved logarithms, now known as common or base 10 logarithms (\log_{10}), in 1617. The widespread use of common logarithms grew rapidly due to their ease in performing complex calculations during a time when calculators were not available. This was mainly due to the fact that our numbering system is built on powers of 10. Nevertheless, the natural logarithm

holds a more prominent place in the history of mathematics because of its impact on the discipline's evolution.

In 1649, Alphonse Antonio de Sarasa, who was previously a student of Grégoire de Saint-Vincent, demonstrated that the area $A(t)$ of the region bounded by the hyperbola $xy = 1$ from $x = 1$ to $x = t$ obeys the following relation common to all logarithmic function:

$$A(t \times u) = A(t) + A(u).$$

It was soon realized that this characteristic could lead to the creation of a new type of logarithm. Mercator, in fact, published the first tables of what is now referred to as the natural logarithm in his book *Logaritmotechnia* in 1668.

3.3 From Logarithms to the Exponential Function

In 1748, Leonhard Euler's classic book *Introductio in analysin infinitorum* (*Introduction to the Analysis of the Infinite*) marked the final step in the development of logarithms, exponential functions, and trigonometric functions. Prior to Euler, these mathematical concepts were usually defined using integral calculus. However, Euler changed this by introducing exponentiation a^x for constant a in the positive real numbers, leading to the creation of the logarithm to base a . He also named the natural logarithm, calling it the "natural or hyperbolic logarithm" due to its connection to the quadrature of the hyperbola. Euler designated number e as the base for the natural logarithm, i.e. the number whose natural logarithm is equal to 1.

Jacob Bernoulli's groundbreaking work in compound interest paved the way for the discovery of the constant later named e by Euler. Bernoulli's contribution can be succinctly described as follows: he examined the growth of capital when invested at an annual interest rate of 100% and is compounded at n intervals. At the end of the year, the capital would have multiplied by a factor of

$$\left(1 + \frac{1}{n}\right)^n.$$

Bernoulli showed that as the number of compounding intervals increases, this factor approaches a constant value between 2 and 3.

Euler expanded upon Bernoulli's work by defining the exponential and natural logarithmic functions as follows:

$$\begin{aligned}\exp(x) &= \lim_{n \rightarrow \infty} \left(1 + \frac{x}{n}\right)^n \\ \ln(x) &= \lim_{n \rightarrow \infty} n(x^{1/n} - 1).\end{aligned}$$

Additionally, Euler established that the exponential function is a exponentiation function with base e ($\exp(x) = e^x$) and that the exponential and logarithmic functions are inverse of each other.

3.4 Transcendence of the Exponential Function

Godfrey H. Hardy wrote in *A Mathematician's Apology* that “a mathematical idea is *significant* if it can be connected, in a natural and illuminating way, with a large complex of other mathematical ideas. Thus a serious mathematical theorem, a theorem which connects significant ideas, is likely to lead to important advances in mathematics itself and even in other sciences.” Hardy used Pythagoras’s proof of the irrationality of $\sqrt{2}$ as an example, highlighting how a simple and elegant theorem can open up new avenues for the development of mathematics.

The exponential function is a prime example of a mathematical idea that has left a lasting impact, not just in mathematics but in other fields as well. It is considered a cornerstone for the advancement of all modern areas of mathematics. Its applications are diverse and can be seen in fields such as physics, where it explains processes ranging from radioactive decay to population growth. In finance, it is employed in modeling interest rates and stock prices. The exponential function is also a critical component in engineering, contributing to the development of electrical circuits, control systems, and communication systems, just to mention a few examples.

In *Introductio in analysin infinitorum*, Euler introduced the equation named after him:

$$e^{ix} = \cos x + i \sin x.$$

Specifically, when $x = \pi$, this formula leads to the well-known Euler identity:

$$e^{i\pi} + 1 = 0.$$

which is considered by many to be one of the most beautiful equations in mathematics, as it combines the three basic mathematical operations (addition, multiplication, and exponentiation) and relates five fundamental mathematical constants (0, the additive identity; 1, the multiplicative identity; the unit of imaginary numbers, i ; e and π). The Euler identity is a point of convergence of various mathematical disciplines, such as arithmetic, trigonometry, and complex number theory.

Euler formula has been a vital aspect in physics and engineering, particularly through Fourier analysis. This method allows the transformation of complex functions into sums of simple trigonometric functions. Some of the most significant uses include:

- Signal processing: Fourier analysis is used to analyze and manipulate signals such as audio, images, and voice.
- Image compression: Fourier analysis is used in image compression algorithms to reduce the amount of data needed to represent an image.
- Spectral analysis: Fourier analysis is applied to study the frequency components of signals, such as those produced by vibrating objects or electromagnetic waves.
- Filter design: Fourier analysis is used to create electronic filters that remove unwanted frequencies from signals.
- Heat transfer: Fourier analysis is applied to examine heat flow in solids and fluids.

- Quantum mechanics: Fourier analysis is used to analyze the behavior of particles in a quantum state.
- Seismology: Fourier analysis is employed to examine the propagation of seismic waves.
- Electromagnetic analysis: Fourier analysis is applied to study the behavior of electromagnetic fields.
- Analysis of neuronal signals: Fourier analysis is used in the study of the electric and magnetic fields emanating from brain activity.
- Analysis of protein structure: Fourier analysis is employed to determine the structure of proteins using X-ray crystallography.

3.5 Discussion

This chapter has chronicled the remarkable journey of the exponential function from its earliest origins to its central role in modern mathematics and sciences. While geometric progressions date back millennia in various ancient cultures, it was not until the foundational work of 17th century figures like Napier, Briggs, and Euler that the exponential and logarithmic functions emerged in their modern formalized forms.

Key developments included the independent invention of logarithms by Napier and Bürgi, establishing the logarithmic relationship between multiplication and addition. Common logarithms streamlined calculations and advanced sciences. Later, the work of figures like Bernoulli, Euler, and Mercator uncovered deeper properties, culminating in Euler's definition of the exponential and natural logarithmic functions using limits.

In summarizing this long history, the chapter has underscored how a single mathematical notion can evolve enormously over centuries through the work of generations of thinkers. It has also conveyed the exponential function's status as a prime example of an abstract mathematical idea that revolutionized scientific understanding through illuminating connections to the natural world. Its influence ensures the story of this fantastic function will undoubtedly continue expanding into new uncharted domains.

Chapter 4

Exponential Decay

Abstract This chapter develops both deterministic and stochastic models to analyze how population size changes over time under the assumption of an age-independent death rate in closed populations. Beginning with a distribution function describing population age structure, a convection equation governs aging in the absence of deaths. Introducing constant mortality leads to exponential decay of total size. A stochastic approach models population size as a random variable and relates transition probabilities, recovering the deterministic solution when averaging expected size. Solving for individual lifetime distributions links dynamics across scales through averaging. Extensions to age-dependent but stationary mortality demonstrate self-organized exponential decay, connecting perspectives from random interactions to emergent collective behaviors. The established foundations connect stochastic and deterministic views on simple populations and lay the groundwork for further complexity.

4.1 Introduction

Population dynamics is the study of how populations change over time and space due to various biological and environmental factors. Central topics in population dynamics include birth, death, immigration and emigration, density dependence, and biotic and abiotic interactions between individuals within a population or between species.

In this chapter, we will begin exploring population dynamics by studying a simple death process in closed populations. Specifically, we will develop both deterministic and stochastic models to analyze how population size changes over time under the assumption of an age-independent death rate. This forms the basis for understanding more complex population dynamics incorporating additional realistic

features like age-structure, density dependence, and other stochastic birth and death mechanisms.

By establishing these foundations, we aim to connect individual-level stochasticity to emergent deterministic behaviors at the population scale.

4.2 Dynamics of Aging

Let us analyze the dynamics of a closed population with no births or deaths over time. We define the function $\eta(\tau, t)d\tau$ as the fraction of individuals in the population with ages in the interval $[\tau, \tau + d\tau]$ at time t . This function fully describes the population state at any given time and how it evolves. Specifically, the total population at any time t is given by:

$$N(t) = \int_0^\infty \eta(\tau', t) d\tau'.$$

In the absence of births, deaths, and migration, individuals can only age over time. This means the plot of the function $\eta(\tau, t)$ shifts to the right as time passes. We can mathematically express this as:

$$\eta(\tau, t + \Delta t) = \eta(\tau - \Delta t, t).$$

Expanding the left-hand side (LHS) and right-hand side (RHS) terms in a Taylor series about t and τ , respectively, gives:

$$\eta(\tau, t) + \frac{\partial \eta}{\partial t} \Delta t + \dots = \eta(\tau, t) - \frac{\partial \eta}{\partial \tau} \Delta t + \dots$$

Simplifying and taking the limit as $\Delta t \rightarrow 0$ yields the governing equation:

$$\frac{\partial \eta}{\partial t} = -\frac{\partial \eta}{\partial \tau}. \quad (4.1)$$

The RHS can be viewed as an age-related flux term. Therefore, this equation expresses conservation of population as the rate of change within an infinitesimal age interval equals the net outflux due to aging.

Since the total population $N(t)$ was assumed to remain constant over time due to no births, deaths, or migration, it follows that:

$$0 = \frac{d}{dt} \int_0^\infty \eta d\tau = \int_0^\infty \frac{\partial \eta}{\partial t} d\tau = - \int_0^\infty \frac{\partial \eta}{\partial \tau'} d\tau'.$$

The last equality expresses the fact that aging redistributes individuals among age classes but does not change the total population size.

4.3 Age-Independent Death Rate

We can modify Eq. (4.1) to account for deaths by including an additional death rate term

$$\frac{\partial \eta}{\partial t} = -\frac{\partial \eta}{\partial \tau} - \mu(\tau)\eta, \quad (4.2)$$

where $\mu(\tau)$ is the death-rate constant for individuals of age τ . It represents the probability per unit time that an individual of age τ dies.

Integrating Eq. (4.2) gives:

$$\frac{dN}{dt} = -\int_0^\infty \mu(\tau')\eta(\tau', t)d\tau'.$$

Now assume that the death rate is independent of age. Then:

$$\frac{dN}{dt} = -\mu N. \quad (4.3)$$

This differential equation has the well-known solution of exponential decay:

$$N(t) = N_0 e^{-\mu t},$$

where N_0 is the initial population size. This demonstrates that under the assumption of a constant, age-independent death rate, the population will decrease exponentially over time.

An important parameter that arises from this solution is the population half-life ($t_{1/2}$), defined as the time required for the population to decrease to half its initial value. Specifically:

$$\frac{N_0}{2} = N_0 e^{-\mu t_{1/2}}$$

Solving this equation for $t_{1/2}$ gives:

$$t_{1/2} = \frac{\ln 2}{\mu} \quad (4.4)$$

4.4 Stochastic Description

In the previous section, we modeled population dynamics deterministically and showed the population decays exponentially over time when death rates are independent of age. Here, we develop a stochastic framework to analyze this process more rigorously.

Let n be a random variable representing population size. Define $P(n = N; t)$ as the probability that the population has a value of N individuals at time t :

$$P(n = N; t)$$

Additionally, let μ denote the probability per unit time that an individual dies independently of others. Considering these variables, the evolution of $P(n = N; t)$ is described by:

$$P(n = N; t + \Delta t) = P(n = N; t)(1 - \mu N \Delta t) + P(n = N + 1; t)\mu(N + 1)\Delta t \quad (4.5)$$

This equation accounts for two possibilities that could result in a population of size N over a short time interval Δt . 1) the population was already size N at time t and no deaths occurred. 2) The population was size $N + 1$ at time t and one death occurred. We assume that Δt is small enough that more than one death is highly unlikely.

We can rearrange Eq. (4.5) to obtain:

$$\frac{P(n = N; t + \Delta t) - P(n = N; t)}{\Delta t} = P(n = N + 1; t)\mu(N + 1) - P(n = N; t)\mu N$$

Taking the limit as the time interval Δt approaches 0 yields the following differential equation governing the time evolution of the probability $P(n = N; t)$:

$$\frac{dP(n = N; t)}{dt} = P(n = N + 1; t)\mu(N + 1) - P(n = N; t)\mu N \quad (4.6)$$

Eq. (4.6) describes the forward Kolmogorov equation for this stochastic death process. It relates the time derivative of the probability of being in state N individuals to the probabilities of transitions between states due to individual death events.

There are several approaches to analyze Eq. (4.6). One method is to take the time derivative of the expected population size, represented by:

$$E_n = \sum_{N=0}^{\infty} NP(n = N; t)$$

By multiplying both sides of Eq. (4.6) by N and taking the sum from 0 to infinity, we obtain:

$$\frac{d}{dt} \sum_{N=0}^{\infty} NP(n = N; t) = \mu \sum_{N=0}^{\infty} N(N + 1)P(n = N + 1; t) - \mu \sum_{N=0}^{\infty} N^2 P(n = N; t)$$

Through some algebraic steps, this equation can be shown to reduce to:

$$\frac{dE_n}{dt} = -\mu E_n \quad (4.7)$$

Notice that Eq. (4.7) is identical to the deterministic Eq. (4.3). This implies the deterministic solution corresponds to the average behavior of repeated stochastic experiments, rather than describing any single experiment. It predicts exponential decay when considering expected population sizes over numerous trials.

Another approach is to find an exact solution to Eq. (4.6). It can be verified through substitution that:

$$P(n = N; t) = \frac{E_n^N(t) e^{-E_n(t)}}{N!},$$

where $E_n(t)$, satisfies Eq. (4.7). This has the form of a Poisson distribution, with mean E_n and standard deviation $\sqrt{E_n}$.

For large values of E_n , the standard deviation becomes negligible compared to the mean. Therefore, even though the deterministic model in Eq. (4.3) does not describe individual stochastic trajectories, its predictions are expected to closely match the behavior of single realizations when population sizes are sufficiently large.

While stochastic fluctuations are prominent for small populations, the deterministic exponential decay approximation becomes increasingly accurate as the number of individuals grows. This solution helps connect the statistical properties of the underlying stochastic process to the emergent deterministic behavior predicted by the differential equation model.

4.5 Individual Lifetime Distribution

As individual death is a stochastic process, the survival time of each individual, denoted by the random variable τ , is also random. Let $P(\tau = T)dT$ represent the probability that an individual survives up to age T and dies between ages T and $T + dT$. We can write an equation for this probability as:

$$P(\tau = T)dT = \left(1 - \int_0^T P(\tau = T')dT'\right) \mu dT$$

The term in parentheses is the probability of surviving until age T , while μdT is the probability of dying between T and $T + dT$.

Differentiating this expression gives the differential equation:

$$\frac{dP(\tau = T)}{dT} = -\mu P(\tau = T)$$

Subject to the normalization condition, the solution is:

$$P(\tau = T) = \mu e^{-\mu T}$$

Therefore, individual lifetimes follow an exponential distribution. The mean lifetime is thus:

$$E_\tau = \frac{1}{\mu}$$

4.6 Discussion

So far, we have analyzed a simple decaying population model considering both deterministic and stochastic frameworks. The key deterministic result was that when death rates are constant over time, the total population size decays exponentially according to Eq. (4.3). By developing a stochastic description, we were able to account for randomness at the individual level. Interestingly, when considering expected population sizes, the deterministic and stochastic descriptions coincide as shown by Eq. (4.7).

This emergence of deterministic behavior from underlying stochastic processes is an important phenomenon. While survival of individuals is inherently random, averaging over many trials washes out variability, resulting in smooth exponential decay. This demonstrates how populations self-organize simpler collective dynamics from complex interactions between constituents.

The death rate parameter μ takes on different meanings depending on the description. Deterministically, it characterized the system's exponential decay profile. Stochastically, it represented the probability of individual mortality. Such multi-scale modeling allows μ to provide insight across descriptive levels.

In summary, even simple population models like exponential decay showcase the interplay between stochastic and deterministic perspectives. Randomness at the individual scale shapes probabilistic population fluctuations, yet deterministic laws emerge at larger scales where variation averages out. This theory establishes foundations for more realistic extensions incorporating additional biological complexities.

4.7 Epilogue

Let us reexamine the population distribution function $\eta(\tau, t)$. We can define the normalized function:

$$\rho(\tau, t) = \frac{\eta(\tau, t)}{N(t)},$$

where $N(t) = \int_0^\infty \eta(\tau', t) d\tau'$. Function $\rho(\tau, t)$ describes the probability density that a randomly selected individual from the population has age τ at time t .

Rewriting Eq. (4.2) in terms of ρ :

$$\frac{\partial \eta}{\partial t} = -\frac{\partial \eta}{\partial \tau} - N(t)\mu(\tau)\rho(\tau, t).$$

Upon integration, this leads to:

$$\frac{dN(t)}{dt} = -\tilde{\mu}(t)N(t), \quad (4.8)$$

where $\tilde{\mu}(t) = \int_0^\infty \mu(\tau')\rho(\tau', t) d\tau'$ is the average death rate.

Notably, if the age distribution $\rho(\tau, t)$ remains stationary (independent of t), then the average death rate $\tilde{\mu}$ is constant. In this case, Eq. (4.8) again predicts exponential decay of $N(t)$, even with age-dependent mortality $\mu(\tau)$.

In conclusion, a stationary age structure is another way of producing exponential population decay through a constant average death rate. Therefore, observing exponential decay alone does not fully characterize the underlying stochastic process. Additional information, such as the lifetime distribution of individuals, is needed to distinguish the underlying stochastic process.

Chapter 5

Exponential Growth

Abstract In the previous chapter, we introduced our first population dynamics model, incorporating deaths alone, and demonstrated that this leads to exponential decay. Here, we expand the model to include both births and deaths. Considering these combined processes, we show that populations can either grow or decline exponentially, depending on whether the birth rate exceeds the death rate or vice versa. We delve more deeply into the phenomenon of exponential growth, investigating its remarkable properties. To build intuition, we first consider a thought experiment exploring the explosive potential of exponential growth in a bacterial culture. We then examine some key mathematical underpinnings, showing how exponential functions exhibit geometric behavior when evaluated over arithmetic sequences. Understanding these fundamental characteristics provides critical insight into how even modest growth rates may translate to astonishingly rapid increases over long timescales. In this chapter, our aim is to develop a richer appreciation for both the power and limitations of exponential growth dynamics.

5.1 Introduction

In the previous chapter, we examined how deaths influence population dynamics. Now, we will expand our study to incorporate the impact of births. It is important to consider that, in the absence of migration, new individuals arise in the population solely through the reproduction of existing individuals, as spontaneous generation is not possible. Therefore, we can modify Eq. (4.2) to accommodate births as follows:

$$\frac{\partial \eta}{\partial t} = -\frac{\partial \eta}{\partial \tau} + \beta(\tau)\eta - \mu(\tau)\eta. \quad (5.1)$$

In this equation, the term $\partial\eta/\partial t$ represents the rate of change of the population density η with respect to time t . The first term on the right-hand side, $-\partial\eta/\partial\tau$, accounts for the effect of aging on the population. The second term, $\beta(\tau)\eta$, introduces the influence of births, where $\beta(\tau)$ represents the birth rate as a function of age (τ). Finally, the third term, $-\mu(\tau)\eta$, considers the mortality rate $\mu(\tau)$, which represents the rate at which individuals of age τ die.

Based on the findings presented in the previous section of Chapter 3, and assuming that the probability density $\rho(\tau, t) = v(\tau, t)/N(t)$ remains stationary, we can integrate Eq. (5.1) to obtain the following expression:

$$\frac{dN}{dt} = \tilde{\beta}N - \tilde{\mu}N, \quad (5.2)$$

where $\tilde{\beta}$ and $\tilde{\mu}$ represent the average birth and death rates, respectively. These parameters are defined as $\tilde{\beta} = \int_0^\infty \beta(\tau')\rho(\tau')d\tau'$ and $\tilde{\mu} = \int_0^\infty \mu(\tau')\rho(\tau')d\tau'$. The population size is represented by $N(t) = \int_0^\infty \eta(\tau')d\tau'$. It is worth noting that, if both β and μ are age-independent, we obtain the same result without requiring the stationarity of η .

By introducing an effective growth rate $\alpha = \tilde{\beta} - \tilde{\mu}$, we can reformulate Eq. (5.2) as follows:

$$\frac{dN}{dt} = \alpha N, \quad (5.3)$$

This differential equation has a solution given by:

$$N(t) = N_0 e^{\alpha t}, \quad (5.4)$$

where N_0 represents the initial population size. If the death rate surpasses the birth rate, as studied in the previous chapter, the population would decay exponentially. However, if the opposite scenario occurs, where the birth rate surpasses the death rate, the population would experience exponential growth.

5.2 Explosiveness of Exponential Growth

To develop an intuitive understanding of exponential growth, let's consider a thought experiment involving an *E. coli* bacterial culture initiated from a single bacterium, assuming it can grow exponentially indefinitely. In such a scenario, the time evolution of the culture's mass is governed by the following equation:

$$m(t) = m_b e^{\alpha t}, \quad (5.5)$$

where m_b represents the initial mass of an individual bacterium, and α denotes the growth rate.

Now, let's explore how long it would take for the culture's mass to reach the magnitude of planet Earth ($M_E \approx 6 \times 10^{24}$ kg). Given that an individual bacterium

weighs approximately 10^{-15} kg and an *E. coli* culture can double its mass every 30 minutes, we can solve for t in Eq. (5.5):

$$t = \frac{1}{\alpha} \ln \frac{m(t)}{m_b}.$$

By substituting $m(t) = M_E$ and $\alpha = \ln(2)/30 \text{ min}^{-1}$, we can calculate the required time:

$$T_E = \frac{30, \text{ min}}{\ln 2} \ln \frac{M_E}{m_b} \approx 4,000 \text{ min} \approx 2.8 \text{ days}.$$

In other words, an exponentially growing bacterial culture starting from a single bacterium would accumulate a mass equal to that of planet Earth in less than 3 days. This thought experiment vividly illustrates the remarkable explosive potential of exponential growth.

5.3 Geometric Sequences and the Exponential Function

To comprehend the explosive nature of exponential growth, it is valuable to explore a fundamental property of the exponential function. Let us consider the function defined as:

$$f(x) = e^{ax}.$$

Now, suppose we have a value x_2 such that:

$$f(x+x_2) = 2f(x).$$

In other words:

$$e^{a(x+x_2)} = 2e^{ax}.$$

By solving for x_2 in the equation above, we find:

$$x_2 = \frac{\ln 2}{\alpha}.$$

Notably, the value of x_2 remains constant regardless of the initial value of x . This implies that, irrespective of the starting point, the value of $f(x)$ doubles when a value of x_2 is added to the argument. Consequently, if we construct an arithmetic sequence of the form:

$$x_{i+1} = x_i + x_2,$$

the sequence:

$$y_i = e^{ax_i},$$

will exhibit geometric behavior ($y_{i+1} = 2y_i$). The remarkable growth potential of geometric sequences has captivated humanity for centuries, giving rise to legends like the one illustrated in Chapter 2.

5.4 Discussion

While the exponential growth model provides valuable insight into population dynamics, it has important limitations when considered over long time periods. As we have seen, even tiny growth rates predict populations will eventually exceed all available resources as their mass approaches infinity. In reality, finite carrying capacities constrain population expansion. Additionally, exponential growth assumes resources are unlimited and external influences negligible, violating the basic principles of resource competition and natural regulation within closed ecological systems. In a forthcoming chapter, we will introduce a more realistic population model called the logistic model. The logistic equation incorporates density-dependent effects like resource competition and saturation, allowing populations to stabilize at an environmental carrying capacity. Studying the logistic model will provide a more nuanced understanding of how biotic and abiotic factors interact to govern long-term population persistence in nature. This will lay the foundation for exploring more complex dynamic interactions between species in ecological communities.

Exercises

1. A geometric progression (S_n) is defined as a sequence of non-zero terms where each subsequent term is obtained by multiplying the previous term by a fixed common ratio (r):

$$S_{n+1} = rS_n$$

An exponential function ($f(x) = Ce^{ax}$) models continuous growth or decay at a constant rate (a). Show that the geometric progression provides a discrete analogue of the exponential function by finding the relation between the common ratio r and the exponent parameter a that allows the geometric progression terms S_n to equal the discrete function values $f(n)$: $S_n = f(n)$.

2. In the previous exercise, we showed that a geometric progression provides a discrete analogue of the exponential function when a specific relationship between their parameters exists. Now consider how the concepts of limits and convergence apply to both of these mathematical objects. Specifically find what conditions must be fulfilled for a geometric sequence and exponential function to converge to zero as the index/input-variable approaches infinity? Relate the convergence condition(s) back to the relationship defined between the common ratio r and exponent parameter a in the prior exercise.

Chapter 6

Local Stability Analysis

Abstract This chapter introduces the key concepts and methods involved in performing a stability analysis of steady states for nonlinear dynamical systems. Steady states, or fixed points, are defined as constant solutions to a differential equation that do not change over time. Their stability determines whether nearby solutions will converge or diverge from the steady state. While graphical analysis can assess stability in 1D, a more rigorous analytical approach is required for higher dimensions. The method developed is to linearize the nonlinear dynamics near a steady state, resulting in a linear approximation governing small perturbations from the fixed point. The stability criterion is then derived from the solution to this linearized system—a steady state will be stable only if perturbations decay over time, indicated by the slope of the original function being negative at that point. This technique allows classification of steady state stability across any system dimensionality using analytical mathematics.

6.1 Introduction

In the preceding chapters, we introduced basic linear population dynamics models and analyzed how their behavior evolves over time. However, more realistic representations often involve nonlinear differential equations. Attaining a rigorous global understanding of these models necessitates a formal stability analysis of their steady states. A steady state corresponds to a constant solution. For a population, this represents an equilibrium point at which birth and death rates precisely balance. Studying the stability of steady states allows for the classification of long-term dynamical behavior and the discernment of global dynamics arising from local perturbations.

Just as a balance at rest indicates equilibrium but imparts no insight into subsequent motion upon disturbance, steady states alone do not reveal dynamical fate.

Their stability determines their attracting or repelling character, with implications for qualitative trajectories that may resemble balls inducted into concavities or convexities. Linearizing functions near steady states permits estimation of the evolution of small deviations, providing local qualitative forecasts. When stability analysis and linearization are combined, they provide qualitative understanding that exceeds model solutions, just as one may predict a ball's motion from terrain alone despite transients obscuring endpoints. This chapter will introduce the tools to perform local stability analysis of 1-dimensional dynamical models.

6.2 Steady States

Consider the univariate ordinary differential equation:

$$\frac{dx}{dt} = f(x), \quad (6.1)$$

wherein $f(x)$ denotes an arbitrary smooth function. Steady states, or fixed points, for this differential equation represent unchanging constant solutions independent of time (t).

Let $x(t) = x^*$ represent a steady state. Its derivative with respect to time is null given its lack of time-dependence. Furthermore, by definition it must satisfy Eq. (6.1). Upon substitution, we obtain:

$$f(x) = 0$$

Accordingly, the steady states equate to the roots of function $f(x)$. This provides a method for determining the fixed points of any first-order ordinary differential equation by resolving the relationship $f(x^*) = 0$.

6.3 Assessment of Fixed Point Stability via Graphical Analysis

Consider the function $f(x)$ depicted in Fig. 6.1. Two roots, denoted x_1 and x_2 , of the equation $f(x) = 0$ are evident. Consequently, these locations define the steady states of the differential equation $dx/dt = f(x)$.

Let us now analyze the stability of the fixed points. Consider x_1 and note the positive slope of $f(x)$ at this location. A positive slope implies that for any initial condition marginally greater than x_1 , the value of $f(x)$ will be positive. Accordingly, this yields a positive rate of change for the value of x . Thus, the solution will move in a progressively greater direction, distancing itself from x_1 . Similarly, for any initial value slightly less than x_1 , the slope is such that the rate of change of x is negative. Consequently, the solution will decrease over time, drifting ever farther from x_1 .

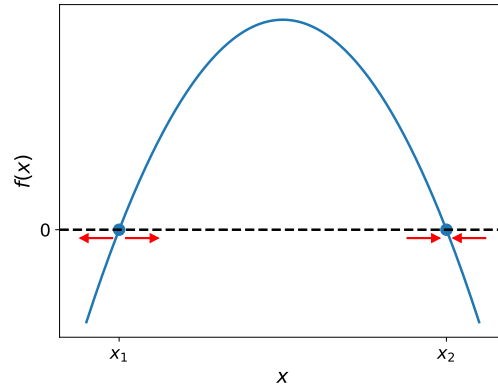


Fig. 6.1 Graphical depiction of the function $f(x)$ with two roots. This figure illustrates the function $f(x)$ which possesses two roots, denoted by x_1 and x_2 . The slope of $f(x)$ is positive in the vicinity of x_1 , as depicted by the upward sloping tangent. In contrast, the slope is negative near x_2 , as shown by the downward sloping tangent. These slope characteristics determine the qualitative behavior of solutions initialized proximate to the steady states. Specifically, red arrows indicate that perturbations tend to diverge from x_1 while converging towards x_2 . Therefore, x_1 represents an unstable fixed point whereas x_2 denotes a stable steady state. This graphical analysis conveys how the slope's sign at steady state locations qualifies their attracting or repelling nature.

From this analysis, we can see that x_1 is unstable as it repels nearby solutions over time.

In contrast, let us examine the stability of the other fixed point, x_2 . At this location, the slope of $f(x)$ is negative. Therefore, for any initial condition marginally greater than x_2 , the value of $f(x)$ will be negative. This implies the rate of change of x will also be negative, causing the solution to decrease in value over time and move closer to x_2 . Similarly, for initial values slightly less than x_2 , the negative slope indicates the rate of change of x is positive. Hence, the solution will increment in value, again tending towards x_2 . We can thus deduce that perturbations from x_2 will be attracted back to this fixed point location over time. Consequently, x_2 is stable as it attracts solutions.

In summary, this graphical analysis demonstrates that the stability of a fixed point for the differential equation $dx/dt = f(x)$ is determined solely by the sign of the slope of the function $f(x)$ evaluated at that fixed point. A positive slope implies perturbations will move further away from the fixed point over time, characterizing it as unstable. In contrast, a negative slope signifies that perturbations will be attracted back to the fixed point location, marking it as stable.

6.4 Local Stability Analysis

While the preceding graphical approach provides useful qualitative insights into fixed point stability for univariate systems, it cannot not be readily generalized to higher dimensions. The graphic analysis relies on visualizing the slope of a scalar-valued function, which is only possible for one-dimensional models. However, real-world phenomena often evolve according to multidimensional dynamical systems that cannot be embedded in two-dimensional space for intuitive slope evaluation. Therefore, a more systematic technique is required that permits stability classification of fixed points for differential equations inhabiting abstract dimensionalities. In this section, we develop the method of local stability analysis through linearization. By approximating nonlinear dynamics near steady states via linear functions, this approach furnishes a quantitative framework to assess stability in any dimensional system. These analytical tools supersede qualitative geometric intuitions, instead providing mathematics directly applicable to complexity beyond what may be visualized.

Consider once more the differential equation:

$$\frac{dx}{dt} = f(x). \quad (6.2)$$

We want to analyze the stability of a steady state value x^* . To do this, we look at an arbitrary solution $x(t)$ that starts out close to x^* . For the steady state to be locally stable, we need to show that $x(t)$ converges to x^* as time goes to infinity:

$$\lim_{t \rightarrow \infty} x(t) = x^* \quad (6.3)$$

It's helpful to define the “distance function” $\delta x(t)$:

$$\delta x(t) = x(t) - x^*. \quad (6.4)$$

This tells us how far $x(t)$ is from the steady state x^* at any time t . For our analysis to work, $\delta x(t)$ needs to stay much smaller than x^* as time passes.

We can write the stability condition in terms of $\delta x(t)$ as well:

$$\lim_{t \rightarrow \infty} \delta x(t) = 0. \quad (6.5)$$

In other words, for x^* to be stable, any small perturbations need to disappear over long times.

We seek to derive the governing differential equation for the dynamics of $\delta x(t)$. It can be readily shown from its definition in Eq. (6.4) that:

$$\frac{d\delta x(t)}{dt} = \frac{dx(t)}{dt}.$$

Substituting this expression and Eq. (6.4) into the original system dynamics in Eq. (6.2) yields:

$$\frac{d\delta x}{dt} = f(x^* + \delta x).$$

Leveraging the assumption that δx is small relative to x^* , we can approximate $f(x^* + \delta x)$ via a Taylor series expansion truncated after the first order term:

$$f(x^* + \delta x) \approx f(x^*) + f'(x^*)\delta x,$$

where $f'(x^*) = df/dx|_{x=x^*}$. Furthermore, since x^* defines a steady state, $f(x^*) = 0$. Thus, the differential equation for δx reduces to the following linear form:

$$\frac{d\delta x}{dt} = f'(x^*)\delta x.$$

The solution to this equation takes the form

$$\delta x(t) = \delta x_0 e^{f'(x^*)t},$$

where δx_0 denotes the initial perturbation from the steady state x^* . It is evident from this last equation that a necessary condition for $\delta x(t)$ to asymptotically approach zero as $t \rightarrow \infty$ is that $f'(x^*) < 0$. In other words, the steady state x^* will only exhibit stable behavior if the slope of the function $f(x)$ is negative when evaluated at $x = x^*$. In summary, local stability is assured only if perturbations decay over time, which occurs solely when the linearized dynamics represented by $f'(x^*)$ are negative.

6.5 Discussion

In this chapter, we introduced the method of local stability analysis and applied it to determine the stability of steady states for a univariate nonlinear dynamical system. Through linearization near steady states and solution of the resulting linear differential equation governing perturbations, we recovered the same criterion for stability established by the graphical analysis in the previous chapter—namely, that stability is ensured only when the slope of the governing function is negative, as evaluated at the steady state. Interestingly, this analysis arrived at the same qualitative conclusion through an analytical approach, rather than a geometric visualization. This mathematical technique has the advantage of being readily generalized to higher-dimensional systems that cannot be depicted graphically. The method of local stability analysis through linearization provides a systematic framework to assess fixed point stability for nonlinear dynamical models of any dimensionality. In this way, insights into long-term dynamical behavior near steady states can be captured quantitatively rather than relying on low-dimensional intuitions. This analytical approach will prove invaluable for nonlinear multi-species population and ecosystem models in subsequent chapters.

Exercises

Find the steady states and characterize their stability for the following one-dimensional differential equations:

1. $\frac{dx}{dt} = 2x - 6.$

2. $\frac{dx}{dt} = x^2 - 4.$

3. $\frac{dx}{dt} = (x - 2)^2.$

4. $\frac{dx}{dt} = -x^3 + 2x.$

Chapter 7

On the Interconnected Origins of Statistics, Probability Theory and Population Dynamics

Abstract This chapter traces the interconnected conceptual origins of statistics, probability theory, and population dynamics that emerged in the 17th century. It examines foundational contributions from figures such as Cardano, Pascal, Graunt, Huygens, and Bernoulli who established the theoretical and empirical bases for analyzing natural and social phenomena using mathematical and data-driven methods. Key advances discussed include the early application of quantitative methods to games of chance by Cardano, the founding of probability theory by Pascal and Fermat, Graunt's establishment of empirical demography, and the development of probabilistic population modeling through life tables. The chapter argues that this transformative period saw the beginning of quantitative, evidence-based approaches across scientific domains through linked conceptual roots in analyzing randomness, uncertainty, and human populations.

7.1 Introduction

The fields of statistics, probability theory, and population dynamics share interconnected conceptual origins that emerged in the 17th century. During this period, mathematicians, philosophers, and early scientists began developing new empirical and mathematical approaches to understand natural and social phenomena. Where previously such domains had been studied through qualitative reasoning or abstract models, quantitative analysis utilizing data and probability concepts now took root.

Three pivotal developments laid the foundation for these disciplines as we understand them today. The first was the establishment of probability theory as a mathematical subject area through the correspondence between Blaise Pascal and Pierre de Fermat in 1654. In establishing clear definitions and analytical techniques for calculating probabilities, their work launched probability as a rigorous field of study.

Concurrently, John Graunt published his study of London mortality records titled *Observations Made upon the Bills of Mortality* in 1662. This work is considered the origin of modern demography and statistics, as Graunt systematically compiled and analyzed parish death data using crude early statistical techniques. His work demonstrated the value of a quantitative, empirical approach and helped establish population modeling and life tables.

Connecting these two threads was the development of probabilistic concepts of population dynamics. Christiaan Huygens and later Nicholas Bernoulli built on Graunt's work by interpreting his partial life table probabilistically. This work in the late 17th century established the theoretical framework for life tables based on probabilistic models of mortality rates.

Together, these developments represented the interconnected foundational concepts of statistics, probability theory and population modeling that are still core to these fields today. Through increasingly mathematical and data-driven methods, scientists began developing powerful new analytical tools for understanding the natural and social world in quantitative terms.

The key sources that informed the development of this chapter were the following works (Bacaër, 2011; Kreager, 1991). Readers interested in exploring these topics in more depth are encouraged to refer to these publications.

7.2 Background

The intellectual context of the 17th century set the stage for the formative developments in probability, statistics and population modeling. Advances in mathematics, along with changing philosophies of science, fostered quantitative and empirical approaches to understanding the natural world.

Mathematicians of the early 1600s had formalized algebra, introducing symbolic notation that allowed solving generalized problems rather than specific numerical examples. This mathematical maturity enabled tackling more complex real-world problems. Concurrently, Francis Bacon and others advocated inductive, experiment-based scientific methods rather than overtly theoretical deduction alone.

Early proto-statistical techniques also emerged. Blood counts recorded by Belgian Lambert van Heemskerck in 1590 showed histograms emerging as a tool to visualize data distributions. Galileo's 1611 displacement experiments laid foundations for experimental design and estimation of measurement error.

In natural philosophy, Aristotelian teleological thought remained dominant yet faced challenges from the mechanistic views of Descartes. John Wallis' *De Algebra* of 1693 signaled a shift towards mathematical representations. Investigation of celestial phenomena like comets, sunspots and nova by Kepler, Brahe and Galileo revealed complexity rather than the astronomically "perfect" former worldview.

This context set the stage for progress. Developing numerical techniques and willingness to quantify real-world phenomena opened the doors for applying mathematics to problems like games, mortality and astronomy. Empirical natural knowl-

edge supplanted overtly theoretical tradition, recognizing phenomena like errors and variation fundamental to scientific understanding. Challenges to established world-views enabled new probabilistic and quantifying perspectives on inherently complex, diverse phenomena. This laid groundwork for probability, statistics and life tables emerging in the mid-1600s.

7.3 Cardano's Work

One of the earliest works to apply mathematical thinking to games of chance was Girolamo Cardano's 1526 treatise *De Ludo Aleae* (*On Games of Chance*). As a physician and polymath deeply engaged in mathematics, Cardano sought to determine equitable rules and stake structures for various gambling activities through probabilistic reasoning. Though he lacked a theoretical framework, Cardano's work marked a pioneering effort in what would later become probability theory.

In *De Ludo Aleae*, Cardano analyzed dice, cards and various board games that involved elements of chance. For each, he aimed to calculate the mathematical expectation of each potential outcome in order to establish fair stakes. For example, in analyzing common dice games, Cardano outlined the relative probabilities of rolling different numbers and their associated payouts. However, his arithmetic calculations contained errors and he did not consistently apply proportional reasoning to determine equitable outcomes.

A problematic endeavor Cardano explored was the "problem of points;" how winnings should be divided between two players if an incomplete game of chance was stopped before a winner was determined. While proposing solutions based on proportional reasoning, Cardano's logic contained logical gaps. For a game half-completed, he suggested stakes be split evenly rather than considering the changing probabilities as the game progressed. This flawed proportional method would continue to plague proposed solutions for some time.

Despite analytical limitations from lacking a rigorous probability system, *De Ludo Aleae* marked an intellectual milestone as one of the earliest works to systematically apply mathematical and quantitative thinking to games involving chance. It helped establish chance and probability as worthwhile subjects of mathematical inquiry. While Cardano's specific solutions were imperfect, his work helped catalyze further development and paved the way for the eventual theoretical foundations later established by Pascal, Fermat, and other 17th century thinkers.

7.4 Pascal and Fermat

The birth of probability theory as a rigorous mathematical discipline owes to the correspondence between the French mathematician Blaise Pascal and French lawyer Pierre de Fermat in 1654. Seeking to solve the unresolved "problem of points," their

letters established fundamental concepts and analytical techniques that formed the basis of probability as a field of study.

Pascal introduced the groundbreaking idea of mathematical expectation, which allowed calculating the average probability-weighted payoff of each possible outcome. Through examining games with varying numbers of trials like rolling dice, Pascal discovered patterns in the binomial coefficients that became known as Pascal's triangle. This arrangement reveals the coefficients of binomial expansions and allowed calculating probabilities and expectations through what is known as the binomial distribution.

Fermat independently devised an analytical approach using proportional reasoning about remaining possibilities. Through comparing solutions, Pascal and Fermat established that their methods agreed, validating that probability could be understood mathematically. They then applied these to systematically solve variations of the problem of points.

Significantly, Pascal provided clear definitions of probability, expectation, and equity in games of chance. This marked the establishment of probability theory as an organized field based on precise definitions and analytical calculations rather than intuition. Their correspondence founded the modern mathematical understanding of probability that remains fundamental to statistics, risk analysis and related disciplines.

7.5 Huygens' Treatise

Building upon the foundational work of Pascal and Fermat, Christiaan Huygens' 1657 treatise *De Ratiociniis in Ludo Aleae* marked an important step forward in developing probability theory. Through elegantly solving problems involving games of chance, Huygens refined key concepts and helped disseminate probabilistic reasoning to a broader intellectual audience.

Huygens presented five problems to demonstrate logical solutions using the mathematical expectation and probability techniques established earlier. His treatment expanded the scope beyond Pascal's original problem of points by considering scenarios like dividing stakes between players leaving ongoing games and determining equitable initial and ongoing stakes.

What distinguished Huygens' approach was his employment of geometric representations to arrive at solutions. By visualizing probabilities and expected values geometrically, he provided intuitive demonstrations accessible to contemporary mathematicians and scholars. Problems involving compound probability or independent events were depicted especially clearly through his innovative geometric approach.

Beyond pragmatic applications, Huygens' treatise introduced theoretical advances. He properly considered cases involving more complex stochastic processes with multiple dependent variables. The concept of independence between events was also more rigorously defined.

Huygens helped cement probability theory as a legitimate field meriting dedicated study. By refining concepts through elegant visual proof, he disseminated probabilistic reasoning to a broader intellectual community. His treatise engaged fellow mathematical thinkers while communicating foundations developed by Pascal and Fermat to a general educated readership.

7.6 Graunt's Bills of Mortality

While Continental mathematicians formalized probability theory, in England John Graunt published his work *Observations Made upon the Bills of Mortality* in 1662. By systematically compiling and analyzing parish mortality records from London, Graunt is considered the founder of modern empirical demography and statistics.

Graunt studied weekly Bills of Mortality listing burials in each parish from 1603-1660. He assessed data quality, discussed trends in mortality from different causes, and noted seasonal patterns. By comparing burial totals to estimated births, Graunt proposed London's total population was around 460,000.

He constructed what is considered the first life table by calculating survivorship ratios at each age based on proportional mortality. While crude, this provided insights into longevity and helped estimate life expectancies. Graunt also tested hypotheses, finding for example that mortality was lower when more births occurred.

Through his careful collection and assessment of real-world evidence, Graunt established demography as an empirical discipline. Unlike earlier works grounded in theory, Graunt emphasized pragmatic, data-driven analysis and population modeling.

Observations Made upon the Bills of Mortality represented an intellectual departure by quantitatively interrogating social phenomena. It influenced later demographers and materially aided statecraft through providing population estimates. Most significantly, Graunt established mortality records and life tables as foundations for future probabilistic population modeling developed by Huygens, Bernoulli and later thinkers.

7.7 Probabilistic Life Tables and Early Insurance Mathematics

Building upon Graunt's empirical establishment of life tables, later 17th century mathematicians developed probabilistic interpretations that represented important conceptual advances. Correspondence between Constantijn and Christiaan Huygens in 1669 began interpreting life tables through expected value calculations, laying early foundations.

However, the first systematic probabilistic construction and interpretation of Graunt's partial life table emerged in Nicholas Bernoulli's 1709 dissertation for the University of Basel. Seeing Graunt's observations as samples from an imagined in-

finite population, Bernoulli established the probability of survival and death at each age based on frequencies in the dataset.

This conceptualization described what is now known as a stationary life table based on regular and consistent mortality probabilities at each age level. Bernoulli fitted Graunt's London figures to his theoretical model to derive survival probabilities and life expectancies, demonstrating how pragmatic demographic records could inform probabilistic population modeling.

Concurrently, nascent life insurance and annuity practices drove interest in mathematically calculating fair premiums and payout values. Jan de Witt evaluated annuity pricing in 1671 based on Dutch life tables, though not fully probabilistically. Edmond Halley's 1693 paper introduced what became known as Halley's life table and outlined uses including insurance pricing, suggesting age-specific rates.

While emerging pragmatically, these developments established the analytical theoretical framework treating populations and longevity in probabilistic terms. Refined life tables coupled with probability concepts formed the mathematical underpinnings for later insurance and social policy applications informed by demographic patterns. They launched systematic population modeling central to modern actuarial science and epidemiology.

7.8 Discussion

By the late 17th century, the conceptual foundations for statistics, probability theory, and population modeling as quantitative fields of study had begun to solidify. Individuals including Cardano, Pascal, Graunt, Huygens, Bernoulli and others made important contributions developing mathematical and empirical approaches for analyzing phenomena involving chance, data, and human populations.

Throughout this period, there was a discernible shift towards more quantitative, data-driven methods of understanding the natural and social worlds. Inspired by early empirical pioneers, scientists increasingly used numerical evidence and mathematical representations to model irregular and complex systems. They developed analytical tools to estimate parameters, assess uncertainties, and test hypotheses rigorously against observations.

Even today, statistics, probability, and population modeling remain interconnected and influence each other's ongoing progress. Advancements in one field often spur developments in related areas. For example, new statistical techniques enable analysts to more accurately model population dynamics when considering demographic uncertainties or changes over time. Similarly, probabilistic methods allow epidemiologists and other scientists to better estimate public health risks and design evidence-based policies. The significant conceptual links established in their 17th century beginnings continue shaping the nature of inquiry across these quantitative fields.

Chapter 8

Logistic Model

Abstract This chapter presents the logistic growth model, a population dynamics model that incorporates density-dependent negative feedback on growth rates. After historically introducing population regulation concepts from Malthus and Verhulst's development of the first quantitative model, we derive the logistic differential equation and its closed-form solution. The model exhibits long-term convergence to a stable carrying capacity regardless of initial conditions. Through local stability analysis of steady states, analytical and graphical approaches confirm the model predicts sigmoidal growth trajectories for starts below half carrying capacity, and monotonic convergence above it. While density-dependence captures universal population constraints, the simplicity of the logistic equation demonstrates how fundamental processes can form the basis for mathematical descriptions reflecting real ecological dynamics over long timescales, making it one of the most widely applied population models.

8.1 Introduction

While the exponential growth model provides a simple and mathematically tractable framework for studying populations over short time periods, it has significant limitations when extrapolated over long timescales. Most notably, the model predicts unconstrained population expansion leading to infinite size, which is not feasible in reality. All natural populations are bound by finite resources in their environment. The exponential model also ignores factors like resource competition and carrying capacity effects that act to slow growth as the population approaches the limits of its habitat. As a result, the model cannot realistically depict long-term population behavior or stability. For populations existing in a closed ecological system with density-dependent influences, another type of population model is needed that incor-

porates limitations on growth from resource limitations and crowding effects. This will allow an investigation of population regulation and equilibrium conditions. The development of such a model, which involves including density-dependent feedback in the growth term, is necessary to more accurately represent population dynamics over long periods aligned with biological timescales.

8.2 A Brief Historical Review

Thomas Malthus was one of the earliest scholars to study population dynamics. In his 1798 treatise *An Essay on the Principle of Population*, Malthus hypothesized that human populations have an inherent capacity to grow exponentially if unchecked by outside forces. This is because populations can increase geometrically through reproduction. In contrast, he argued that the food resources required to support growing populations only increase in an arithmetic progression over time. As populations grow exponentially yet resources increase linearly, Malthus recognized that individuals would inevitably come into competition for limiting resources like food, space, and other necessities of life. This competition, he proposed, serves to slow population growth from its unchecked exponential rate down to a level sustainable given the available resources. Malthus' ideas introduced the concept that populations are regulated by external factors related to resource availability and by the scarcity and struggle for existence that arises due to overpopulation. His insights formed the basis for later formal mathematical models of population dynamics.

While Malthus recognized that populations cannot grow exponentially indefinitely, he did not provide a mathematical model to describe how growth becomes limited over time. It was the Belgian mathematician Pierre Verhulst who first developed an explicit equation incorporating this regulation mechanism. In 1838, Verhulst modified the simple exponential growth model based on Malthus' arguments about competition for resources. He proposed adding a negative feedback term that increases in proportion to the population size, representing the growing scarcity and resultant effect on per capita growth rate as the population approaches the environment's carrying capacity.

8.3 The Logistic Model

We begin by recalling the differential equation that governs exponential population growth:

$$\frac{dN}{dt} = \alpha N,$$

where α is a constant growth rate parameter. Verhulst proposed modifying this model by substituting parameter α with a decreasing function of the population size N , denoted $\alpha(N)$. Specifically, he proposed a linear decay function of the form:

$$\alpha(N) = r \left(1 - \frac{N}{K} \right),$$

where r represents the intrinsic per capita growth rate in the absence of density-dependent effects. Meanwhile, K denotes the environment's biological carrying capacity; the maximum sustainable population size given resource constraints. This negative feedback term grows proportionally as N approaches K , introducing density-dependent regulation into the exponential growth formulation. Verhulst's ingenious substitution of a variable growth rate function was a landmark development that produced the first quantitative model embodying Malthus' concept of self-limitation through resource competition.

Through this modification, Verhulst produced the following nonlinear ordinary differential equation to govern population dynamics:

$$\frac{dN}{dt} = rN \left(1 - \frac{N}{K} \right). \quad (8.1)$$

Verhulst named the solution to this differential equation the “logistic function”. By extension, the overall model is commonly referred to as the “logistic model” of population growth. However, it is also appropriately termed the “Verhulst model”

We can solve the logistic differential equation (Eq. 8.1) using variable transformations. First, introduce the change of variable $x = 1/N$. This transforms Eq. (8.1) to:

$$\frac{dx}{dt} = rx \left(\frac{1}{K} - x \right).$$

Next, define the variable $y = x - 1/K$, yielding:

$$\frac{dy}{dt} = -ry.$$

This has the solution $y(t) = y_0 e^{-rt}$, where y_0 is the initial value. Transforming back through the steps, we arrive at the solution for the original variable N :

$$N(t) = \left[\frac{1}{K} + \left(\frac{1}{N_0} - \frac{1}{K} \right) e^{-rt} \right]^{-1}. \quad (8.2)$$

Through judicious variable substitutions, we have derived an explicit closed-form solution to the logistic differential equation governing population dynamics.

Eq. (8.2) is the well known logistic function. Consider the characteristics of this solution. The first term inside the brackets, $1/K$, represents the asymptotic carrying capacity. As time increases, the exponential term e^{-rt} monotonically decays to zero. Therefore, in the limit of large time, the population N will approach the value:

$$\lim_{t \rightarrow \infty} N = K.$$

This shows that regardless of the initial population N_0 , the solution will always converge to the environmental carrying capacity K . Physically, this makes sense; as time progresses, density-dependent effects will gradually dampen the growth rate until it balances perfectly with mortality to establish an equilibrium at the maximum sustainable size. The timescale to reach this steady state depends on the intrinsic growth rate r , but the ultimate attractor is always K . Therefore, the logistic model comprehensively captures the self-regulation of populations towards their local resource limits envisioned by Malthus.

8.4 Local Stability of Steady States

While we were able to derive an analytical solution to the logistic equation in the previous section, this is not always possible for nonlinear dynamical systems. Even when a closed-form solution cannot be obtained, important qualitative insights into dynamic behavior can still be gained by analyzing the system's steady states and their local stability properties. Though analytical solutions offer complete descriptions of trajectories over time, local stability analysis offers a general, mathematically rigorous technique to characterize global qualitative behaviors. In this section, we will use such an approach by finding steady states of the logistic model and applying linear stability theory to assess their stability.

To perform a local stability analysis, we first rewrite the logistic differential equation (Eq. 8.1) in the general form:

$$\frac{dN}{dt} = f(N),$$

where $f(N) = rN(1 - N/K)$. The steady state solutions, also known as fixed points, correspond to values of N where $f(N) = 0$. One can readily show that the fixed points are $N_1^* = 0$ and $N_2^* = K$.

We next calculate the derivative of $f(N)$ to determine the slope at each fixed point:

$$f'(N) = r - \frac{2rN}{K}.$$

Evaluating f' gives: $f'(N_1^*) = r > 0$ and $f'(N_2^*) = -r < 0$. This indicates that perturbations will grow near $N_1^* = 0$, making it unstable. Meanwhile, near the carrying capacity $N_2^* = K$, perturbations will decay over time, signifying stability.

The previous analytic stability analysis can be visualized graphically. Fig. (8.1) depicts the growth rate function $f(N) = rN(1 - N/K)$. This illustrates the two fixed points where $f(N)$ intersects the horizontal axis, representing steady state solutions.

The fixed points occur at population values of $N_1^* = 0$ and $N_2^* = K$, coinciding with the steady state solutions found earlier. To assess local stability, we evaluate the slope of $f(N)$ at each fixed point. At $N_1^* = 0$, the positive slope means nearby trajectories will diverge over time. Therefore, N_1^* denotes an unstable node, shown

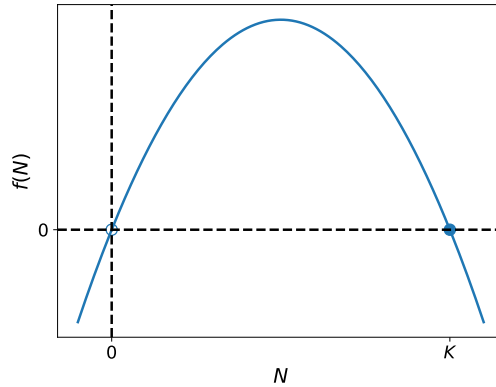


Fig. 8.1 Graphical analysis of fixed points and stability in the logistic growth model. This figure shows the growth rate function $f(N) = rN(1 - N/K)$. The two roots of this function, where it intersects the horizontal axis, are the fixed points (steady state solutions): $N_1^* = 0$ and $N_2^* = K$. Local stability is determined by the slope of $f(N)$ at each fixed point. At $N_1^* = 0$, the slope is positive indicating nearby trajectories will diverge over time. Therefore, N_1^* denotes an unstable fixed point, represented by an open circle. In contrast, the slope of $f(N)$ is negative at the carrying capacity $N_2^* = K$. Thus, small perturbations will contract back towards the fixed point. This characterizes N_2^* as a stable steady state solution, shown as a filled circle.

as an open circle. In contrast, the negative slope at the carrying capacity $N_2^* = K$ implies small perturbations will decay back to this fixed point. This characterizes N_2^* as locally stable, represented by a filled circle.

The graphical analysis in Fig. 8.1 provides additional qualitative insights into solution trajectories. Since the function $f(N)$ is increasing over the range $0 < N < K/2$, populations initialized below half the carrying capacity ($N_0 < K/2$) will experience accelerated growth as they approach this midpoint. However, as $f(N)$ is decreasing for $K/2 < N < \infty$, these solutions will then decelerate as diminishing resources induce density-dependent regulation toward the asymptote. Thus, trajectories beginning below $K/2$ exhibit the characteristic S-shaped sigmoid curve.

On the other hand, solutions starting above half the carrying capacity ($N_0 > K/2$) will converge directly to K in a qualitatively different manner, as $f(N)$ is negative over this interval. Their approach will be steadily dampened regardless of whether their initial value is below or above the stable steady state $N_2^* = K$. Therefore, by examining the increasing and decreasing intervals of $f(N)$, we gain insight into qualitatively distinct population growth dynamics depending on initial population size relative to the system's threshold midpoint value.

The qualitative insights gained from analyzing the growth rate function $f(N)$ can be validated by plotting the solutions of the logistic differential equation over time. Fig. 8.2 plots the logistic function given by Eq. (8.2) for a range of initial population sizes N_0 . This illustrates how initial conditions smaller than half the carrying capacity $K/2$ exhibit sigmoidal growth curves, consistent with the posited trajectory

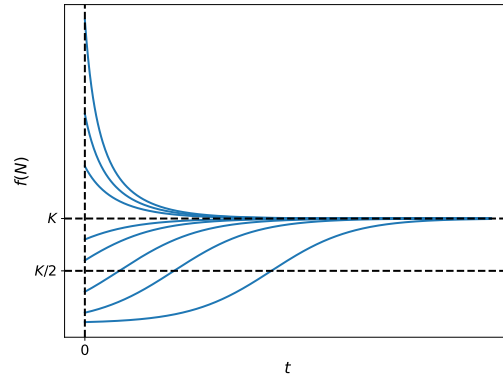


Fig. 8.2 Qualitative trajectories of the logistic solution for varying initial conditions. This figure graphically depicts the logistic function given by Eq. (8.2) over time for different initial population sizes N_0 . Solutions initialized below half the carrying capacity $K/2$ exhibit characteristic sigmoidal growth curves, accelerating as they approach the midpoint before slowing down due to density dependence. In contrast, populations starting above $K/2$ demonstrate qualitatively different monotonic convergence (without an inflection point) to the stable steady state at carrying capacity K , regardless of whether they start above or below the fixed point.

shapes based on the increasing and decreasing intervals of $f(N)$. Solutions initialized above $K/2$ also match expectations, showing direct monotonic convergence.

By comparing the predicted dynamics from analytic and graphical stability analysis (Fig. 8.1) against analytic solutions in Fig. 8.2, we find strong agreement between the local mathematical characterization near fixed points and the emergent global qualitative behaviors of the overall system across a spectrum of initial conditions. This corroborates that the linearization techniques employed to analyze steady states provide insights extending well beyond the local neighborhood of equilibria to inform our broader understanding of logistic population growth models.

8.5 Discussion

The logistic equation, despite its simple mathematical form, captures essential qualitative features of real-world population dynamics. The inclusion of nonlinear density-dependent feedback simulates the influence of finite resources and competition on growth. This confers carrying capacity behavior observed universally in populations, from microbial colonies to animal populations. Thus the logistic model has broad relevance in ecology, providing a starting point to understand outbreaks, booms, and stabilization in a variety of species. Its success stems from distilling dynamics to fundamental processes without species-specific complexity. As one of the earliest and most widely employed models in mathematical biology, it demonstrates

how even minimal representations can reflect key characteristics of living populations, especially those of unicellular organisms like bacteria exhibiting exponential growth followed by limited expansion.

While analytic solutions offer complete trajectories when attainable, local stability analysis provides a generalizable technique for characterizing nonlinear dynamical systems. By linearizing near fixed points, it allows classifying long-term qualitative fates of solutions based on mathematical stability criteria. As demonstrated here for the logistic equation, this approach correctly predicts global dynamic attributes from investigation of a system's local equilibrium properties. Even without closed-form solutions, local analysis thus remains a powerful approach for divining qualitative insights into complexity arising from nonlinear feedbacks governing real natural and engineered systems. Where full descriptions remain elusive, studying stability properties of steady states provides an alternative lens into qualitative behaviors that may emerge from complexity near points of balance.

Exercises

1. Find the steady states of the following variation of the logistic model

$$\frac{dN}{dt} = rN \left(1 - \frac{N}{K} \right) - \delta.$$

Study the stability of steady states and discuss the implications in comparison with the behavior of the original model.

2. Find the steady state and study their stability for the Gompertz model:

$$\frac{dN}{dt} = rN \ln \frac{K}{N}.$$

Contrast the findings with those of the logistic model.

Chapter 9

Extending the logistic model

9.1 Introduction

In the previous chapter, we introduced the basic logistic population growth model and analyzed its dynamic behavior. This model assumes that density-dependent competition for resources limits exponential growth. However, more complex interactions can also shape population dynamics. Here we extend the logistic equation to incorporate two additional realistic effects: increased mortality and the Allee effect.

9.2 Increased mortality

Up to this point, our logistic population model has assumed that the effective growth rate (the difference between the growth and death rates) is a linearly decreasing function of the population size. In some circumstances, environmental factors unrelated to population density, such as stressors or resource limitation, can elevate mortality. To incorporate this effect, we modify the logistic differential equation. Specifically, we add a term representing density-independent background mortality:

$$\frac{dN}{dt} = rN(1 - N/K) - aN. \quad (9.1)$$

Here, the parameter $a \geq 0$ controls the strength of increased background mortality. When $a = 0$, this model reduces to the basic logistic equation.

To perform a local stability analysis, we first rewrite the logistic differential equation, Eq. (9.1), in the general form:

$$\frac{dN}{dt} = f(N),$$

where $f(N) = rN(1 - N/K) - aN$. The steady state solutions, also known as fixed points, are given by values of N that satisfy $f(N) = 0$. This yields two fixed points: the extinction state $N_1^* = 0$, and the non-zero equilibrium $N_2^* = K(r - a)/r$.

To determine stability, we calculate the derivative of the function $f(N)$ to obtain the slope at each fixed point. The derivative is:

$$f'(N) = (r - a) - \frac{2rN}{K}.$$

Evaluating f' at the two fixed points gives: $f'(N_1^*) = r - a$ and $f'(N_2^*) = a - r$. This reveals that when $a < r$, the extinction state N_1^* is unstable while the positive equilibrium N_2^* is stable. However, when the mortality rate exceeds the intrinsic growth rate ($a > r$), the stability of the fixed points switches; now the extinction state is stable, whereas the non-zero state N_2^* becomes unstable.

Geometrically, we can gain insight into this transition by visualizing how the fixed points vary with the mortality rate parameter a , as illustrated in Fig. 9.1. As a increases through the critical value of r , the two fixed points collide at $a = r$ and trade stability. Topologically, this behavior corresponds to a transcritical bifurcation. Physically, it indicates that beyond a threshold level of background mortality, high death rates outweigh new births even at very low population sizes, thereby preventing the population from persisting over long-term. The bifurcation analysis thus provides a framework for understanding how environmental stresses influence population viability through changes in demographic rates.

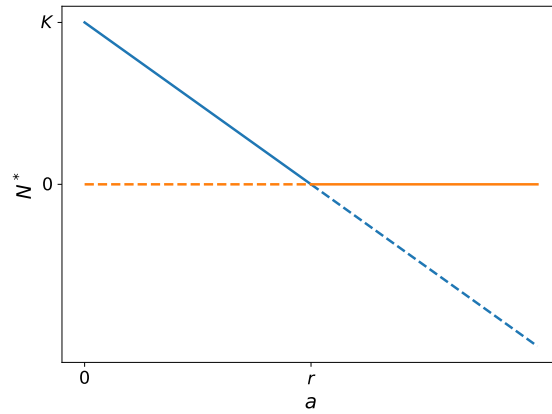


Fig. 9.1 Bifurcation diagram showing how the two steady state solutions, population extinction (N_1^*) and the positive equilibrium population size (N_2^*), vary dynamically with changes to the background mortality rate parameter (a). The extinction fixed point is depicted with orange lines, while the positive equilibrium is shown in blue. Stable steady states are depicted with solid lines, and unstable states with dashed lines. As a increases beyond the critical threshold value r , equivalent to the intrinsic growth rate, the fixed points intersect at the transcritical bifurcation point. This bifurcation signifies the exchange of stability between the two solutions, where population persistence loses stability and extinction gains stability with further increases in environmental mortality.

This model exhibits the first bifurcation encountered in this textbook. It is therefore worthwhile to discuss bifurcations in more detail. By definition, a bifurcation refers to a qualitative change in dynamical behavior that can emerge from small perturbations to parameter values. Specifically, at a bifurcation point the number and/or stability properties of fixed point solutions may abruptly shift. Some common types of bifurcations include:

- Saddle-node bifurcation: this occurs when two fixed points coalesce and annihilate one another.
- Transcritical bifurcation: a stable and unstable fixed point exchange stability at the critical parameter value.
- Pitchfork bifurcation: a single fixed point loses stability, splitting into three solutions of which two are stable.

Bifurcations are significant because they delineate boundaries between distinct qualitative solution behaviors attainable within a model. Identifying these transition points provides insight into how sensitive model predictions are to perturbations of the governing equations.

In the modified logistic population model presented here, the bifurcation that occurs with rising background mortality is of the transcritical type. This bifurcation demarcates how increasing non-density dependent death rates can irreversibly drive the population to extinction once they surpass the capacity for growth. Specifically, as mortality rises past the critical threshold equal to the intrinsic per capita growth rate, the transcritical bifurcation causes the stable fixed point solution representing long-term population persistence to exchange stability with the unstable extinction point. Consequently, above this bifurcation value, mortality dominates reproduction even at very low densities throughout the entire parameter space. This example demonstrates that environmental stressors can precipitate a population tipping point between ongoing viability versus extinction by tilting the demographic balance through small alterations to basic rates of birth and death. Identifying such bifurcation-defined thresholds provides insight into how susceptible population persistence is to fluctuations in underlying biological parameters.

9.3 Allee Effect

Small populations face additional hurdles that threaten their long-term sustainability. This phenomenon, known as the Allee effect, arises due to difficulties finding mates and engaging in beneficial forms of cooperation at very low densities, resulting in decreased per capita growth. To represent this intrinsic difficulty in the logistic model, we introduce an Allee term as follows:

$$\frac{dN}{dt} = rN \left(1 - \frac{N}{K} \right) \left(\frac{N}{A} - 1 \right). \quad (9.2)$$

In this formulation, parameter $0 < A < K/2$ represents a population threshold below which the effective per capita growth rate becomes negative, meaning that deaths exceed births.

Let us analyze Eq. (9.2) in its general functional form, $\dot{N} = f(N)$, where $f(N) = rN(1 - N/K)(N/A - 1)$. The form of this function $f(N)$ is depicted graphically in Fig. 9.2. As seen in the figure, $f(N)$ intersects the horizontal axis at three distinct points, indicating the presence of three steady state solutions: population extinction at $N_1^* = 0$, an interior equilibrium at $N_2^* = A$, and a second fixed point at the carrying capacity $N_3^* = K$. Furthermore, the derivatives $f'(N_1^*) < 0$, $f'(N_2^*) > 0$, and $f'(N_3^*) < 0$. This confirms that N_1^* and N_3^* are stable nodes, while N_2^* is an unstable saddle point.

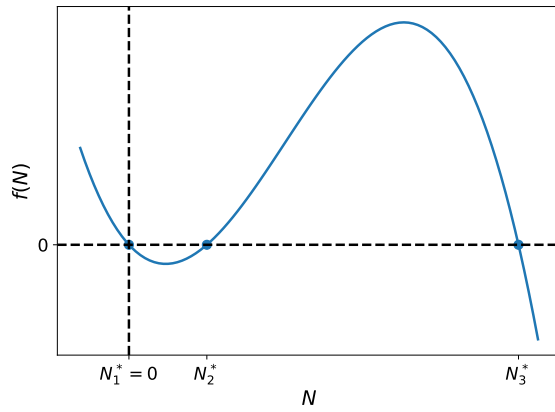


Fig. 9.2 Graphical depiction of the function $f(N) = rN(1 - N/K)(N/A - 1)$ describing per capita growth rate in the Allee effect model—Eq. (9.2). The function intersects the horizontal axis at three fixed points, indicating three steady state solutions: population extinction at $N_1^* = 0$, an interior unstable equilibrium at $N_2^* = A$, and the second interior stable fixed point at carrying capacity $N_3^* = K$. The first and third fixed points are stable nodes whereas the interior point is an unstable saddle, as shown by the signs of the derivatives $f'(N_1^*) < 0$, $f'(N_2^*) > 0$, and $f'(N_3^*) < 0$.

The existence of two locally stable fixed points separated by an unstable steady state in this modified logistic model, namely the extinction state N_1^* and the positive carrying capacity N_3^* , gives rise to bistability in the system's dynamics. Biologically, bistability implies that the population can persist indefinitely at either stable state of extinction or carrying capacity, with the final outcome dependent on initial conditions. Stochastic fluctuations may cause the population to randomly switch between attractors.

The logistic equation exhibiting an Allee effect is the first example in this textbook to demonstrate bistability. As a key feature of nonlinear systems, bistability will emerge again in other examples throughout this textbook, continually deepening our understanding of its consequences for real-world ecological and biological systems.

9.4 Discussion

In this chapter, we explored two extensions to the basic logistic population growth model: increased background mortality and an Allee effect. By incorporating density-independent mortality through an additional death term, the model exhibited a transcritical bifurcation whereby changes to the mortality rate could precipitate a population tipping point between ongoing viability and extinction. This demonstrated how environmental stresses may trigger abrupt, irreversible transitions in population state through subtle parameter changes.

Incorporating an Allee effect produced bistability, in which the population could persist indefinitely at either the extinction or carrying capacity stable states depending on initial conditions. Bistability highlights the sensitivity of ecological systems to random perturbations, with the potential for sudden shifts between alternative community states. It is a nonlinear phenomenon with significant implications for population persistence and community resilience.

More broadly, this chapter demonstrated the utility of dynamical systems theory and tools like bifurcation analysis for gaining mechanistic understanding of population viability. Such approaches aim to tease apart how multiplicative interactions between intrinsic biological processes and density-dependent feedbacks shape complex, often counterintuitive population dynamics over time.

Chapter 10

A Brief History of Nonlinear Dynamics

Abstract The field of nonlinear dynamics emerged from late 19th century efforts to understand complex phenomena that resisted traditional mathematical analysis. Pioneers like Henri Poincaré and Alexander Lyapunov developed qualitative and geometric techniques to study systems' long-term behaviors without exact solutions. Over the 20th century, mathematicians and scientists significantly advanced the original foundations. They formulated theories of stability, bifurcations, and chaos. Thinkers such as George Birkhoff, Aleksandr Andronov, and René Thom categorized fundamental changes in systems' behavior. Late 20th century experiments and computation unlocked deterministic chaos and strange attractors, revolutionizing views of unpredictability. Today, nonlinear dynamics provides a rigorous framework that illuminates order in apparent randomness across scales, from fluid motions to heart rhythms. This chapter surveys the origins and major developments of the field, from its roots in celestial mechanics to its modern role across science in understanding change over time.

10.1 Introduction

The natural world contains complexity from nonlinear interactions between simple components. Phenomena like flocking birds abruptly changing direction or turbulent flows appear unpredictable long-term despite deterministic rules. Understanding such behaviors has posed scientific challenges.

In the late 19th century, planetary motion presented intractable equations for three or more gravitating bodies. Motivated by these problems, Henri Poincaré developed qualitative techniques to characterize systems without exact solutions, founding a field of study.

Over decades, theorists defined concepts like stability, bifurcations and chaos, categorizing key transitions. Experiments revealed deterministic chaos from non-linearity, defying beliefs randomness required statistics. Progress accelerated with computers enabling simulations and visualization of strange phenomena.

Today, nonlinear dynamics provides rigorous frameworks for complexity across scales, illuminating mysteries from weather to heart rhythms. Analyses inform materials design and neural coding. The field drives conceptual links between microscopic chaos and macroscopic transport.

This chapter traces the emergence and historical developments of nonlinear dynamics, from its roots in studying celestial motion to its widespread applications across science today. In developing this overview, the following sources informed the key topics and milestones presented: (Kingsland, 1995; Goodstein, 2007). Readers seeking a more comprehensive understanding of nonlinear dynamics' conceptual foundations and evolution are encouraged to refer to these publications.

10.2 The Origins of a Field

10.2.1 *The Genius of Henri Poincaré*

By the late 19th century, mathematicians struggled to solve problems involving the gravitational interactions of three or more celestial bodies, as such systems evaded algebraic analysis due to their nonlinearities. Henri Poincaré believed qualitative geometric methods held the key to understanding these intractable dynamical systems.

Poincaré's brilliance was realizing that continuous systems described by differential equations could be transformed into discrete mappings through a process he termed "sectioning." By considering how variables changed between intersections of a chosen surface, trajectories were reduced to iterative functions. This allowed probing systems' long-term properties without requiring algebraic solutions.

Through these mappings, Poincaré unveiled profound insights that remain fundamental today. He showed that fixed points, where iterations return to the same value, correspond to periodic motions in the original system. Poincaré also introduced pioneering concepts like limit cycles and novel stability classifications that characterized behavior through geometry rather than algebra.

By elucidating analogies between continuous and discrete representations through their qualitative properties over infinite time horizons, Poincaré established deep conceptual connections. While others viewed such systems as impossibly complex, he perceived an underlying geometric order comprehensible through analysis of mappings and geometric reasoning. By applying these methods to problems in celestial mechanics, Poincaré laid the philosophical and conceptual groundwork for qualitative analyses in nonlinear dynamics.

10.2.2 Formalizing Stability

Building on Poincaré's foundations, Alexandre Lyapunov developed a rigorous mathematical theory of stability for dynamical systems. Lyapunov's key insight was to quantitatively describe stability through characteristic exponents, which measure the rate of convergence or divergence between nearby trajectories over time. He showed that negative exponents ensure convergence, implying the system is stable against small perturbations, while positive exponents indicate divergence and instability.

Crucially, Lyapunov introduced concepts that classified stability on a global scale, rather than just locally near equilibrium points. In particular, his introduction of Lyapunov functions established a powerful theoretical framework allowing conclusions about stability to be drawn without requiring detailed solutions—an approach that heavily influenced later work in control engineering.

Through his rigorous mathematical innovations, Lyapunov elevated stability analysis from geometric intuition to a robust formal discipline. His techniques revealed how stability is intrinsic to a system's inherent geometry and dissipative properties. His theorems ensured stability analysis became a cornerstone of applied mathematics, with influence in fields including engineering and celestial mechanics.

10.2.3 Additional Pioneers

While Poincaré and Lyapunov established the theoretical foundations, other mathematicians made important contributions in the late 19th and early 20th centuries. Jules Hadamard studied non-smooth systems like billiards, proving that invariant curves could persist near non-differentiable points. Tullio Levi-Civita and Angelo Cigala focused on the stability of periodic orbits, developing tools beyond linearization to analyze problems involving planetary motion. Their techniques addressed perturbations' effects on repetitive orbital paths.

Across Europe, pioneers including Moïse Lattès, Gaston Julia, and Pierre Fatou conducted research exploring global properties of dynamical mappings and complex iterative functions. Their work helped define the self-similar structures called Julia sets that summarize long-term recursive behavior. Luitzen Brouwer's fixed point theorems related continuous transformations to topology and established existence principles for equilibrium states.

Together, these early contributors helped shift qualitative analysis from specific systems to more rigorous general frameworks.

10.3 Advancing the Foundations

10.3.1 Birkhoff's Contributions

The mathematician George Birkhoff built significantly on the foundations laid by Poincaré in the field of dynamics. By classifying maps of mechanical systems, Birkhoff proved concepts that revealed illuminating qualitative similarities across system trajectories. He introduced new coordinate systems that enabled geometric analysis of surfaces and volume-preserving transformations.

Birkhoff found analogs in maps to concepts like periodic orbits through iterative cycling. His work further uncovered invariant manifolds that separate different behavioral regimes. Studying “twist mappings” of oscillatory dynamics led to new stability insights dependent on oscillation amplitude.

Most profoundly, Birkhoff's phase space studies established the foundations of ergodic theory and geometric mechanics. While Poincaré intuitively linked continuous and discrete representations, Birkhoff formalized these relationships and established a framework that embraces both chaos and invariant ordered behavior.

Building rigorously on Poincaré's foundations through more geometric qualitative methods, Birkhoff advanced the field of dynamics by establishing an understanding of how order can arise within nature's complex dynamical behaviors. His work showed how classification of maps could reveal common qualitative features of trajectories and provide geometric insight into system properties like invariants and stability.

10.3.2 The Rise of Soviet Dynamical Thought

Two prominent centers of dynamical systems research emerged in the early 20th century Soviet Union, making profound contributions through contrasting yet complementary approaches.

In Moscow, Aleksandr Andronov's school pioneered the use of simplified “relay element” models to represent real oscillating systems in reduced conceptual form. By coarsely approximating complexity, these discrete representations provided mechanistic insights across diverse fields through intuitively accessible models.

Meanwhile in Kiev, the school of Nikolay Krylov and Nikolay Bogoliubov developed rigorous mathematical techniques informed by fluid stability problems. Their innovative “method of multiple scales” derived approximate analytic solutions near critical parameters using scaling arguments.

Asymptotic analyses from this method unveiled entirely new qualitative behaviors, such as bifurcations where smooth driving causes abrupt shifts in dynamics. This revelation inspired the modern theory classifying transitions between different equilibrium states.

While employing divergent methodologies, the Moscow and Kiev schools proved remarkably synergistic. Andronov's intuitive models motivated analytical tool development, while advances from the Kiev school continually strengthened connections between rigorous theory and its applications in mechanics, electronics, and more.

Under visionary leaders, these Soviet schools cultivated a research culture maintaining a dynamic interplay between practical and theoretical progress in nonlinear dynamics, significantly impacting the international field. Their complementary approaches drove new conceptual and methodological frontiers.

10.3.3 The emergence of Bifurcations

As the 20th century progressed, mathematicians continued refining analytical tools for studying nonlinear systems. One particularly influential development emerged from the pioneering work of the Krylov-Bogoliubov school in Kiev on fluid flows.

Employing asymptotic methods to analyze flows near stability thresholds, they discovered scenarios where smooth variations in a system parameter could abruptly alter its qualitative dynamics at critical values. Specifically, they found equilibrium states could suddenly transform or transition between alternative configurations in a discontinuous, non-smooth manner at these points.

They termed these ambiguous parameter values where behavior splits or branches “bifurcations,” drawing an analogy to biological branching. In doing so, they conceived the new field of bifurcation theory, providing a framework for classifying topological changes in attractor structures as system parameters evolve.

Concurrently, René Thom developed complementary topological techniques using singularity theory to geometrically represent dynamics occurring near bifurcations. His concept of “unfolding” a potential function in the vicinity of its singularities proved insightful for illuminating how small perturbations influence qualitative dynamics at the boundary between alternative dynamical regimes.

Generalized far beyond fluid systems, bifurcation theory demonstrated that nonlinear transformations exhibit intrinsic organizational transitions intimately tied to parameter values, contrary to expectations of uniform behavior. Its development revealed dynamics to be highly ordered, even at points evading explicit solutions.

10.4 The Emergence of Chaos and Beyond

10.4.1 The Discovery of Deterministic Chaos

By the 1970s, the field of nonlinear dynamics was poised for revolutionary changes in perspective. Controlled experiments on simplified electronic circuits and fluid

flow systems upended prevailing beliefs that seemingly random fluctuating behaviors necessarily implied underlying stochastic processes.

Through these benchtop systems governed by just a few mathematical equations, unambiguously unpredictable dynamics were observed that defied straightforward statistical characterization. Yet these phenomena were shown to arise from strict deterministic laws, not stochasticity as previously assumed.

Around this time, a serendipitous computer experiment by meteorologist Edward Lorenz would captivate the scientific world. Seeking to better understand atmospheric convection patterns through numerical modeling, Lorenz initialized a simplistic simulation with truncated initial conditions. However, the long-term evolution computed from even slightly different starting points diverged dramatically over time.

Intrigued, Lorenz plotted successive state values in phase space, discovering an unusual shape—resembling a butterfly—that served to encapsulate the attracting set summarizing the system’s overall long-run behavior. This “strange attractor” demonstrated how even deterministic dynamical systems could exhibit extreme sensitivity to initial conditions, manifesting as erratic yet unambiguously predictable fluctuations.

Lorenz’s startling discovery launched the foundational concept of “deterministic chaos,” showing how seemingly random phenomena observed in nature can in fact arise solely from strict, non-stochastic laws of dynamics. It provided evidence that irregular fluctuations did not necessarily imply an underlying stochastic essence.

His insights resonated broadly, spurring further experiments and modeling across scientific fields that revealed intricately structured yet unpredictable chaotic dynamics were in fact pervasive in both artificial and natural phenomena. The notion of deterministic unpredictability was born.

10.4.2 Illuminating Complexity Across Scales

By the late 20th century, the conceptual tools and theoretical perspectives developed over prior decades in nonlinear dynamics had coalesced into a robust mathematical framework for studying complexity in natural systems. Deep insights into phenomena like strange attractors, bifurcations, and chaos theory provided powerful explanations and predictions of behaviors observed across diverse realms, from fluid turbulence and mixing to cardiac rhythms and neuronal firing patterns.

Studies of phenomena like period-doubling cascades revealed the subtle step-by-step dynamical transformations that enable the emergence of qualitative unpredictability in seemingly deterministic systems. At the same time, interdisciplinary collaborations uncovered new dimensions of intricacy even within classically-understood systems, such as discoveries that chaotic states can coexist alongside regular laminar flows in fluid mechanics problems.

Advances in supporting fields also drove major advances. For example, breakthroughs in ergodic theory connected the microscopic world of chaos in ODE/PDE

systems to macroscopic phenomena like diffusion. Unification of geometric and measure-theoretic perspectives via areas like fractal geometry, topological conjugacy, and smooth ergodic theory synthesized mathematical views.

New conceptual lenses emerged from this activity as well, such as chaotic scattering and transition to turbulence, which provided profound insights across scientific domains. Powerful computational simulation finally made it possible to visualize strange dynamical objects that had scarcely been imaginable just a few years prior, such as solitons, defect-mediated chaos, and chimera states.

The synergistic combination of dynamical systems theory, computational modeling, and interdisciplinary collaboration had given rise to a powerful modern theoretical framework for illuminating the intricate ordered patterns that can emerge even within complexity—across microscopic to astrophysical scales. By century's end, nonlinear science was permeating all domains addressing temporal change and unpredictability.

10.5 Discussion

Over decades, tools from nonlinear dynamics like bifurcation theory, attractor analysis, and chaos theory coalesced into a robust mathematical framework. Insights into phenomena such as strange attractors, period-doubling routes, and self-organized criticality provided explanations for a diverse range of behaviors observed in fluids, cardiac systems, and beyond.

New conceptual lenses emerged as well, such as chaotic scattering and transitions to turbulence, providing insights across scientific disciplines. Powerful computational simulations made it possible for the first time to visualize objects like solitons, chimera states, and defect-mediated chaos.

By synthesizing dynamical systems theory, computation, and collaboration across spatial and temporal scales, the field established a powerful mathematical framework for elucidating order within nature's complexity, from the microscopic to the astrophysical. By century's end, nonlinear science had permeated research on problems involving temporal change, unpredictability, and emergent phenomena across diverse domains.

Chapter 11

Local Stability Analysis in 2D Systems

Abstract This chapter develops the technique of local stability analysis for two-dimensional nonlinear dynamical systems modeled by sets of coupled ordinary differential equations. Steady states, or fixed points, where both equations are simultaneously satisfied, are classified into nodes, saddles, and spirals by analyzing the eigenvalue structure of the 2×2 Jacobian matrix computed from the system's partial derivatives near each fixed point. Analytical criteria are derived requiring both eigenvalues to have negative real parts for stability, reducing determination to the Jacobian's trace and determinant. Qualitative analysis of eigenvalue configurations provides insight into global trajectory behavior near different steady state types, equipping nonlinear dynamical modeling with a rigorous yet accessible mathematical approach for stability-based analysis. The methodology introduced generalizes directly to higher dimensions and serves as a foundation for stability-based modeling across sciences involving ordinary differential equations.

11.1 Introduction

In Chapter 6, we developed the method of local stability analysis to characterize the behavior of steady states in one-dimensional nonlinear dynamical systems. This approach reduces the stability criterion to checking the sign of the slope of the governing function at the steady state. However, many natural and engineered systems are described by models with two or more dimensions that cannot be intuitively visualized or analyzed using one-dimensional techniques. It is therefore necessary to generalize the technique of local stability analysis to higher-dimensional systems described by sets of coupled ordinary differential equations.

In this chapter, we extend the methodology of local stability analysis to two-dimensional nonlinear dynamical systems represented by a pair of coupled ordinary

differential equations. While graphical analysis is no longer suitable, the algebraic framework of linearization remains valid. We will see that steady states are now defined as simultaneous solutions to two equations. Linearizing the system dynamics locally yields a 2×2 Jacobian matrix governing small perturbations near the steady state. The matrix's eigenstructure determines stability and allows a qualitative classification.

By deriving analytical stability criteria from the Jacobian eigenvalues, this approach provides insights into even relatively simple 2D models that are inaccessible through low-dimensional intuition alone. The methodology generalizes directly to higher dimensions through matrix analysis. Local stability analysis thus equips the study of multidimensional dynamical models with a systematic and mathematically rigorous technique.

11.2 Steady States in 2D Systems

We begin by considering a general two-dimensional dynamical system governed by a pair of first-order ordinary differential equations:

$$\frac{dx}{dt} = f(x, y), \quad (11.1)$$

$$\frac{dy}{dt} = g(x, y), \quad (11.2)$$

where $f(x, y)$ and $g(x, y)$ are smooth functions determining the rate of change of x and y with respect to time t .

In the one-dimensional case studied previously, a steady state or fixed point was defined as a location x^* where the system's behavior does not change over time. To generalize this concept to two dimensions, we require the system to be stationary at a particular point (x^*, y^*) in the x - y plane. Mathematically, a fixed point (x^*, y^*) satisfies:

$$\left. \frac{dx}{dt} \right|_{(x^*, y^*)} = 0, \quad \left. \frac{dy}{dt} \right|_{(x^*, y^*)} = 0.$$

Substituting the definitions of dx/dt and dy/dt yields:

$$f(x^*, y^*) = 0, \quad g(x^*, y^*) = 0.$$

Therefore, steady states or fixed points in two-dimensional systems are points (x^*, y^*) that are simultaneous solutions to the equations $f(x, y) = 0$ and $g(x, y) = 0$.

11.3 Local Linearization and Stability Analysis

To analyze the stability of a fixed point (x^*, y^*) , we study how small perturbations from this point evolve over time. Let $\delta x = x - x^*$ and $\delta y = y - y^*$ represent deviations of an arbitrary trajectory from the fixed point coordinates. By definition, these perturbations satisfy:

$$\frac{d\delta x}{dt} = \frac{dx}{dt}, \quad \frac{d\delta y}{dt} = \frac{dy}{dt}.$$

Substituting the ODE definitions yields:

$$\begin{aligned} \frac{d\delta x}{dt} &= f(x^* + \delta x, y^* + \delta y), \\ \frac{d\delta y}{dt} &= g(x^* + \delta x, y^* + \delta y). \end{aligned}$$

Performing a Taylor series approximation truncated to the linear term renders:

$$\begin{aligned} \frac{d\delta x}{dt} &= f_x \delta x + f_y \delta y, \\ \frac{d\delta y}{dt} &= g_x \delta x + g_y \delta y \end{aligned}$$

where the partial derivatives are evaluated at the fixed point:

$$f_x = \left. \frac{\partial f}{\partial x} \right|_{(x^*, y^*)}, \quad f_y = \left. \frac{\partial f}{\partial y} \right|_{(x^*, y^*)}, \quad g_x = \left. \frac{\partial g}{\partial x} \right|_{(x^*, y^*)}, \quad g_y = \left. \frac{\partial g}{\partial y} \right|_{(x^*, y^*)}.$$

These linearized equations can be written compactly in matrix form as:

$$\frac{d\delta \mathbf{r}}{dt} = \mathbf{J} \delta \mathbf{r}, \quad (11.3)$$

in which the Jacobian matrix \mathbf{J} contains the partial derivatives, and $\delta \mathbf{r}$ is the perturbation vector.

$$\mathbf{J} = \begin{bmatrix} f_x & f_y \\ g_x & g_y \end{bmatrix}, \quad \delta \mathbf{r} = \begin{bmatrix} \delta x \\ \delta y \end{bmatrix}.$$

Based on the one-dimensional analysis, we expect perturbations to evolve exponentially near the fixed point. Specifically, we make an ansatz that the solution takes the form:

$$\delta \mathbf{r} = \mathbf{v} e^{\lambda t}, \quad (11.4)$$

where vector \mathbf{v} and the scalar parameter λ remain to be determined.

Substitution of Eq. (11.4) into Eq. (11.3) yields

$$\lambda \mathbf{v} = \mathbf{J} \mathbf{v}. \quad (11.5)$$

This reveals that for the ansatz to be a valid solution, the parameters λ and \mathbf{v} must satisfy the eigenstructure of the Jacobian matrix \mathbf{J} . Specifically, λ must be an eigenvalue of \mathbf{J} and \mathbf{v} the corresponding eigenvector.

Since a 2x2 matrix like the Jacobian will generally have two eigenpairs, the complete solution is a superposition of the exponential modes:

$$\delta \mathbf{r} = C_1 \mathbf{v}_1 e^{\lambda_{t_1}} + C_2 \mathbf{v}_2 e^{\lambda_{t_2}}, \quad (11.6)$$

with $(\lambda_1, \mathbf{v}_1)$ and $(\lambda_2, \mathbf{v}_2)$ the eigenpairs of \mathbf{J} , while constants C_1 and C_2 are determined by the initial conditions. We can deduce the asymptotic behavior from Eq. (11.6): $\delta \mathbf{r}$ decays to zero as $t \rightarrow \infty$ if both eigenvalues have negative real parts. In this case, the fixed point is declared locally stable.

11.4 Steady-State Classification

The eigenstructure relation in Eq. (11.5) can be expressed as:

$$(\mathbf{J} - \lambda \mathbf{I}) \mathbf{v} = 0,$$

where \mathbf{I} is the 2D identity matrix. This represents a system of two homogeneous linear equations with the components of \mathbf{v} as unknowns. Generally, the only solution to such a system is the trivial solution $\mathbf{v} = \mathbf{0}$. However, this trivial solution implies $\delta \mathbf{r}(t) = \mathbf{0}$, meaning that the considered solution is already at the fixed point. This prevents analysis of the stability. A non-trivial solution exists only when the determinant of the coefficient matrix vanishes, i.e. when:

$$\det(\mathbf{J} - \lambda \mathbf{I}) = 0.$$

Expanding this determinant condition gives:

$$(f_x - \lambda)(g_y - \lambda) - f_y g_x = 0,$$

Which can be written compactly in terms of the trace $\tau = f_x + g_y$ and determinant $\Delta = f_x g_y - f_y g_x$ of the Jacobian matrix \mathbf{J} as:

$$\lambda^2 - \tau \lambda + \Delta = 0. \quad (11.7)$$

Eq. (11.7) takes the form of a characteristic quadratic polynomial, whose roots correspond to the eigenvalues of the Jacobian matrix \mathbf{J} . The eigenvalues, $\lambda_{1,2}$, can be explicitly computed by solving the characteristic polynomial:

$$\lambda_{1,2} = \frac{\tau \pm \sqrt{\tau^2 - 4\Delta}}{2}.$$

An analysis of this equation reveals key properties of the eigenvalues based on the values of the trace and determinant. Specifically:

- If the determinant $\Delta < 0$ (region I in Fig. 11.1), then one eigenvalue will be positive while the other is negative, regardless of the sign of the trace τ .
- If $\Delta > 0$ and the discriminant $\tau^2 > 4\Delta$ (regions II and V in Fig. 11.1), then both eigenvalues will be real and have the same sign as the trace τ .
- If $\Delta > 0$ but the discriminant $\tau^2 < 4\Delta$, then the eigenvalues form a complex conjugate pair in which τ is the real part (regions III and IV in Fig. 11.1). Notably, when the trace $\tau = 0$, the solutions eigenvalues are purely imaginary numbers.

The above analysis has delineated how the values of coefficients Δ and τ determine the possible configurations of the eigenvalues. We now aim to connect these eigenvalue configurations to criteria for classifying the stability of the fixed point.

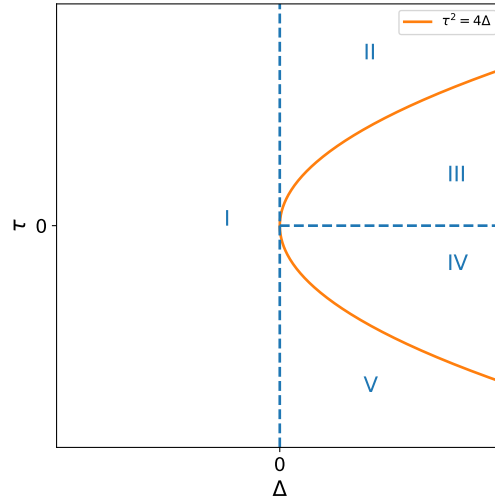


Fig. 11.1 Regions in the trace-determinant plane delineating qualitative configurations of the Jacobian matrix eigenvalues. The trace τ and determinant Δ values determine whether the eigenvalues are real or complex and their relative signs. Region I corresponds to eigenvalues of opposite sign, yielding a saddle node. Regions II and V exhibit real eigenvalues of the same sign, giving rise to unstable and stable nodes, respectively. Regions III and IV contain a complex conjugate eigenvalue pair, resulting in spiral node behavior characterized by rotational motion around the fixed point with exponential decay or growth modulated by the real part of the eigenvalues.

Recall that the general solution of the linearized system is given by Eq. (11.6). When the eigenvectors \mathbf{v}_1 and \mathbf{v}_2 are unitary and linearly independent, they form a basis of the δx - δy space, and the terms $C_1 e^{\lambda_1 t}$ and $C_2 e^{\lambda_2 t}$ can be interpreted as the coordinates of the perturbation $\delta \mathbf{r}(t)$ at time t in this eigenbasis.

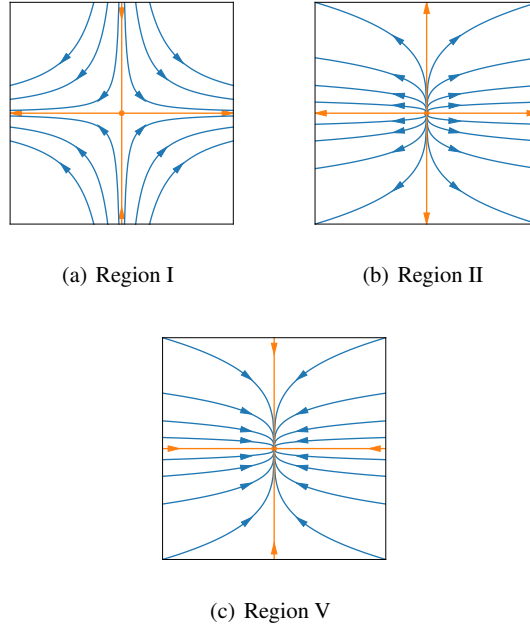


Fig. 11.2 Illustration of phase portraits for different eigenvalue configurations near a fixed point. (a) Region I of Fig. 11.1 exhibits saddle node behavior, with trajectories flowing away along one direction and toward the fixed point along the orthogonal direction. (b) Region II displays an unstable node, where all trajectories exponentially diverge from the fixed point. (c) Region V corresponds to a stable node, with converging trajectories.

Considering the full solution as $\mathbf{r}(t) = \mathbf{r}^* + \delta\mathbf{r}(t)$, we see that $C_1 e^{\lambda_1 t}$ and $C_2 e^{\lambda_2 t}$ determine how the linearized solution $\mathbf{r}(t)$ evolves in a reference frame defined by the Jacobian eigenvectors and anchored at the fixed point \mathbf{r}^* .

When the eigenvalues are real, the eigenbasis coordinates $C_1 e^{\lambda_1 t}$ and $C_2 e^{\lambda_2 t}$ will exponentially decay or grow over time depending on the sign of the respective eigenvalues. A positive eigenvalue leads to exponential growth of the corresponding coordinate, while a negative eigenvalue implies exponential decay. This characterization of the perturbation growth informs the trajectory sketches shown in Fig. 11.2 for regions I, II and V of Fig. 11.1.

The steady state in region I, where one eigenvalue is positive and one is negative, corresponds to a saddle node. Near a saddle node, trajectories will flow away in one eigen-direction and towards the fixed point in the other direction, as illustrated in 11.2a. A steady state in region II, where both eigenvalues are positive, is referred to as an unstable node. In this case, small perturbations will always grow exponentially, leading trajectories to flow outward from the fixed point in all directions, as shown in Fig. 11.2b. In region V, where both eigenvalues are negative, the steady state is said to be a stable node. Here, perturbations decay exponentially fast, causing

trajectories to converge onto the fixed point from all surrounding points in phase space, as depicted in Fig. 11.2c.

When the eigenvalues are complex, the linearized system possesses oscillatory behavior near the fixed point. For regions III and IV in Fig. 11.1, where the trace τ and determinant Δ satisfy $\tau^2 < 4\Delta$, the eigenvalues form a complex conjugate pair $\lambda_{1,2} = \alpha \pm i\beta$. Substituting this into the general solution of the linearized system in Eq. (11.6) yields:

$$\delta \mathbf{r}(t) = C_1 \mathbf{v}_1 e^{\alpha t} \cos(\beta t) + C_2 \mathbf{v}_2 e^{\alpha t} \sin(\beta t)$$

Observe that the perturbation undergoes rotational motion, with an exponential decay or growth modulated by the real part α of the complex eigenvalues. Since $\alpha = \tau/2$, where τ is the trace of the Jacobian matrix, the sign of τ dictates whether the oscillations decay or grow exponentially over time. Specifically, when $\tau > 0$ the real part is positive ($\alpha > 0$), corresponding to region III of Fig. 11.1 where perturbations spiral outward from the fixed point with exponential growth. Conversely, for $\tau < 0$ the real part is negative ($\alpha < 0$), describing region IV where oscillations spiral inward to the fixed point in a decaying manner. These behaviors are illustrated in Fig. 11.3.

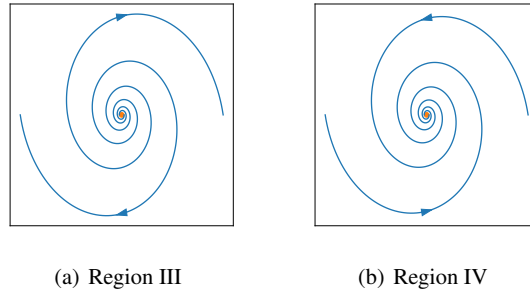


Fig. 11.3 Phase portraits for regions III and IV displaying spiral node behavior near the fixed point. (a) In region III of Fig. 11.1, where the trace $\tau < 0$, perturbations decay along a clockwise spiral trajectory towards the fixed point. (b) For region IV with $\tau > 0$, perturbations grow along a counterclockwise spiral, diverging from the fixed point. The real and imaginary parts of the complex eigenvalues determine the exponential decay/growth and rotational motion of perturbations in these cases.

11.5 Discussion

In this chapter, we have presented a framework for classifying the behavior near steady state solutions of 2D dynamical systems using linear stability analysis. By

analyzing the eigenvalues of the Jacobian matrix (\mathbf{J}) evaluated at a fixed point (\mathbf{r}^*), we can gain qualitative insight into how perturbations will evolve in the local vicinity of that steady state.

There are three main categories of steady state behavior that emerge based on the signs and types of eigenvalues:

1. Node: All real eigenvalues lead to exponential decay or growth along principal directions, yielding stable or unstable equilibria.
2. Saddle: Mixed stability with one growing and one decaying eigenvalue mode. Trajectories flow away along one direction and towards the fixed point along the other.
3. Spiral: A complex conjugate eigenvalue pair yields stable or unstable rotational motion around the fixed point, with exponential modulation by the real part of the pair.

The stability of nodes and spirals is determined by the sign of the real part of the eigenvalues.

The classifications provided by this local linear stability analysis framework offer powerful insights into the full nonlinear dynamics of the system. Specifically, the local dynamic behavior near steady states allows for a qualitative description of the global behavior of trajectories throughout the phase space. When combined with numerical techniques, this framework enables comprehensive characterization of system dynamics. In the following chapters, we will explore detailed examples that demonstrate these concepts.

Chapter 12

Historical Origin of Population Ecology

Abstract This chapter traces the historical development of population ecology from its conceptual foundations in the mid-19th century through the emergence of quantitative modeling approaches in the early 20th century that established it as the discipline of population ecology. It examines the influential ideas of early thinkers like Darwin, Spencer and Forbes and how the works of Clements, Adams, Lotka, and Volterra formalized theoretical understandings into foundational mathematical expressions of population growth, competition, and predator-prey relations. By outlining the progression and integration of ideas between these pioneering scientists across disciplines, the chapter delineates how population ecology emerged as a rigorous field centered on predictive modeling of demographic processes and the biotic and abiotic factors that influence population change over successive generations.

12.1 Introduction

The discipline known today as mathematical biology is the confluence on many traditions and research fields. One of them is population ecology, which aims to understand the dynamics of biological populations and the factors that cause fluctuations in population size over time. This includes seeking to explain how intrinsic growth rates interact with environmental constraints like resource availability, competition, and predation. While these questions have intrigued biologists and natural philosophers for centuries, it was not until the late 19th century that population ecology truly emerged as a distinct discipline within ecology.

This chapter traces the historical origin and development of population ecology as a quantitative, mathematical field of study. It explores the influential early thinkers who established the conceptual foundations, from Darwin and Spencer's formative works on competition and population regulation, to Forbes pioneering

quantitative field studies. The chapter then focuses on the key figures around the early 20th century who significantly advanced population ecology through new theoretical and modeling approaches—Clements, Adams, Lotka, and Volterra. Their innovative works helped define population ecology not just as a field of qualitative explanations, but as a discipline incorporating quantitative modeling of factors driving demographic change in populations.

By examining these pioneering scientists and how their ideas intertwined and built upon one another, this chapter aims to outline the lineage of thought that ultimately established population ecology as a the investigative framework still used today. The objective is to recognize population ecology's intellectual roots and appreciate how incremental progress occurs in science through the efforts of diverse thinkers synthesizing different perspectives over generations. In crafting this overview of key topics and milestones, the chapter drew upon insights from the publication by Mira (1997). For readers seeking deeper exploration of population conceptual underpinnings and progressive development, the referenced work offers more encompassing examination of these subjects.

12.2 Early Foundations of Population Ecology

The foundations of population ecology emerged in the mid-19th century, paralleling the rise of ecology more broadly. Charles Darwin and Alfred Russel Wallace made enormous contributions through their formulation of the theory of evolution by natural selection. In *On the Origin of Species* (1859), Darwin established competition between individuals for limited resources as a key mechanism driving evolutionary change. He recognized populations as growing exponentially until constrained by environmental carrying capacities.

Herbert Spencer built on these ideas in *Principles of Biology* (1864) with one of the first conceptual frameworks of population regulation. He theorized that populations achieve stable size through a balance of “nurturant” forces like reproduction and “accidental” forces like mortality. This introduced the principles of opposing demographic factors achieving dynamic equilibrium. Spencer envisioned ecology as encompassing networks of interdependencies rather than just adaptation.

Around the same time, the German biologist Ernst Haeckel coined the term “ecology” and defined it as the study of organism-environment interactions. He highlighted interdependence between organisms and their environments, foreshadowing systems-thinking in ecology. Haeckel developed one of the first energy flow frameworks, seeing communities as integrated systems maintained through negative feedback loops.

Stephen Alfred Forbes conducted extensive field work on Illinois lakes in the late 1800s. His meticulous surveys provided empirical evidence supporting early theories, demonstrating density fluctuations between predator and prey populations over time. Forbes was also the first to propose that populations self-regulate through

birth and death responses to environmental variables like resource availability. His work helped establish population ecology as an empirical, quantitative science.

12.3 Formative Years of the Discipline

Frederic Clements, a botanist, studied plant succession and published an influential book called *Plant Succession* in 1916. He developed the analogy that plant communities mature through predictable stages of development akin to an organism. Clements stressed the community as a holistic superorganism shaped over time by interspecific cooperation as well as competition for resources.

While criticized for underestimating stochastic events, Clements' organismic perspective shaped early theoretical ecology. He recognized that populations do not fluctuate independently but are interconnected, with species influencing community trajectories through direct and indirect effects on one another. Clements also highlighted the importance of long-term ecological processes like facilitation and inhibition in driving dynamic changes to communities.

Joseph Adams' background in physical chemistry strongly influenced his development of quantitative population models. Concepts from statistical mechanics and chemical kinetics inspired Adams to mathematically relate observed macro-level population patterns to underlying micro-level reproductive and mortality processes.

Models from physical chemistry describing how reaction rates change over time also motivated Adams to capture variation in demographic rates based on density dependence and environmental conditions. Additionally, viewing chemical systems as dynamic and open, rather than closed and static, aligned with Adams' thinking of populations as regulated through inputs and outputs over generations.

Adams was also influenced by emerging ideas in the field of geology during his career. Geologists were developing theories of dynamic equilibrium in integrated Earth systems achieved through compensatory positive and negative feedbacks acting over long timescales. These likely informed Adams' consideration of population regulation around equilibrium levels.

Through such interdisciplinary lenses, Adams published highly influential works in the 1920s and 30s that established conceptual and methodological foundations for modern demographic analyses. His formulation of exponential and logistic population growth models represented pioneering efforts to quantitatively model intra-specific regulating factors theoretically posited by past scholars.

Adams' approach helped shift population ecology towards a more predictive science based on mathematical descriptions of population behavior over time. His integration of both empirical field data and theoretical modeling lenses established population ecology as a distinct quantitative discipline within ecology.

12.4 Lotka's Interdisciplinary Approach and Influence from Adams

Like Adams, Alfred Lotka's diverse educational and professional background proved formative for his groundbreaking theoretical population ecology work. Lotka studied chemistry and worked as both a chemist and actuary, applying mathematical techniques to insurance calculations.

This quantitative training was evident in Lotka's 1925 paper, where he published differential equations modeling predator-prey populations over time. Lotka was directly influenced by Adams' prior logistic modeling concept, which he built upon by including additional interspecific interactions such as predation. Lotka's 1925 work demonstrated how physical chemistry principles could be applied to biological systems. Inspired by concepts of energy flows and dissipation from his chemistry background, Lotka framed evolution as optimizing energy pathways through ecological networks.

This interdisciplinary energy perspective proved highly influential and represents an early application of systems thinking to theoretical ecology. By synthesizing demographic and interspecific modelling approaches, Lotka established theoretical population ecology's focus on quantifying factors driving changes in population size and composition over generations.

12.5 Lotka-Volterra Equations

Lotka's 1925 differential equation model of predator-prey population change became highly influential and established the foundation for modern population ecology. However, Lotka was not the only pioneering thinker formulating such models at this time.

The Italian mathematician Vito Volterra independently developed near-identical nonlinear equations describing oscillating predator and prey densities in 1926. Published in Italian, Volterra's work went initially unnoticed by the international science community.

However, subsequent discussions between Lotka and Volterra revealed their remarkable convergence in conceiving mathematical population models. Their collaborative connection helped define what are now universally known as the Lotka-Volterra equations.

Volterra brought his advanced mathematical expertise, allowing for the first rigorous analysis of conditions defining stable limit cycles predicted by the prey-predator framework. His contributions helped establish theoretical population ecology on a firm theoretical footing through analytical validation of early modeling approaches.

Their seminal collaboration highlights how great scientific progress emerges through the intersecting ideas of diverse thinkers globally exploring challenges through their own insightful lenses.

12.6 Discussion

This chapter has outlined the major developments that established population ecology as a theoretical, quantitative field of study. It traced ideas from early conceptual works of Darwin, Spencer and Forbes through to modelers like Adams, Lotka and Volterra who incorporated mathematics.

Their contributions defined population ecology not just as natural history observation, but as a predictive discipline seeking to understand population behaviors and interdependencies through quantitative models of birth, death and interaction over successive generations.

While individual pioneers built upon each other, their synergistic efforts collectively transformed population ecology into a rigorous mathematical science. Concepts like intra-specific constraints, inter-trophic level connections, and achieving dynamic equilibrium through opposing factors endure as foundational principles.

Later 20th century population modelers drew upon this lineage, extending formulations to incorporate more complex influences like age structure, nonlinear feedbacks and stochasticity. Their works have found diverse interdisciplinary applications from economics to epidemiology.

The intellectual lineage outlined highlights both incremental progress through extended works, as well as how convergence of independent yet complementary views can drive paradigm shifts. It recognizes population ecology's multifaceted roots and distributed nature of scientific thinking that together establish robust new fields.

Chapter 13

Competitive Lotka-Volterra Model

Abstract This chapter presents and analyzes the Lotka-Volterra competitive modeling framework, which describes the population dynamics of two competing species. The framework uses coupled logistic growth differential equations to represent the per capita growth rates of each species, with these rates being reduced by interspecific competition. The chapter examines the equilibrium states of the system and performs phase plane analysis to determine the long-term trajectories defined by different competition coefficient regimes. It also analyzes the stability of the equilibria, relating the competitive hierarchies to the resulting community outcomes. Despite the simplifying assumptions inherent in the model, it provides valuable explanatory insights into patterns that conform to Gause's competitive exclusion principle. By conceptually formulating the interspecific interactions through basic growth and competition functions, the Lotka-Volterra framework demonstrates how even simple conceptual theory can generate ecological understanding of community assembly, focusing on elucidating the underlying mechanisms rather than pursuing precise prediction.

13.1 Introduction

Intraspecific competition describes interactions between individuals of the same species competing for limited resources. In contrast, interspecific competition characterizes interactions between distinct but ecologically similar species that utilize overlapping resource pools. Past chapters have addressed intraspecific competition mathematically through the logistic model of population growth regulation.

This chapter focuses on interspecific competition, which occurs when multiple species utilize the same limited resources in a single area. As populations of coexisting species continuously interact through competition for necessities like food and

shelter, their relative abundances shift in complex ways over time. Describing these population dynamics mathematically provides insights into how competition shapes community structure and long-term species coexistence.

We explore the competitive Lotka-Volterra model, one of the earliest and most influential models developed to study interspecific competition. First introduced independently by Lotka in 1925 and Volterra in 1926, this seminal model formulated competition between species using coupled logistic growth functions. Over a century later, the Lotka-Volterra model remains fundamental to understanding phenomena like competitive exclusion and the conditions permitting diverse communities to coexist simultaneously.

13.2 The Competitive Lotka-Volterra Model

Lotka and Volterra developed one of the first mathematical formulations of interspecific competition by extending the logistic growth model to multiple interacting species. Their competitive Lotka-Volterra model describes the population dynamics of two species, which we will refer to as species 1 and 2, competing for a shared limiting resource.

The model assumptions are:

- Each species exhibits logistic population growth in the absence of the other.
- Competition arises through each species reducing the per capita growth rate of the other.

Based on these, the governing equations are:

$$\frac{dN_1}{dt} = r_1 N_1 \left(1 - \frac{N_1}{K_1} - a_{12} \frac{N_2}{K_2} \right), \quad (13.1)$$

$$\frac{dN_2}{dt} = r_2 N_2 \left(1 - \frac{N_2}{K_2} - a_{21} \frac{N_1}{K_1} \right), \quad (13.2)$$

where:

- N_1 and N_2 are the population sizes of species 1 and 2.
- r_1 and r_2 are the intrinsic growth rates.
- K_1 and K_2 are the carrying capacities.
- a_{12} and a_{21} are the interspecific competition coefficients.

This pair of coupled nonlinear ordinary differential equations represent the simplest mathematical model capturing the dynamics of competing populations based on limiting resources. We will analyze its properties and implications in subsequent sections.

It is convenient to non-dimensionalize the model by introducing the following scaling:

$$\begin{aligned}
n_1 &= N_1/K_1, \\
n_2 &= N_2/K_2, \\
\tau &= r_1 t.
\end{aligned}$$

This scales population sizes relative to the corresponding carrying capacities and time relative to the intrinsic growth rate of species 1. Substituting these into the original model equations gives:

$$\frac{dn_1}{d\tau} = n_1(1 - n_1 - a_{12}n_2), \quad (13.3)$$

$$\frac{dn_2}{d\tau} = \rho n_2(1 - n_2 - a_{21}n_1), \quad (13.4)$$

with $\rho = r_2/r_1$.

13.3 Analysis of the Non-Dimensional Model

We now analyze the dynamics and behavior of the non-dimensional competitive Lotka-Volterra model derived in the previous section. We first examine the equilibrium points of the system, found by setting (13.1) and (13.2) equal to zero and solving the resulting system of algebraic equations. This gives four possible equilibrium points:

$$\begin{aligned}
E_1 &= (0, 0), & E_2 &= (1, 0), \\
E_3 &= (0, 1), & E_4 &= \left(\frac{1-a_{12}}{1-a_{12}a_{21}}, \frac{1-a_{21}}{1+a_{12}a_{21}} \right)
\end{aligned}$$

The equilibrium points E_1 , E_2 , and E_3 correspond to boundary equilibria representing the extinction of one or both species. Specifically, E_1 is the point of double extinction, E_2 is the extinction of species 2, and E_3 is the extinction of species 1.

The point E_4 is an interior equilibrium where both species can potentially coexist. Notably, E_4 exists in the positive quadrant where population sizes are greater than zero only when the interspecific competition coefficients satisfy either $a_{12}, a_{21} < 1$ or $a_{12}, a_{21} > 1$.

To analyze the stability of the equilibrium points, we compute the Jacobian matrix of the system defined by Eqs. (13.3)-(13.4). Taking the partial derivatives, the Jacobian is:

$$J = \begin{bmatrix} 1 - 2n_1 - a_{12}n_2 & -a_{12}n_1 \\ -\rho a_{21}n_2 & \rho(1 - 2n_2 - a_{21}n_1) \end{bmatrix}. \quad (13.5)$$

Evaluated at each equilibrium point E_i , the Jacobian matrix $J(E_i)$ characterizes the linearized behavior near that point. The stability type is determined by the eigenvalues of each $J(E_i)$ matrix.

Evaluating the Jacobian at the equilibrium point $E_1 = (0, 0)$ gives:

$$J(E_1) = \begin{bmatrix} 1 & 0 \\ 0 & \rho \end{bmatrix}.$$

As this is a diagonal matrix, its eigenvectors are aligned with the n_1 and n_2 axes. The corresponding eigenvalues are 1 and ρ . Since both eigenvalues are positive, the Jacobian evaluation indicates that E_1 is an unstable node, where small perturbations will drive the populations away from the double extinction equilibrium.

The Jacobian evaluated at E_2 gives

$$J(E_2) = \begin{bmatrix} -1 & -a_{12} \\ 0 & \rho(1 - a_{21}) \end{bmatrix}.$$

One of its eigenvectors is aligned with the n_1 axis and its corresponding eigenvalue is -1. The other eigenvector is

$$\left(\frac{a_{12}}{\rho(a_{21} - 1) - 1}, 1 \right),$$

while its associated eigenvalue is $\rho(1 - a_{21})$. Therefore, when $a_{21} > 1$ the eigenvalue is negative and the fixed point is a stable node. Contrarily, when $a_{21} < 1$ the eigenvalue is positive and the fixed point is a stable node. Notably, the stability of the fixed point where species n_1 is the sole survivor is determined by its aggressiveness.

The Jacobian evaluated at E_2 gives

$$J(E_2) = \begin{bmatrix} -1 & -a_{12} \\ 0 & \rho(1 - a_{21}) \end{bmatrix}.$$

One of its eigenvectors is aligned with the n_1 axis and its corresponding eigenvalue is -1. The other eigenvector is

$$\left(\frac{a_{12}}{\rho(a_{21} - 1) - 1}, 1 \right),$$

while its associated eigenvalue is $\rho(1 - a_{21})$. Therefore, when $a_{21} > 1$, this eigenvalue is negative and the fixed point E_2 is a stable node, representing the stable extinction of species 2. Contrarily, when $a_{21} < 1$ the eigenvalue is positive and E_2 is an unstable node, meaning small perturbations will drive the system away from the extinction of species 2. In summary, the stability of the fixed point where only species 1 survives depends on the competitiveness of species 2, represented by the parameter a_{21} .

The Jacobian evaluated at E_3 is:

$$J(E_3) = \begin{bmatrix} \rho(1 - a_{12}) & 0 \\ -a_{21} & -1 \end{bmatrix}.$$

The eigenvector aligned with the n_2 axis has an eigenvalue of -1. The other eigenvector is

$$\left(1, \frac{a_{21}}{\rho(a_{12}-1)-1}\right)$$

with associated eigenvalue $\rho(1-a_{12})$. Therefore, when $a_{12} > 1$ this eigenvalue is negative and E_3 is a stable node, representing the stable extinction of species 1. However, when $a_{12} < 1$ the eigenvalue is positive and E_3 is an unstable node, meaning small perturbations will drive the system away from the extinction of species 1. Analogous to E_2 , the stability of the fixed point where only species 2 survives depends on the competitiveness of species 1, given by the parameter a_{12} .

The Jacobian at the interior coexistence equilibrium E_4 is:

$$J(E_4) = \frac{1}{1-a_{12}a_{21}} \begin{bmatrix} a_{12}-1 & a_{12}(a_{12}-1) & \rho a_{21}(a_{21}-1) & \rho(a_{21}-1) \end{bmatrix}$$

The stability of E_4 depends on the eigenvalues of $J(E_4)$, which are given by:

$$\lambda_{1,2} = \frac{\tau \pm \sqrt{\tau^2 - 4\Delta}}{2},$$

where the trace τ and determinant Δ are:

$$\tau = \frac{(a_{12}-1) + \rho(a_{21}-1)}{1-a_{12}a_{21}}, \quad \Delta = \frac{\rho(a_{12}-1)(a_{21}-1)}{1-a_{12}a_{21}}$$

It can be shown that:

$$\tau^2 - 4\Delta = \frac{[(a_{12}-1) + \rho(a_{21}-1)]^2 + 4\rho a_{12}a_{21}(a_{12}-1)(a_{21}-1)}{(1-a_{12}a_{21})^2}$$

Since E_4 only exists in the positive quadrant when $a_{12}, a_{21} < 1$ or $a_{12}, a_{21} > 1$, this further implies that the eigenvalues are real. If $\Delta > 0$, the eigenvalues have the same sign as τ , while one is positive and one negative otherwise. Finally, E_4 is a saddle when $a_{12}, a_{21} > 1$ because $\Delta < 1$, but a stable node when $a_{12}, a_{21} < 1$ since $\Delta > 0$ and $\tau < 0$.

The previous analysis reveals four possible long-term scenarios based on the competition coefficients a_{12} and a_{21} , as illustrated in Fig. 13.3:

1. When $a_{12} > 1$ and $a_{21} < 1$, the extinction equilibrium E_2 is the sole steady state. In this case, species 1 dominates competition and excludes species 2 in the long run for nearly all starting population levels.
2. Conversely, when $a_{12} < 1$ and $a_{21} > 1$, E_3 is the only equilibrium. Now species 2 is competitively superior and drives species 1 extinct in the long run.
3. When a_{12} and a_{21} are both less than 1, E_4 represents the sole steady state. Here, interspecific competition is weak enough to allow the long-term coexistence of both species for most initial conditions.
4. Finally, if a_{12} and a_{21} both exceed 1, the extinction equilibria E_2 and E_3 become stable, creating a bistable system. In this case, the phase plane separates into two basins of attraction defined by a separatrix running through E_1 and E_4 .

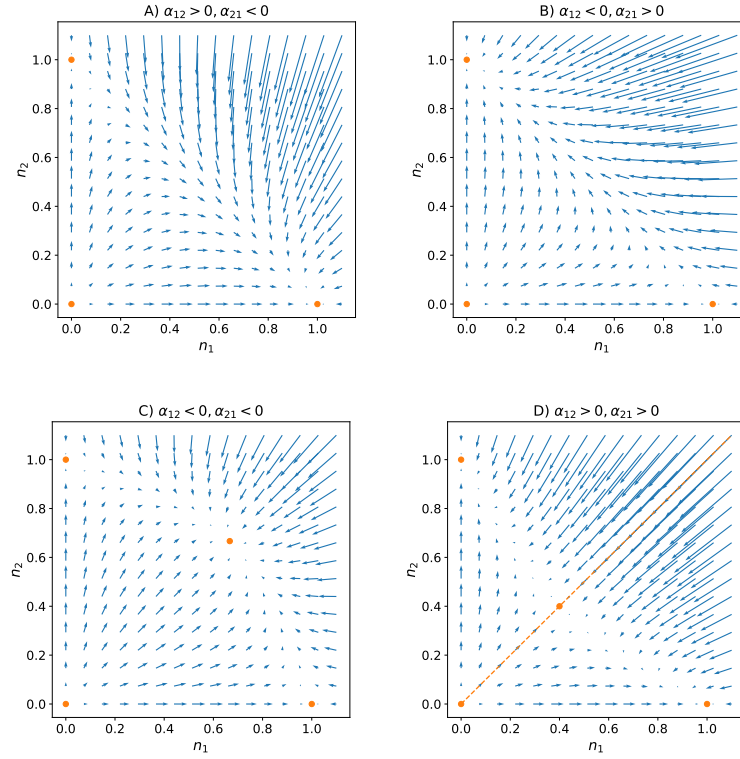


Fig. 13.1 Qualitative behavior of the competitive Lotka-Volterra model in the four regimes defined by the competition coefficients a_{12} and a_{21} . Arrows indicate the direction of flow and stable steady states are shown as filled circles. (A) When $a_{12} > 1$ and $a_{21} < 1$, species 1 competitively excludes species 2 and the system flows to the E_2 equilibrium. (B) For $a_{12} < 1$ and $a_{21} > 1$, species 2 outcompetes species 1 and the long-term outcome is the E_3 equilibrium. (C) When mutualism or weak competition occurs ($a_{12}, a_{21} < 1$), both populations can stably coexist at E_4 . (D) Under strong reciprocal competition ($a_{12}, a_{21} > 1$), the system exhibits bistability between the exclusion of species 1 or 2, separated by a separatrix that passes through E_1 and E_4 .

Populations beginning in either basin asymptotically approach either the E_2 or E_3 equilibrium exclusively.

The results of this model analysis have important implications for understanding competitive interactions and community assembly in ecological systems. When interspecific competition is strong, meaning one species is highly dominant over the other, the model predicts that stable coexistence is not possible long-term. The inferior competitor will be excluded from the community. This upholds Gause's principle of competitive exclusion, which states that no two species can occupy the same niche indefinitely if competing for the same limiting resources.

However, when interspecific competition is weak or mutualistic, the model indicates stable coexistence may occur. Only under conditions of weak resource overlap or facilitation between species can a diverse competitive community persist over generations. This provides insight into how biodiversity is maintained; strong niche differentiation or weak competitive effects allow multiple similar species to stably co-occupy an area together. Overall, the results tie competitive hierarchies directly to potential long-term diversity outcomes, deepening our comprehension of community structure and dynamics.

13.4 Discussion

While simple and stylized, the competitive Lotka-Volterra model yields important insights into interspecific interactions and their implications for community organization. By capturing the essential dynamics of competing populations through logistic growth and competitive reductions to per capita growth rates, the model provides a mathematical framework for exploring how competition shapes long-term community outcomes.

Despite many unrealistic assumptions, such as constant competition coefficients and symmetrical interspecific effects, the Lotka-Volterra model successfully describes the four qualitative behaviors that can emerge from competitive interactions. These regimes, distinguished by the relative competitive abilities of each species, predict different long-term fates ranging from coexistence to exclusion. In this way, the model functions well as an abstract, conceptual explanatory model rather than a quantitatively predictive one.

Explanatory models like Lotka-Volterra aim to provide mechanistic understanding of natural phenomena, rather than detailed forecasts of real populations. They distill the essence of a process into mathematical terms to investigate general principles and properties. While simplifying assumptions neglect ecological complexities, this allows revealing underlying dynamics that may otherwise remain obscure. The insights generated can then guide more realistic, data-driven modeling as our comprehension progresses.

Naturally, limitations arise from unrealistic assumptions. Despite this, the Lotka-Volterra model fulfills its purpose of building foundational understanding rather than accurate prediction for any specific system. Its enduring usefulness demonstrates the power of conceptual models to advance ecology conceptually. Overall, the Lotka-Volterra model exemplifies how simple theory can provide explanatory insights that stimulate new hypotheses and guide more sophisticated modeling in future.

Chapter 14

SIR Model

Abstract The chapter introduces the fundamental SIR modeling framework, which is used to study the dynamics of infectious disease transmission. The SIR model categorizes a population into three compartments: susceptible, infected, and recovered individuals. Changes in the size of each compartment are represented by a system of differential equations, formulated based on assumptions of homogeneous mixing and exponential recovery rates. The model equations are non-dimensionalized and analyzed to identify fixed points and determine stability through Jacobian analysis. This analysis reveals a critical transition at the basic reproduction number $R_0 = 1$, which governs whether a disease can invade and become established in the population. Various extensions and applications of the SIR model are also discussed, demonstrating how it can provide both qualitative and quantitative insights into real disease systems.

14.1 Introduction

Mathematical modeling of infectious disease transmission has been crucial for understanding and controlling epidemics. One of the simplest yet most influential epidemiological models is the SIR model. Proposed in the early 20th century, the SIR model divides a population into three categories—Susceptible, Infected, and Recovered—and represents transmission through a system of differential equations.

Despite its assumptions of homogeneous mixing and exponential recovery rates, the SIR model has provided fundamental insights into disease dynamics. Threshold quantities like the basic reproduction number R_0 characterize when an outbreak will occur based on transmission rates. Analytic solutions also demonstrate a range of epidemiological behaviors from disease invasion and persistence to endemic equilibrium.

The basic SIR framework has served as a starting point for extending models to consider additional biological and external influence realistically. Yet even in its simple form, the model illustrates how self-organizing transmission processes alone can lead to complex episodic outbreak patterns on the population scale. SIR analyses and simulations provide an elegant, versatile tool to study disease control strategies from targeted quarantines to vaccination programs.

In this chapter, we will introduce the SIR modeling framework in detail. We will formulate the compartmental differential equations, obtain analytic solutions, and explore simulation-based analyses. Examples will demonstrate how this basic setup can be applied to real disease systems while also motivating extensions. The goal is to establish the conceptual and technical foundations of SIR modeling as a foundation for more complex and realistic epidemiological representations.

14.2 Model Formulation

The SIR model divides population into three mutually exclusive compartments based on disease status: susceptible (S), infected (I), and recovered (R). The following assumptions are made:

- Individuals mix homogeneously; the probability of contact between any two individuals is equal.
- Upon infection, individuals immediately become infectious.
- Transmission occurs through contact between susceptible and infected individuals. The rate of new infections is thus proportional to both the number of susceptible (S) and infected (I) individuals, with proportionality constant β known as the transmission rate.
- Infected individuals recover at a constant rate γ and acquire lifelong immunity.
- The population birth rate is constant and denoted by α .
- Individuals in all compartments die due to causes other than disease at constant rate μ , and infected individuals also die due to causes directly associated to the disease at a constant rate δ .

These mechanisms are schematically represented in Fig. 14.2 which pictures infection dynamics as flux-balance processes. Taking this into consideration, the population evolution in all compartments can then be expressed as a system of ordinary differential equations:

$$\begin{aligned}\frac{dS}{dt} &= \alpha - \beta SI - \mu S, \\ \frac{dI}{dt} &= \beta SI - (\gamma + \mu + \delta)I, \\ \frac{dR}{dt} &= \gamma I - \mu R.\end{aligned}$$

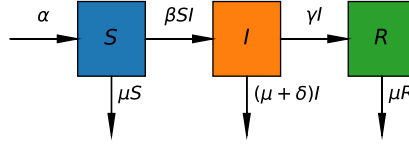


Fig. 14.1 Schematic representation of the SIR model compartmental structure and transitions. Susceptible individuals (compartment S) become infected at a rate proportional to contacts with infectious individuals in compartment I . Infected individuals recover at rate γ and enter the recovered compartment R with lasting immunity. All compartments face a baseline death rate μ . Additionally, infectious individuals face an extra disease-induced death rate δ owing to pathogenic effects.

14.3 Normalizing the Model

We can non-dimensionalize the system of differential equations by introducing the following normalized variables:

$$\begin{aligned} s &= \frac{S}{\alpha/\mu}, \\ i &= \frac{I}{\alpha/(\gamma + \mu + \delta)}, \\ r &= \frac{R}{\alpha/\mu}, \\ t' &= \mu t \end{aligned}$$

With this, the ODE system becomes:

$$\begin{aligned} \frac{ds}{dt'} &= 1 - R_0 si - s, \\ \frac{di}{dt'} &= \rho(R_0 si - i), \\ \frac{dr}{dt'} &= \varepsilon i - r, \end{aligned}$$

where

$$\begin{aligned} R_0 &= \frac{\alpha\beta}{\mu(\gamma + \mu + \delta)}, \\ \rho &= \frac{\gamma + \mu + \delta}{\mu}, \\ \varepsilon &= \frac{\gamma}{\gamma + \mu + \delta}. \end{aligned}$$

The normalization process yields several advantages. First, it reduces the original model with 5 parameters to an equivalent model with only 3 non-dimensional lumped parameters. This simplifies the analysis. Second, some of these lumped parameters have special epidemiological meaning. In particular, R_0 is known as the basic reproductive number. To understand its significance, rewrite R_0 as:

$$R_0 = \beta \frac{\alpha}{\mu} \frac{1}{\mu + \gamma + \delta}.$$

β represents the number of new infections generated by each infectious individual per unit time. α/μ is the disease-free population size. Thus, $\beta\alpha/\mu$ gives the number of infections generated per unit time by one infectious individual introduced into a completely susceptible population. Meanwhile, $1/(\mu + \gamma + \delta)$ is the average time an individual spends in the infectious compartment before either recovering or dying. Multiplying these terms gives R_0 , which can thus be interpreted as the expected number of secondary infections produced by a single infectious individual introduced into a wholly susceptible population. The dynamical significance of this threshold will become clear in subsequent analysis.

14.4 Fixed Points and Stability Analysis

The first two differential equations of the normalized SIR model, governing the dynamics of s and i , form an autonomous subsystem that is decoupled from the equation for r . This subsystem can be analyzed independently of r , then the solutions for i can be substituted into the third equation to solve for r .

Focusing first on the independent (s, i) subsystem will allow us to characterize the overall infection dynamics without consideration of the recovered population. Solving this core transmission model will provide insight into whether the disease can invade and establish infection within the population.

Rewriting this subsystem

$$\begin{aligned} \frac{ds}{dt} &= 1 - R_0 si - s, \\ \frac{di}{dt} &= \rho(R_0 si - i). \end{aligned}$$

It is straightforward to prove that it has two different fixed points:

$$(1, 0), \quad \left(\frac{1}{R_0}, 1 - \frac{1}{R_0} \right).$$

To analyze the stability of the disease-free equilibrium, we compute the Jacobian matrix of the reduced subsystem:

$$J = \begin{bmatrix} -1 - R_0 i & -R_0 s \\ \rho R_0 i & \rho(R_0 s - 1) \end{bmatrix}.$$

Evaluating this at the disease-free fixed point $(1, 0)$ gives:

$$J(1, 0) = \begin{bmatrix} -1 & -R_0 \\ 0 & \rho(R_0 - 1) \end{bmatrix}.$$

The eigenvectors of the Jacobian matrix are:

$$\begin{aligned} v_1 &= (1, 0), \\ v_2 &= \left(-\frac{R_0}{1 + \rho(R_0 - 1)}, 1 \right), \end{aligned}$$

with corresponding eigenvalues:

$$\lambda_1 = -1, \quad \lambda_2 = \rho(R_0 - 1).$$

These results indicate that the disease-free fixed point is locally asymptotically stable when $R_0 < 1$, and unstable otherwise, transitioning to a saddle point structure at the critical value of $R_0 = 1$. This stability switches at the epidemic threshold of $R_0 = 1$.

We can investigate the stability of the endemic equilibrium by evaluating the Jacobian matrix at $(1/R_0, 1 - 1/R_0)$:

$$J(1/R_0, 1 - 1/R_0) = \begin{bmatrix} -R_0 & -1 \\ \rho(R_0 - 1) & 0 \end{bmatrix}.$$

Rather than computing the eigenvalues directly, which could yield cumbersome expressions, we analyze the Jacobian trace (τ) and determinant (Δ) as explained in Chapter 11 and summarized in Fig. 11.1:

$$\begin{aligned} \tau &= -R_0, \\ \Delta &= \rho(R_0 - 1). \end{aligned}$$

From these results, we see that $\Delta < 0$ when $R_0 < 1$, indicating the endemic equilibrium is a saddle node in this case. Additionally, for $R_0 > 1$, $\Delta > 0$ and $\tau < 0$, implying that the endemic equilibrium is locally asymptotically stable. In summary, the trace and determinant criteria reveal that the endemic fixed point undergoes a transcritical bifurcation, transitioning from a saddle to a stable node as R_0 passes through the threshold value of 1.

Fig. 14.4 summarizes the findings of the local stability analysis. Observe that, in the endemic state, i^* takes negative values when $R_0 < 1$. This means that, in practice, only the disease-free steady state exists when the average number of secondary infections produced by a single infectious individual introduced into a wholly susceptible population is less than one.

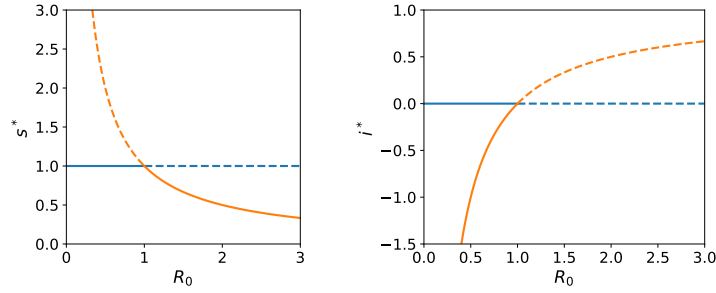


Fig. 14.2 Steady-state values and stability domains as a function of the basic reproduction number, R_0 . (Left) In the disease-free state, the fraction of susceptible individuals, s^* , remains at 1, represented by the blue curve. However, in the endemic-disease state s^* decreases inversely with R_0 , shown by the red curve. (Right) The normalized infected fraction at equilibrium, i^* , is zero in the disease-free state (blue curve) and increases as $1 - 1/R_0$ in the endemic-disease state (red curve). A transcritical bifurcation occurs at $R_0=1$. For $R_0 < 1$, the disease-free equilibrium is stable (solid lines) while the endemic steady state is unstable (dashed lines). At the bifurcation point, the two equilibria collide and their stability reverses for $R_0 > 1$.

In summary, the SIR model predicts two possible long-term outcomes depending on the value of R_0 . Specifically, the model has two steady states: a disease-free equilibrium where the infection is eliminated, and an endemic equilibrium where the disease persists at a constant level in the population.

The stability analysis revealed that a critical transition occurs at $R_0 = 1$. For $R_0 < 1$, the disease-free state is locally asymptotically stable, meaning any small perturbation will fade out as the infection dies from the population. However, when $R_0 > 1$, the disease-free equilibrium loses stability. This same threshold governs the stability of the endemic equilibrium, which undergoes a bifurcation at $R_0 = 1$. Below the threshold, the endemic state is a saddle node and unstable. But for $R_0 > 1$, it transitions to a stable node.

Biologically, R_0 represents the average number of secondary cases produced by one infected individual in a fully susceptible population. Hence, by determining whether R_0 is above or below one, we can predict if a disease invasion is likely to succeed or fail at establishing long-term transmission within the community. The stability analysis therefore provides key insights into disease dynamics based on the epidemiological threshold defined by R_0 .

Based on the definition of R_0 , there are a few measures that can be taken to reduce its value:

- Reduce transmission rate (β). Public health interventions that decrease the risk of transmission during contact, such as hand hygiene, masks, distancing, and ventilation, will lower β . Non-pharmaceutical interventions like lockdowns and restrictions on gatherings that reduce social contact frequency also impact β .
- Increase recovery rate (γ). Providing supportive medical care and targeted treatment to infected individuals can help speed their recovery and shorten the duration that they remain infectious, effectively increasing parameter γ .

- Increase removal rate (δ). In agricultural or wildlife settings, humane culling of visibly infected individuals can effectively increase the disease-induced mortality rate parameter δ . However, in human populations a more ethical approach is to quickly identify infectious individuals through widespread testing and rigorous contact tracing and place them in isolation.
- Reduce influx into susceptible class (α). Rather than interpretation as birth rate, α is better viewed as the rate at which new individuals become susceptible, such as through loss of immunity. Vaccination upon birth or entrance into the susceptible population lowers this parameter without unwanted demographic effects.
- Combination of approaches: The most effective strategies often combine multiple types of measures simultaneously. This creates additive reductions in R_0 through independent pathways compared to single measures.

14.5 Discussion

While the basic SIR model makes several restrictive assumptions, it has proven remarkably capable of capturing fundamental mechanisms of disease transmission dynamics. The model's enduring value stems from its ability to isolate a minimal set of elements necessary to mathematically represent infectious propagation through a population based on transmission between individuals. Though heterogeneous mixing, temporary immunity, and other real-world complexities are ignored, the model framework provides conceptual and predictive insights that have remained highly relevant.

Despite its limitations, the SIR model elucidated critical but unintuitive properties like the existence of epidemic thresholds defined by epidemic quantities like R_0 . Threshold effects and bifurcation behaviors revealed through model analysis explain why certain interventions can entirely curb outbreaks while others have negligible impact. Such lessons challenge naïve assessments and guide rational intervention design.

Perhaps most remarkably, the simple SIR rules give rise to complex and varied overall infection patterns at the system scale depending on parameter conditions. Self-organized criticality and phase transition phenomena emerge from local inter-individual interactions alone. These phenomena shed light on how diseases can transition between disparate outbreak modes from fleeting invasion to endemic stability.

The model's intrinsic value also lies in its explanatory character; by distilling phenomena to essential mathematical elements, relationships between underlying factors and observable behaviors are uncovered. This enhances conceptual understanding beyond empirical observations alone. The model serves as a framework upon which more realistic representations can be built through principled expansions, while preserving core transmission dynamics.

In summary, despite being formulated over a century ago with limited data and computational power, the SIR model has proven to transcend its restrictive assumptions through theoretical and practical insights that remain highly relevant today.

Its minimal yet fundamental representation of transmission acts as the cornerstone upon which our quantitative understanding of infectious disease dynamics continues to be built.

Chapter 15

A Matter of Scales

Abstract This chapter examines biological scaling principles and their implications for depicting size changes in organisms. Scaling relationships govern how structures like bones evolve in proportion to size to cope with mechanics. Metabolic rates also scale predictably with mass to maintain homeostasis across magnitudes. Evolution enforces proportional tuning of all traits through natural selection. Together, these multi-level scaling constraints reveal why artificially modifying size alone produces non-viable designs. Popular scenarios of miniaturization/magnification in films disregard life's exquisitely calibrated, scaled architecture. Mathematical modeling faces challenges representing biology's polyscalar complexity across organizational levels from molecules to ecosystems. Studying scaling laws provides perspectives on what engineered modifications respect life's constraints and informs authentic portrayals in storytelling by highlighting the intrinsically scaled nature of life.

15.1 Introduction

For decades, science fiction films have entertained audiences with fantastical scenarios of humans and animals transformed to novel sizes. From the iconic miniaturization procedure aboard the submarine in *Fantastic Voyage*, to the hapless kids shrunk to ant proportions in *Honey I Shrunk the Kids*, popular cinema has long toyed with the possibilities of manipulating scale. However enthralling these cinematic tales may be, a closer examination of biological scaling principles reveals such size-changing scenarios violate the rigorous constraints shaping life at even its most fundamental levels.

While celebrated pioneers like Galileo Galilei first began piecing together the mathematical rules governing structural scaling across the natural world, modern

integrative biology has further illuminated why modification of size alone disrupts the interdependent design of organisms. Through detailed analysis of traits from bone dimensions to metabolic rates, scientists now understand structures, functions and processes have all evolved in coordinated balance to suit a species' particular stature. Size is but one facet of an exquisitely calibrated architecture, a single thread in the woven tapestry of form and function.

This chapter examines how biological structures and processes scale in relation to size at different levels, from bones to metabolism to evolution. This helps explain why scenarios of artificially changing an organism's size portrayed in movies are unrealistic given the intricate relationships required for life. It also demonstrates Biology's "scaled" nature—the way phenomena exist across a vast range of magnitudes, from molecules to entire populations, and can only be understood by considering the appropriate scale.

15.2 Structural scaling

One of the earliest scientists to recognize patterns in animal body sizes was Galileo Galilei in the 1600s. Even without modern technology, he carefully observed bone structures across species of different masses. In his work *Dialogues Concerning Two New Sciences*, Galileo described finding consistent relationships when comparing the femurs (thighbones) of land animals.

He noticed that as an animal's overall bulk increases, the diameter of weight-bearing long bones like the femur expands at a faster rate than the bone's length. What did this mean? Simply put, bigger animals need sturdier bones to carry their heavier weight. While a femur's length relates to body size, mass grows exponentially with increasing size. Additionally, bone strength comes mainly from its thickness, not length.

Using basic mechanics, Galileo reasoned that for an animal's femur to withstand the extra stress of greater mass, its width must increase more quickly than overall growth. His discovery launched quantitative studies of how material properties and designs cope with size-dependent stresses.

This scaling relationship helps explain why miniaturizing or enlarging creatures as shown in movies is unrealistic if proportions stay the same. For example, shrinking a human while preserving relative femur dimensions would result in bones much thicker than needed, limiting movement. Stretching proportions to enlarge a mouse would create femurs too slender to hold its increased weight without breaking. Nature has perfectly evolved size-calibrated solutions through evolutionary scaling of structures and functions.

15.3 Metabolic Scaling

While structural design accommodates size-dependent mechanical loads, another critical factor influenced by scale is an organism's metabolism. Warm-blooded animals like mammals and birds maintain a relatively constant internal temperature higher than their surroundings, necessitating continual heat production to offset heat loss.

All objects lose heat through their external surface area. Hence, for any given temperature difference from the environment, smaller animals lose heat faster relative to their bulk than larger organisms. Mathematically, surface area scales with mass elevated to the two-thirds power, whereas the internal volume heating the body scales closer to mass. This means that heat flux away from small bodies is disproportionately large versus what their mass alone would suggest.

At the same time, bodies generate metabolic heat through the biochemical reactions of cells. Cellular number scales close to an organism's mass, but volumetrically within its three-dimensional form. Putting these scaling rules together, scientists expect metabolic rate to rise with approximately the two thirds power of mass for warmth to be evenly distributed regardless of size.

Intriguingly, empirical studies confirm most mammals and birds qualitatively adhere to power-law scaling of basal metabolism. This is exemplified by hummingbirds working furiously to offset fast cooling. Artificial size changes isolated from evolutionary context would similarly cause metabolic misalignments causing overheating or shutdown of smaller or larger fabricated bodies. Nature has incrementally tuned metabolism in harmony with structure over immense time through non-arbitrary, size-specific selection pressures.

15.4 Evolutionary Scaling Constraints and Lessons Learned

The scaling relationships governing both structure and metabolism demonstrate why size change in isolation from evolutionary context produces non-viable designs. Natural selection shapes life through proportional, multi-generational modifications aligning form and function across scales in response to environmental forces. While size itself may change gradually over extended periods, the proportional tuning of all supporting parameters remains subject to strict biological scaling laws.

When considering evolutionary requirements, it becomes clear that simply shrinking or stretching an organism would disrupt the exquisite interdependencies so carefully optimized through natural processes. Studying biological scaling elucidates life's inherent multi-scalar character, as traits manifest and vary contingent on the level of analysis. Phenomena appear only when observing the relevant magnitude; molecules, cells, individuals, ecosystems and beyond all influence one another. Mathematically modeling such complexity also requires representing relationships flexibly across domains.

Ultimately, these principles demonstrate both the stringent design constraints on bioengineering novel sizes and what we gain by evaluating hypotheses through a scale-aware lens. Popular films depicting scaling may entertain, but examining what naturally evolved scaling laws reveal new perspectives on possibility and impossibility. Continued scaling investigations also hold promise to inform more nuanced illustrations merging scientific accuracy with compelling storytelling in future works.

15.5 Discussion

In this chapter, we have explored how biological structure, function, and evolution are intrinsically shaped by size through various scaling relationships. From Galileo's foundational observations of bone geometry, to quantitative analyses of metabolism and selection pressures, close examination reveals that life is calibrated optimally only within an organism's adapted scale. Artificial modification of size alone violates these multi-level interdependencies so precisely tuned through natural processes over immense time.

Understanding nature's stringent scaled blueprints holds important implications not only for scientific fields, but also provides a basis for more evidence-based approaches in other domains like storytelling. Scaling principles offer a profound lens for both appreciating life's intricacy.

Chapter 16

Simplified SIR Model

Abstract This chapter develops and analyzes a simplified version of the classic SIR compartmental model. The goal is to illuminate the intrinsic transmission-recovery dynamics that govern the short-term propagation of an infection during the initial stages of an outbreak, when demographic effects have a negligible impact. The model is formulated as a system of ordinary differential equations, and analytical techniques are employed to determine key characteristics of outbreak behavior as functions of epidemiological parameters, such as the basic reproduction number. Stability analysis reveals threshold conditions for outbreak potential based on this metric, while linearization allows for the quantification of initial growth or decay trajectories. Further exploration of the governing equations provides insights into the forces shaping the temporal prevalence profiles over the course of an epidemic. By focusing on the fundamental transmission-recovery dynamics, this simplified SIR model offers a valuable tool for understanding the early dynamics of an outbreak, independent of complicating demographic factors.

16.1 Introduction

Outbreaks of infectious diseases can have major public health and socioeconomic impacts. It is therefore important to understand the dynamics of disease spread and characterize factors determining outbreak size and duration. The classic SIR compartmental model provides a useful framework for modeling infection transmission at the population level. It incorporates demographic fluxes due to births and deaths. However, in many outbreak settings, the timescales over which infections and recoveries occur are much faster than demographic turnover.

As such, during the initial spread and peak of an outbreak, the influence of births and deaths can be neglected as a first approximation. In this chapter, we develop and

analyze a simplified version of the SIR model that ignores demographic fluxes. This allows us to focus specifically on the short-term infection dynamics over the course of an outbreak. Understanding how the basic infection and recovery processes drive temporal changes in disease prevalence at this timescale is highly relevant from a public health perspective.

Key determinants of outbreak size and duration need to be identified to effectively target intervention strategies. The simplified SIR model provides a tractable framework for characterizing the influence of transmission rate, recovery rate, and other epidemiological parameters on short-term infection dynamics. Analytical insights will be used to explore model predictions and make connections to real-world outbreak settings. Overall, this analysis aims to complement the full demographic SIR model by illuminating infection spread mechanisms operating over a distinct, epidemiologically important short-term timescale.

16.2 Model development

We develop a compartmental model to describe the transmission dynamics of an infectious disease within a closed population. The population is divided into three mutually exclusive health states: susceptible (S); infected (I); and recovered (R). Individuals transition between states according to the following processes:

- Susceptible individuals contract the infection upon contact with infectious individuals. The per capita rate of new infections is proportional to the product of the number of susceptible and infectious individuals, with proportionality constant β known as the infection rate.
- Infected individuals recover at a constant per capita recovery rate γ .
- In the absence of demographic factors like birth, death, immigration or emigration, the total population size $N = S + I + R$ remains fixed.

These assumptions allow formulation of the following system of ordinary differential equations:

$$\frac{dS}{dt} = -\beta SI, \quad (16.1)$$

$$\frac{dI}{dt} = \beta SI - \gamma I, \quad (16.2)$$

$$\frac{dR}{dt} = \gamma I. \quad (16.3)$$

The total population size is non-dimensionalized to 1 by defining normalized variables $s = S/N$, $i = I/N$, $r = R/N$ and a rescaled time $t' = \gamma t$. In terms of these, the equations become:

$$\frac{ds}{dt'} = -R_0 si, \quad (16.4)$$

$$\frac{di}{dt'} = R_0 si - i, \quad (16.5)$$

$$\frac{dr}{dt'} = i, \quad (16.6)$$

where $R_0 = \beta N/\gamma$ denotes the basic reproductive number, defined as the average number of secondary infections produced by an infectious individual in a fully susceptible population. In subsequent sections, we analyze this system to characterize outbreak dynamics based on R_0 .

16.3 Analysis of Disease-Free Equilibria

We first analyze the steady state solutions of the system of equations given by (16.4)-(16.6). A steady state occurs when the time derivatives vanish such that $ds/dt' = di/dt' = dr/dt' = 0$. This condition is satisfied whenever the number of infected individuals is $i = 0$, regardless of the values of s and r . Hence, there exists a continuum of disease-free equilibria (DFE) given by:

$$s^* = \eta, \quad i^* = 0, \quad r^* = 1 - \eta,$$

where η can range between 0 and 1, representing all possible mixtures of the susceptible and recovered populations when the disease is absent.

To assess stability, we calculate the Jacobian matrix J and evaluate it at each DFE. This yields:

$$J(\eta, 0, 1 - \eta) = \begin{bmatrix} 0 & -R_0\eta & 0 \\ 0 & R_0\eta - 1 & 0 \\ 0 & 1 & 0 \end{bmatrix}. \quad (16.7)$$

The eigenvalues are $\lambda_1 = R_0\eta - 1$, $\lambda_2 = \lambda_3 = 0$. Since $\lambda_2 = \lambda_3 = 0$ variations in s and r (the directions determined by \vec{v}_2 and \vec{v}_3) decay at rate zero. That is, the DFE is neutrally stable to perturbations in these directions. However, perturbations in the direction of \vec{v}_1 decay for $R_0\eta < 1$ but grow for $R_0\eta > 1$, indicating stability below epidemic threshold and instability above. When the entire population is susceptible ($\eta = 1$), stability requires $R_0 < 1$. Therefore, an outbreak occurs if $R_0 > 1$, allowing small infectious perturbations to amplify rather than decay.

16.4 Characterizing Outbreak Dynamics

We have shown that the disease-free equilibrium (DFE) is stable when $R_0\eta < 1$, resulting in disease extinction, but unstable for $R_0\eta > 1$, allowing potential out-

breaks. To further characterize outbreak dynamics, we analyze the behavior near the DFE. Considering the Jacobian in Equation (16.7), linearization of Equations (16.4)-(16.6) yields:

$$\begin{aligned}\frac{d\delta s}{dt'} &= -R_0\delta i, \\ \frac{d\delta i}{dt'} &= (R_0\eta - 1)\delta i, \\ \frac{d\delta r}{dt'} &= \delta i,\end{aligned}$$

where $\delta s = s - s^*$, etc. Taking $s^* = \eta$, $i^* = 0$, $r^* = 1 - \eta$, this implies:

$$\begin{aligned}\frac{ds}{dt'} &= \eta - R_0i, \\ \frac{d\delta i}{dt'} &= (R_0\eta - 1)i, \\ \frac{d\delta r}{dt'} &= (1 - \eta) + i.\end{aligned}$$

These equations further imply that introduction of infected individuals causes a decrease in susceptibles and increase in recoveries. On the other hand, the behavior of $i(t)$ depends on the sign of $R_0\eta - 1$: for $R_0\eta < 1$, infections decay, while for $R_0\eta > 1$, outbreaks ensue as infections amplify initially.

Outbreaks cannot persist indefinitely, however, as implied by Equation (16.5): infections arise from contacts between s and i , but are lost through recoveries at rate i . As s decreases while i increases over time, recoveries will eventually dominate, terminating the outbreak at a new DFE with $R_0\eta' < 1$.

16.5 Discussion

In this chapter, we developed and analyzed a simplified SIR model that ignores demographic fluxes to describe the spread and short-term dynamics of an infectious disease over the initial stages of an outbreak. By formulating the model as a system of ordinary differential equations and non-dimensionalizing variables, we were able to characterize key features of outbreak behavior depending on epidemiological parameters like the basic reproduction number R_0 .

Analysis of the disease-free steady states revealed that outbreaks occur when R_0 exceeds the threshold value of 1. Linearization near the disease-free state then allowed quantification of initial growth or decay depending on stability criteria. These findings aligned with epidemiological theory regarding outbreak potential based on the expected number of secondary cases produced in a fully susceptible population.

Going beyond stability analysis, we also explored outbreak profiles by examining the forces governing changes in compartment sizes over time. This elucidated the

competing influences of new infections versus recoveries on the infectious class. It was shown that outbreaks arise due to an initial influx domination but wane once recovery outpaces transmission as susceptibility decreases.

Overall, the simplified SIR model provided valuable insights into the intrinsic infection dynamics driving temporal changes in prevalence over an outbreak timescale. Both analytical and numerical approaches complemented each other to strengthen understanding. It demonstrates how even highly idealized models can offer meaningful public health insights when paired with epidemiological context.

Chapter 17

The Interdisciplinary Journey of Oscillators: From Transatlantic Navigation to Neurophysiology

Abstract Oscillators have proven profoundly versatile, weaving through numerous disciplines to unlock innovations. In this chapter, we explore how oscillators have had a significant impact on the advancement of science and technology throughout history. Both mechanical and electromagnetic oscillators, along with the mathematical models that describe them, have played a crucial role in various fields such as navigation, communications, and the study of neurophysiology. Key contributions in the science of oscillators that have left a lasting influence on other areas are highlighted, and the influence of figures like John Harrison, James C. Maxwell, Heinrich Hertz, Balthasar van der Pol, Alan Hodgkin, and Andrew Huxley is emphasized. We discuss how they continue to be essential in current research and the development of advanced interdisciplinary approaches.

17.1 Introduction

Physics encompasses a number of notable concepts that have shaped the course of scientific and technological progress. The ideal gas and the black-body radiator, for example, have had a significant impact on various branches of physics and inspired the development of novel technologies. However, the harmonic oscillator is arguably the most profound and versatile concept of all.

The study of oscillators has a long and rich history, weaving together ideas and discoveries from diverse disciplines including physics, mathematics, engineering, biology, and medicine. Research on oscillators has unlocked fundamental insights about the natural world while also enabling transformative technologies.

This chapter will trace the winding journey of oscillator research over centuries, highlighting interdisciplinary collaborations that produced groundbreaking innovations. We will explore how the quest for accurate timekeeping at sea drove inno-

ventions in clock engineering, and how this converged with discoveries in electromagnetism to enable radio technology. Electrical oscillator models would come full circle, providing key insights into biological oscillators underlying heart rhythms and nerve impulses. By tracing this vivid narrative, we will reveal how the incessant human drive to understand and manipulate oscillatory systems has profoundly reshaped civilization. Those interested in learning more are referred to the following sources (van der Pol, 1926; van der Pol and van der Mark, 1928; Bremmer et al., 1960; Sobel, 2007; Brown, 2020; Parry, 1992; Hodgson, 1977; Cipolla, 2003; Baigrie, 2006; Maxwell, 2011a,b; Clarke, 2011; Shamos, 1987; Izhikevich and FitzHugh, 2006).

17.2 The Longitude Problem and the Development of Clocks

In the 2nd century BCE, the Silk Road was established as a network of trade routes linking China with the Mediterranean region, fostering the exchange of goods, ideas, and technologies between Asia and Europe. However, after the fall of Constantinople in 1453, the Silk Road was disrupted, making trade routes to Asia and the Middle East more cumbersome and expensive for Europeans. To circumvent this challenge, explorers set out to discover direct sea routes to Asia, leading to voyages such as Christopher Columbus' discovery of the Americas in 1492, Vasco da Gama's expedition that reached India by sailing around Africa in 1498, and the voyage of circumnavigation initially commanded by Ferdinand Magellan and completed in 1522 (Parry, 1992). These journeys were soon followed by others from various European powers, marking the beginning of the Age of Exploration, which spanned from the 15th to the 18th century and produced significant changes in global trade, culture, and politics.

The contributions of Islamic scholars during the Islamic Golden Age, which spanned from the 8th to the 14th century, in the fields of mathematics, astronomy, medicine, and geography are partly responsible for the accomplishments of the Age of Exploration (Hodgson, 1977). They contributed significantly to the translation and preservation of works from the Greek and Roman eras, which had a major impact on philosophers of the European Renaissance. Since navigation relied heavily on the observation of celestial bodies prior to the 18th century, the contributions in astronomy and mathematics were particularly notable. However, astronomical methods only allowed sailors to determine their latitude, or their north-south position, while determining longitude was a more challenging task. This challenge came to be known as the longitude problem.

Accurate determination of longitude was vital for ensuring safe navigation, particularly during lengthy voyages. Vessels capable of precisely calculating their position faced reduced risks of grounding, collision, or becoming lost at sea. This not only protected the lives of sailors but also safeguarded valuable cargo, minimizing losses for ship owners and merchants. Additionally, efficient navigation reduced travel time, enabling ships to undertake more voyages and enhance profitability. To

promote advancements in this crucial area, the British government introduced the Longitude Prize, also referred to as the Longitude Act, in 1714. This competition aimed to encourage the creation of a dependable and feasible method for determining longitude at sea (Sobel, 2007).

John Harrison, a British clockmaker, successfully tackled the problem of determining longitude. Harrison recognized the importance of accurate timekeeping in solving this problem. Rather than relying on celestial observations, Harrison proposed that a meticulously crafted timepiece could allow sailors to keep track of the time at a reference location and compare it to the local time. By comparing the local and reference times, it was possible to convert the difference in hours, minutes, and seconds into a reliable indicator of longitude.

John Harrison was born in 1693 in Yorkshire, England. From a young age, he displayed exceptional skill as a carpenter and clockmaker. In the 1720s, Harrison moved to London and began designing innovative clocks, including long-case clocks with novel mechanisms. Interested in the Longitude Prize, he set out to design a marine chronometer that could maintain accuracy under the harsh conditions encountered on transoceanic voyages.

Following on the steps of scientists and clock-makers like Christiaan Huygens, Harrison crafted a series of marine chronometers. The first, known as H1, was finished in 1735. It pioneered innovations such as the use of “grasshopper escapement” and temperature compensation through a bimetallic strip. However, issues with operation at sea meant further refinements were needed.

Over the next few decades, Harrison went on to develop the H2, H3 and finally the H4 models, incrementally improving the timekeeping accuracy and durability. The H4 chronometer, completed in 1759, was a compact, high-performance device that fully met the demands of marine navigation. In rigorous sea trials, it kept time to within a few seconds per day, allowing longitude to be calculated to within half a degree.

The Board of Longitude was reluctant to fully award Harrison the prize money, leading to a prolonged dispute. However, his chronometers were widely recognized as a monumental achievement. Their unprecedented accuracy revolutionized navigation and enabled the great voyages of exploration that expanded global knowledge.

At its core, Harrison’s ingenious solution to the longitude problem required developing a sustained mechanical oscillator that could remain perpetual and constant for months under the harsh conditions of ocean voyages. The marine chronometer’s clockwork mechanism is precisely an oscillator in which energy dissipated through friction is continually replenished. This allows the periodic motion to be maintained indefinitely, enabling accurate timekeeping over long periods.

17.3 Harnessing Oscillators for Wireless Communication

The chronometer's sustained mechanical oscillations enabled advances in global navigation and mapping. However, the nineteenth century ushered in a new paradigm as scientists sought to harness the power of electromagnetic waves. Just as the perpetual motion of Harrison's clocks arose from carefully sustaining a harmonic system, steady electrical oscillations would prove vital for powering modern wireless communication.

The pioneering experiments on electricity and magnetism conducted in the eighteenth and early nineteenth centuries laid the foundation for understanding oscillatory electrical phenomena (Baigrie, 2006). Notable contributions came from Hans Christian Ørsted's discovery of the connection between electricity and magnetism in 1820, demonstrating that an electric current produces a magnetic field, and the efforts of Michael Faraday to quantitatively relate electric and magnetic forces. However, it was James Clerk Maxwell who, through his seminal treatise published in 1873, unified the previously fragmented theories into a comprehensive framework (Maxwell, 2011a,b).

Maxwell synthesized prior knowledge within a system of equations describing the interrelation between electric and magnetic fields. A key insight was that these fields could propagate through space as waves, spreading energy outward from a source. One remarkable conclusion was that light itself was simply a high-frequency electromagnetic wave. However, generating such waves to study their properties proved challenging. It was not until 1887 that Heinrich Hertz conclusively demonstrated the existence of electromagnetic waves (Shamos, 1987).

In his laboratory, Hertz sought to generate and detect the elusive electromagnetic waves predicted by Maxwell's equations. To achieve this, he devised an electrical oscillator circuit connected to a dipole antenna. When operated at high voltages, oscillations in the circuit induced corresponding oscillations in the antenna, launching electromagnetic radiation. To detect the waves, Hertz used a separate loop antenna connected to another resonant circuit. When placed in the path of the radiation, oscillations were induced in this receiver loop, providing experimental evidence of propagating electromagnetic waves.

The apparatus engineered by Hertz definitively confirmed Maxwell's theories and opened up a new paradigm in physics. Additionally, Hertz measured properties of the waves including polarization, reflection, refraction and interference, verifying that they obeyed the same rules as visible light. This cemented light's electromagnetic basis.

Hertz's experiments proved that coordinated electrical oscillations could be harnessed to generate and receive wireless signals. However, the capabilities of Hertz's apparatus were limited. While suitable for laboratory studies, more powerful and efficient oscillators would be needed to enable practical applications like radio communication.

Early radio transmitters used crude ore detectors and inefficient spark gap generators to produce electromagnetic radiation. Generating steady, high-frequency electrical oscillations was key to enabling continuous wave radio broadcasts. This relied

on certain analogies with mechanical oscillators like those used in chronometers. A resonant LC circuit can exhibit oscillations, but losses due to resistance will dampen the oscillations over time. To sustain continuous oscillations, energy must be continually fed into the system, analogous to rewinding the chronometer's drive spring. In an electronic oscillator, amplifying elements like vacuum tubes are used to replenish the energy dissipated in the resonant tank circuit. This negative resistance precisely counteracts losses, allowing persistent high-frequency oscillations. By maintaining energy balance in an electrical harmonic system, electronic oscillators enabled modern wireless communication.

The parallels between mechanical and electrical oscillators highlight the continuity in physics concepts across disciplines. Whether weighing a clock's escapement or balancing amplifiers and dissipation in a radio transmitter, the goal of sustaining an oscillator despite losses united these efforts. Powered by electronic oscillators, radio technology would fundamentally reshape society in the 20th century (Clarke, 2011).

17.4 Modelling Neural Excitation with Oscillators

The transmission of signals in nerves and muscles relies on the propagation of electrical impulses known as action potentials. Understanding the nonlinear dynamics underlying excitation in neurons and cardiac cells would require integrating concepts from physics, mathematics and biology. Once again, oscillator models would provide vital insights, this time by mimicking the spikes and rhythms produced by biological cells.

The Dutch physicist Balthasar van der Pol joined Philips Research Laboratories after receiving his doctorate in 1913. During his time there, he made significant contributions to the field of electronics, especially in radio technology. Van der Pol was a key figure in the development of the Philips radio receiver, which was a huge success at the time. According to one of his biographers, "Radio might have remained a field of haphazard empiricism along with wild commercial ventures, but for the influence of men like Van der Pol who stressed the need for a more scientific approach" (Bremmer et al., 1960, Introduction).

In 1926, van der Pol derived a nonlinear differential equation to describe the behavior of vacuum tube circuits used in early radios. While analyzing his model equations, van der Pol made an intriguing discovery. When the value of a parameter known as the damping coefficient was small, the system exhibited the familiar traits of a harmonic oscillator. However, as the damping coefficient increased to larger values, the model solutions diverged from the conventional behavior of harmonic oscillators. Instead of following smooth periodic sinusoidal oscillations, the model solutions displayed alternating periods of rapid and slow changes. Van der Pol coined the term "relaxation oscillations" to describe this behavior (van der Pol, 1926).

The spiking behavior of Van der Pol oscillator was analogous to the action potentials transmitted along neurons and the cells of the heart pacemaker. Building on this, van der Pol created a circuit with three oscillators to reproduce the electrical behavior of the heart. Using this method, he successfully replicated specific cardiac arrhythmias, demonstrating the model's ability to capture the complex dynamics of cardiac electrical activity (van der Pol and van der Mark, 1928).

In parallel to the oscillator modeling work, new technologies enabled direct measurements of neural electrical signals. The development of operational amplifiers (op-amps) in the early 1940s was a key advance. Op-amps can perform high-gain voltage amplification and mathematical operations like addition, subtraction, integration and differentiation. This made signal processing and analysis much more feasible. In 1949, Kenneth Cole and Howard Curtis invented the voltage clamp technique using an op-amp based feedback circuit to control the voltage across a cell membrane (Brown, 2020). This allowed the underlying ionic currents to be precisely measured for the first time.

Fundamental discoveries in thermodynamics and physical chemistry by pioneers like Max Planck and Walther Nernst also contributed to understanding the electrical behavior of cell membranes. Nernst's work led to his eponymous equation in 1889, relating an ion's equilibrium potential to its concentration gradient. The Nernst-Planck equations described the motion of charged particles, extending diffusion to include electrostatic effects.

Also important was Cole's adoption of the squid giant axon as a model for studying membrane electrical properties in 1936, following J. Z. Young's suggestion. The size and spacious lumen of the squid axon made it more amenable to experimental techniques such as intracellular recording, which were previously impractical with smaller axons.

While collaborating with Cole in the 1930s, Hodgkin realized the potential of using the squid giant axon to record intracellular action potentials. Returning to Cambridge in 1938, he recruited the undergraduate Andrew Huxley. Huxley's outstanding physics and mathematics background paired with Hodgkin's neurophysiology expertise. Their collaborative project resulted in a series of papers providing quantitative insights into the biophysical basis of the action potential (Brown, 2020).

The culminating paper in the Hodgkin and Huxley series established the field of quantitative membrane biophysics, integrating mathematical modeling with empirical measurements. Hodgkin and Huxley developed a model of interconnected differential equations and performed painstaking calculations to match the model output to their voltage clamp data. Lacking access to early computers, Huxley relied on a desktop mechanical calculator, achieving remarkable precision.

The Hodgkin-Huxley model marked a breakthrough in neuroscience, offering the first quantitative, mechanistic picture of neural excitability. Their integrative approach combining math and biology yielded insights into ion channel function while spurring new fields like computational neuroscience. This achievement emerged from interdisciplinary collaboration, as experts in physics, mathematics and physiology united around the common goal of demystifying the action potential. The

Hodgkin-Huxley collaboration highlights the power of bridging disciplinary divides to propel discovery.

The complexity of the Hodgkin-Huxley model posed challenges for broader usage in an era before digital computers. In the 1960s, Richard FitzHugh at the NIH sought to investigate the model's mathematical properties using nonlinear dynamics techniques. To solve the equations across parameters, FitzHugh collaborated with John Moore to build an analog computer from op-amps, multipliers and plotters (Izhikevich and FitzHugh, 2006). This allowed them to graphically visualize solutions, though operating the intricate analog simulator required sophisticated engineering and math skills. The model complexity and lack of digital computing motivated efforts to derive simplified models of neural excitation.

Guided by Cole's insights, FitzHugh modified van der Pol's relaxation oscillator equations to distinguish key features of the Hodgkin-Huxley model. The aim was to separate the dynamics of sodium and potassium ion flow across the membrane from the regenerative excitation process. Originally called the Bonhoeffer-van der Pol equations, these were later renamed the FitzHugh-Nagumo equations because, around the same time, Japanese engineer Jin-Ichi Nagumo invented an electronic circuit using tunnel diodes that reproduced the key cubic nonlinearity. The simplified FitzHugh-Nagumo model provided an accessible approximation to the complex Hodgkin-Huxley system. Reconfiguring the analog computer to solve these reduced equations enabled more extensive mathematical analyses of neural excitation dynamics.

The quest to understand the electrical basis of neural signaling exemplifies the potency of cross-disciplinary pollination. Integrating oscillator models from physics and engineering with emerging techniques to probe nerve impulses yielded insights into the mechanisms of neural excitation. Constructing fruitful analogies between biological and man-made oscillators led to accessible mathematical representations that captured the essence of spiking dynamics. By breaking down barriers between physics, mathematics and physiology, pioneers transformed understanding of the fundamental processes underlying thought itself. The intertwined narrative of biological and technological oscillators underscores how synthesizing diverse perspectives propels discovery.

17.5 Conclusion

The history of oscillators unveils the intricate relationship between science and technology. Driven by practical needs, advancements in timekeeping brought about significant changes in navigation. Not only this pursuit had profound political and economical effects but also led to fundamental scientific discoveries.

Likewise, electronic oscillators played a crucial role in powering wireless communication systems that transformed society. Yet, when examined through mathematical models, they also shed light on the electrical rhythms of the nervous system. Time and again, the manipulation of oscillatory systems for engineering purposes

unintentionally deepened our scientific understanding, crossing disciplinary boundaries.

The enduring significance of oscillators lies in their versatility as model systems. The concept of the harmonic oscillator provides an approximate description for a wide range of systems, including physical, biological, and engineering domains. This commonality across different areas facilitates analogies that enhance the process of discovery.

By tracing the history of oscillations through the centuries, we gain insight into the very evolution of science itself. While curiosity guides exploration in specialized fields, it's the process of synthesis that breathes life into the deepest ideas. The journey of oscillators highlights how collaborative human effort, aimed at understanding natural rhythms, regardless of their origin, propels us toward a deeper understanding of nature and contributes to the shaping of our civilization.

Finally, oscillators still play a crucial part in today's science and technology. High-frequency electronic oscillators act like the heartbeat of modern computers, making sure that different parts work together and share information at the right time. In computer science, they facilitate complex calculations and data processing by synchronizing clock cycles and enabling high-speed data transfer within computer systems. In the internet, they play a central role in precise data transmission, ensuring the uninterrupted flow of information during digital interactions. These unsung heroes quietly contribute to the seamless operation of computer technology and the interconnected world we rely on daily.

Chapter 18

The Damped Harmonic Oscillator

Abstract This chapter introduces the canonical second-order differential equation governing damped harmonic motion as one of the most fundamental and ubiquitous models for describing oscillatory behavior near equilibrium across physics, engineering, and biology. The governing equation is derived from first principles using physical analogs including a spring-mass system, pendulum, and RLC electrical circuit. Analytical solutions to the differential equation are explored and qualitative analysis of its dynamics is performed by reformulating it as a system of first-order equations, characterizing stability properties through eigenvalue analysis and classifying oscillatory regimes. Overall, the chapter establishes the broad relevance of the damped harmonic oscillator framework while providing context for future examination of oscillatory phenomena through dynamical systems theory.

18.1 Introduction

The harmonic oscillator is one of the most ubiquitous models found across physics, engineering, and biology. At its simplest, a harmonic oscillator describes the oscillatory motion of a mass attached to an ideal linear spring. Due to the restoring force exerted by the spring in response to displacement from equilibrium, the motion takes the form of simple harmonic oscillations.

More generally, any physical system that displays oscillatory behavior about an equilibrium point can be approximated as a harmonic oscillator, provided the restoring force is proportional to displacement and acts in the opposite direction. Examples include the vibrations of molecules, pendulums with small amplitude swings, electrical circuits containing inductors and capacitors, and even whole organs or organisms displaying rhythmic dynamics like the beating of the heart or circadian rhythms.

In reality, no oscillator is truly isolated from its environment. Damping forces arising from friction or dissipation act to sap the oscillator's energy over time. This gives rise to the damped harmonic oscillator model, where a force proportional but opposed to velocity is included. The damped harmonic oscillator provides a minimal yet remarkably versatile modeling framework applicable across science and engineering.

In this chapter, we introduce the damped harmonic oscillator differential equation from three physical perspectives: a mass-spring system, a pendulum, and an electrical RLC circuit. Through linearization and stability analysis techniques, we explore the oscillator's steady state behavior and classify different regimes of underdamped, critically damped, and overdamped motion. Finally, we discuss examples of biological oscillators that adhere to damped harmonic dynamics, establishing the broad relevance and fundamental importance of this ubiquitous model.

18.2 Spring-mass system

We begin our examination of the damped harmonic oscillator by considering the classical spring-mass system. As shown in Fig. 18.1, this consists of a point mass m attached to an ideal linear spring with stiffness constant K . The spring exerts a restoring force F_s proportional to the displacement x of the mass from its equilibrium position, according to Hooke's law: $F_s = -Kx$.

In addition to the conservative restoring force of the spring, the system experiences a dampening force F_d due to friction as the mass oscillates. We model this as a viscous drag force proportional to velocity: $F_d = -b\dot{x}$, where b is the damping coefficient.

By Newton's second law, the equation of motion for this system is given by:

$$m\ddot{x} = F_s + F_d = -Kx - b\dot{x} \quad (18.1)$$

By scaling time by $1/\sqrt{K/m}$, the equation takes the form:

$$\ddot{x} + 2\zeta\dot{x} + x = 0 \quad (18.2)$$

where the damping ratio $\zeta = b/(2\sqrt{km})$ characterizes the relative contribution of damping forces.

This spring-mass representation provides a straightforward mechanical depiction of the damped harmonic oscillator and will serve as a useful reference point for discussion. The normalized equation governs a wide range of oscillatory systems, as we will explore in subsequent sections.

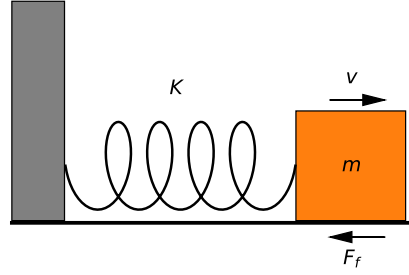


Fig. 18.1 Spring-mass system with friction.

18.3 Pendulum

We next consider how the damped harmonic oscillator model applies to small oscillations of a physical pendulum. As illustrated in Fig. 18.2, this consists of a point mass m hanging from a rigid rod of length L , which is fixed at one end to a pivot.

For small angular displacements θ from the hanging equilibrium position, the gravitational torque on the mass can be approximated as $\tau \approx -mgL\theta$. Additionally, the pivot exerts a viscous damping torque $\tau_f = -b\dot{\theta}$ opposing the angular velocity.

Treating the mass-rod system as a rigid body with moment of inertia $I = mL^2$, Newton's second law for rotational motion gives:

$$I\alpha = \tau + \tau_f \quad (18.3)$$

where $\alpha = \ddot{\theta}$ is the angular acceleration. This yields the equation of motion:

$$mL^2\ddot{\theta} = -mgL\theta - b\dot{\theta} \quad (18.4)$$

Non-dimensionalizing via the rescaling $t \rightarrow t/\sqrt{g/L}$, we obtain the normalized form of the damped harmonic oscillator with damping ratio $\zeta = b/(2m\sqrt{g/L})$:

$$\ddot{\theta} + 2\zeta\dot{\theta} + \theta = 0 \quad (18.5)$$

Thus, despite involving circular rather than linear motion, the mathematical description of small oscillations in a simple pendulum is identical to that of the spring-mass system. Both phenomena are governed by the ubiquitous damped harmonic oscillator equation near their equilibrium points.

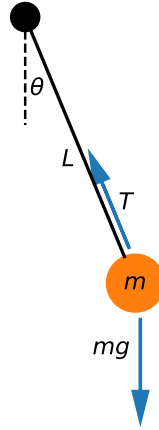


Fig. 18.2 Pendulum displaying small angular displacement θ .

18.4 RLC Circuit

We now show that oscillatory behavior in an electrical RLC circuit is also described by the damped harmonic oscillator model. Consider the series circuit in Fig. 18.3 consisting of a resistor R , inductor L , and capacitor C .

Using Kirchhoff's voltage law around the closed loop, we write:

$$V = L\dot{I} + RI + \frac{1}{C} \int_0^t I, dt' \quad (18.6)$$

where I is the current through the inductor. The first term accounts for the back electromotive force induced in the inductor according to Faraday's law. The second term represents resistive voltage drop from Ohm's law. The final term incorporates the voltage accumulated across the capacitor from charge integration.

Taking the time derivative and rearranging yields the governing differential equation:

$$L\ddot{I} + RI + \frac{1}{C}I = 0 \quad (18.7)$$

Upon non-dimensionalizing time as $t \rightarrow t/\sqrt{LC}$ and defining the damping ratio $\zeta = R/(2\sqrt{L/C})$, we obtain the normalized damped harmonic oscillator equation:

$$\ddot{I} + 2\zeta\dot{I} + I = 0. \quad (18.8)$$

Thus, oscillations in the RLC circuit are mathematically equivalent to those in the spring-mass and pendulum systems near equilibrium. Despite physical differences, the key attribute shared is oscillatory dynamics governed by a second-order differential equation with damping. This establishes a fundamental systems-level correspondence that will prove insightful moving forward in analyzing oscillatory phenomena across diverse domains.

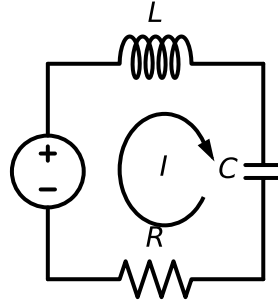


Fig. 18.3 RLC series circuit.

18.5 Steady State Analysis

We can gain further insights by recasting the damped harmonic oscillator equation as a system of first-order differential equations. Starting from the second-order form:

$$\ddot{x} + 2\zeta\dot{x} + x = 0. \quad (18.9)$$

Define a new variable $y = \dot{x}$ to represent velocity. This allows us to write the original equation as a coupled system:

$$\dot{x} = y, \quad (18.10)$$

$$\dot{y} = -2\zeta y - x. \quad (18.11)$$

In vector form:

$$\dot{\vec{r}} = \mathbf{J}\vec{r}, \quad (18.12)$$

where $\vec{r} = (x, y)^T$ while the Jacobian matrix is:

$$\mathbf{J} = \begin{bmatrix} 0 & 1 \\ -1 & -2\zeta \end{bmatrix}.$$

Due to the linearity of the system, it possesses a single fixed point given by the zero vector, $\vec{r}^* = (0, 0)$. We can determine the general solution by exploiting the eigenstructure of the Jacobian matrix \mathbf{J} . Specifically, the eigenvalues $\lambda_{1,2}$ and corresponding eigenvectors $\vec{v}_{1,2}$ of \mathbf{J} allow us to write the solution as:

$$\vec{r}(t) = C_1 \vec{v}_1 e^{\lambda_1 t} + C_2 \vec{v}_2 e^{\lambda_2 t}, \quad (18.13)$$

with C_1 and C_2 arbitrary constants determined by the initial conditions.

The eigenvalues of the Jacobian matrix at the origin are:

$$\lambda_{1,2} = -z \pm \sqrt{\zeta^2 - 1} \quad (18.14)$$

For a damping ratio of $\zeta = 0$, the eigenvalues are purely imaginary, indicating that the fixed point is a center. When $0 < \zeta < 1$, the eigenvalues form a complex conjugate pair with negative real parts. Therefore, the fixed point is a stable spiral; perturbations will result in damped oscillations converging towards the steady state. This regime corresponds to underdamped oscillations. Finally, for $\zeta > 1$, the eigenvalues are both real and negative. In this case, the fixed point is a stable node; perturbations decay monotonically without oscillation. The system is said to be in the overdamped regime.

In closing, we note that the only means of achieving truly undamped oscillations with $\zeta = 0$ would be in an idealized, isolated system without any dissipative effects. However, the second law of thermodynamics dictates that all real physical systems experience some form of damping or energy loss over time. The damping terms in our analysis have accounted for these non-conservative effects that cause oscillatory motions to gradually lose energy and amplitude. The type of decay—overdamped, critically damped, or underdamped oscillations—depends sensitively on the relative strength of damping represented by the dimensionless ratio ζ .

18.6 Application to Biological Systems

Many fundamental biological processes exhibit oscillatory dynamics that can be modeled as damped harmonic oscillators. Some key examples include:

- **Muscle contraction/relaxation:** The cyclic interaction of actin and myosin filaments, driven by ATP hydrolysis, gives rise to damped oscillations. The viscoelastic properties of muscle fibers introduce damping.
- **Neural oscillations:** Large populations of neurons can fluctuate collectively near a limit cycle regime. Damping regulates transitions between distinct firing states.
- **Cardiovascular system:** Each heartbeat and respiratory cycle involves pressure and volume oscillations that are smoothed by viscous damping into pressure-volume loops.

- Gene regulation: Negative feedback in transcription/translation causes gene expression levels to oscillate. Molecular noise and resource depletion attenuate the oscillations over time.

While real biological systems are high-dimensional and stochastic, damped oscillator theory provides qualitative insights into self-sustained rhythms, resonance effects, and characteristic relaxation timescales. For instance, analysis of damping ratios could inform drug delivery strategies that modulate the rate at which oscillations decay.

However, the damped harmonic oscillator has limitations in describing some biological oscillators. In particular, relaxation oscillators may better capture the repetitive behavior of autoregulated cells like cardiac pacemaker cells. Relaxation oscillators exhibit alternating periods of stasis and rapid switching between states, resembling a staircase waveform arising from thresholds in the system dynamics. In the next section, we analyze relaxation oscillators to understand the core properties underlying rhythmic behaviors in tissues such as the heart.

18.7 Discussion

In this chapter, we explored the damped harmonic oscillator model; a fundamental oscillatory system found throughout physics and biology. We derived the canonical second-order differential equation that governs damped harmonic oscillations and analyzed its properties both analytically and qualitatively.

We also showed how real-world phenomena involving oscillatory motion in springs, pendulums, and electrical circuits can often be approximated as damped harmonic oscillators. This revealed the broad applicability and insights provided by studying these foundational systems.

However, damped harmonic oscillator have some limitations in capturing certain biological oscillators. In particular, relaxation oscillators may better describe the behavior of excitable cells like cardiac pacemaker cells that exhibit an alternating staircase-like waveform.

This sets the stage for the next chapter, where we will introduce and analyze relaxation oscillators. Characterizing these self-sustained oscillating systems will advance our quantitative and mechanistic understanding of rhythmic processes in living tissues and their relationship to cellular-level properties of excitability and threshold dynamics.

The overarching goal of examining damped and relaxation oscillators is to build dynamical system models that provide conceptual links between distinct realms which, at the component level, may seem very different but share underlying mathematical commonalities at a system-wide scale.

Chapter 19

The van der Pol Oscillator

Abstract Oscillatory phenomena are ubiquitous in nature and underlie diverse biological and physical processes. The van der Pol oscillator introduced by Balthasar van der Pol in 1926 established a seminal mathematical framework for describing self-sustained oscillations that arise via a distinctive relaxation mechanism. This chapter analyzes the dynamical properties of the van der Pol oscillator through analytical and qualitative techniques. We derive the governing equation of motion from first principles using a spring-mass analog and examine its behavior both near and far from equilibrium. Through linearization and phase plane analysis, we classify oscillation regimes and determine stability properties of steady states. We also relate the system's dynamics to physiologically relevant relaxation oscillations in excitable media like cardiac tissue. Overall, the chapter establishes the van der Pol oscillator as a foundational model exhibiting nonlinear relaxation phenomena of widespread relevance across science and engineering disciplines.

19.1 Introduction

Oscillators have widespread applications in science and engineering. In the early 20th century, the field of telecommunications faced the challenge of developing self-sustained oscillators capable of powering wireless communication over long distances. Pioneering researchers experimented with resistor-capacitor-inductor (RCL) circuits and introduced amplifiers to counteract energy losses and enable sustained oscillations. However, a more rigorous understanding of these oscillator systems was needed to facilitate their further development and practical applications.

In 1926, the Dutch physicist Balthasar van der Pol made seminal progress in this area with his oscillator model. Van der Pol recognized that amplifiers behave as negative resistors at low oscillation amplitudes, effectively amplifying signals. In an

ideal system, an amplifier could then induce ever-growing oscillations by substituting the resistor in an RCL circuit. However, van der Pol also realized that unbounded growth was not observed in practice, suggesting the presence of a mechanism curtailing growth.

To address this, van der Pol introduced a model term that mimicked an amplifier at low amplitudes but behaved like a resistor at high amplitudes, limiting oscillation growth. Through analyzing this model, van der Pol demonstrated that under certain parameters, self-sustained oscillations could arise via a distinctive “relaxation-type” behavior. This conceptualization of relaxation oscillations was highly influential.

Importantly, van der Pol also recognized the relevance of his model to describing the rhythmic electrical activity underlying cardiac pacemaker cells. He developed related models to simulate cardiac arrhythmias, providing novel insights.

In this chapter, we will explore the oscillatory dynamics of van der Pol’s system. Studying this model aims to deepen understanding of engineered and biological self-oscillators exhibiting relaxation phenomena.

19.2 The van der Pol model

To build his model, van der Pol substituted the linear damping term in the harmonic oscillator equation with a nonlinear term, as follows:

$$\frac{d^2x}{dt^2} - \mu(1 - x^2) \frac{dx}{dt} + x = 0.$$

The key feature of this model is the nonlinear term $-\mu(1 - x^2)$, which mimics the behavior of an amplifier at low amplitudes (when $|x| < 1$) but acts like a resistor at high amplitudes (when $|x| > 1$). The parameter μ controls the strength of the nonlinear damping. When $\mu = 0$, the system reduces to the standard harmonic oscillator. However, for nonzero μ , the nonlinear damping term gives rise to richer dynamical behavior that will be explored in later sections. Specifically, as μ increases, the system exhibits oscillations that converge to a stable, finite-amplitude closed orbit called a *limit cycle*.

It is insightful to rewrite the model as a system of first-order differential equations. Here, we apply the Liénard transformation $y = x - x^3/3 - \dot{x}/\mu$, which yields:

$$\dot{x} = \mu \left(x - \frac{x^3}{3} - y \right), \quad (19.1)$$

$$\dot{y} = \frac{1}{\mu} x. \quad (19.2)$$

This formulation enables analysis techniques like phase plane analysis, which provide insight into the limit cycle behavior. Specifically, we can examine the nullclines

and flow field to understand how oscillations converge to the stable limit cycle trajectory.

19.3 Steady State and Stability Analysis

To analyze the dynamics of the van der Pol oscillator, we first investigate its steady state behavior (recall that at the steady state, both derivatives \dot{x} and \dot{y} are equal to zero). It is insightful to examine the concept of nullclines in this analysis. A nullcline is defined as the set of points where one of the time derivatives is equal to zero, while the other is allowed to vary. For the van der Pol system, the x -nullcline consists of the points where $\dot{x} = 0$, which corresponds to $y = x - x^3/3$ based on Eq. (19.1). The y -nullcline consists of the points where $\dot{y} = 0$, given by $x = 0$ from Eq. (19.2).

By definition, steady states occur at the intersection of both nullclines. Evaluating the nullclines for the van der Pol system, we find that they intersect only at the origin, with coordinates $(x, y) = (0, 0)$. Therefore, this point represents the lone steady state, or fixed point, of the system. Fig. 19.1 illustrates the nullclines and this fixed point.

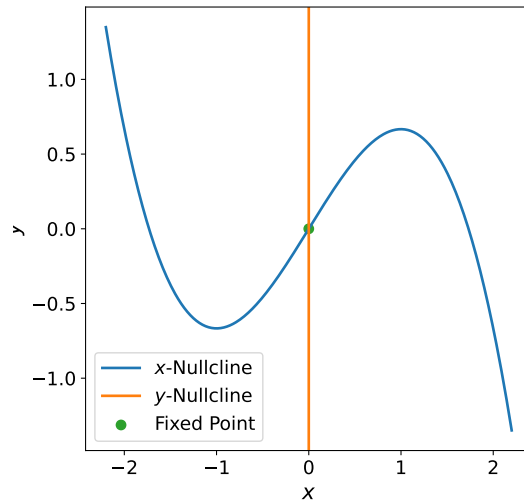


Fig. 19.1 Phase plane portrait of the van der Pol oscillator. Nullclines are shown as thick red lines, with the x -nullcline given by $y = x - x^3/3$ and the y -nullcline along the vertical axis $x = 0$. The lone fixed point is located at the origin $(0,0)$.

To analyze stability, we compute the Jacobian matrix \mathbf{J} of the system and evaluate it at the fixed point. The Jacobian of the 2-dimensional van der Pol model is given by:

$$\mathbf{J} = \begin{bmatrix} \mu(1-x^2) & -\mu \\ 1/\mu & 0 \end{bmatrix}$$

Evaluating at the fixed point yields

$$\mathbf{J} = \begin{bmatrix} \mu & -\mu \\ 1/\mu & 0 \end{bmatrix}$$

Its eigenvalues and eigenvectors are:

$$\lambda_{1,2} = \frac{\mu \pm \sqrt{\mu^2 - 4}}{2},$$

$$\vec{v}_{1,2} = \left(\mu \frac{\mu \pm \sqrt{\mu^2 - 4}}{2}, 1 \right)^T$$

Observe that the eigenvalues are either complex conjugate with positive real part or real positive numbers. In either case, the fixed point is locally unstable: a spiral in the first case and a node in the second. In the particular case in which $\mu \gg 2$, $\lambda_1 \gg \lambda_2$, whereas the first component of \vec{v}_1 is much greater than the second component of the same vector and both components of \vec{v}_2 . This means that all trajectories starting in the neighborhood of the steady state will tend to rapidly move away in a direction almost parallel to the x axis.

19.4 Existence of a limit cycle

Fig. 19.4 illustrates the phase portraits of the van der Pol system for different values of the parameter μ , overlaid with the nullclines. As seen, trajectories far from the origin converge to the x -nullcline and for a while move along it in the direction of the steady state, in accordance with Eq. (19.2). Meanwhile, the unstable nature of the fixed point causes nearby trajectories to repel outwards. According to the Poincaré-Bendixon theorem, the only closed trajectory consistent with these opposing dynamics within a bounded region of phase space is a stable closed orbit, known as a limit cycle.

In contrast to a center equilibrium, there is no family of closed trajectories surrounding the fixed point here. Moreover, after a perturbation, trajectories return to the limit cycle if it is stable, or diverge from it if unstable. Critically, the emergence of a limit cycle implies the existence of a periodic solution—with trajectories repeating their motion indefinitely along the closed orbit. This periodic behavior explains the self-sustained oscillations exhibited by the van der Pol and similar relaxation oscillator systems.

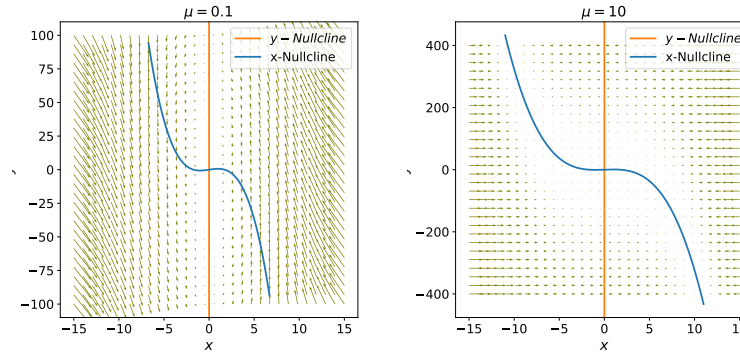


Fig. 19.2 Phase portraits of the van der Pol oscillator for parameter values $\mu = 0.1$ and $\mu = 10$, overlaid with nullclines (thick red lines). Arrows indicate vector field flow.

19.5 Relaxation Oscillations

In the limit where $\mu \rightarrow \infty$, additional insights can be gained about trajectory behavior in the van der Pol system. According to Eq. (19.2), flows are nearly horizontal everywhere except in close proximity to the x -nullcline. This is evident in the right panel of Fig. 19.4, which shows trajectories rapidly approaching one of the lateral branches of the x -nullcline.

Once a trajectory lands on a lateral branch, it slowly creeps in the vertical direction—descending along the left branch or ascending the right branch. However, when the trajectory reaches a local maximum or minimum of the lateral branch, where it meets the unstable middle branch of the x -nullcline, it is unable to continue progressing along the middle branch. Instead, it abruptly jumps to the opposite lateral branch. Specifically, a trajectory descends the left branch until the local minimum, at which point it cannot progress further and abruptly jumps rightward to ascend the rising right branch instead. Similarly, upon reaching the local maximum of the right branch, the trajectory jumps left to descend along the left branch once more.

This rapid approach and slow movement along the stable branches, interrupted by abrupt jumps between branches at turning points, gives rise to the characteristic relaxation oscillations observed in the van der Pol oscillator when $\mu \gg 2$. The system alternates between episodes of rapid evolution and sluggish progression as it repeatedly hops between the lateral branches of the x -nullcline. This peculiar oscillatory behavior distinguishes relaxation oscillators from conventional sinusoidal oscillations.

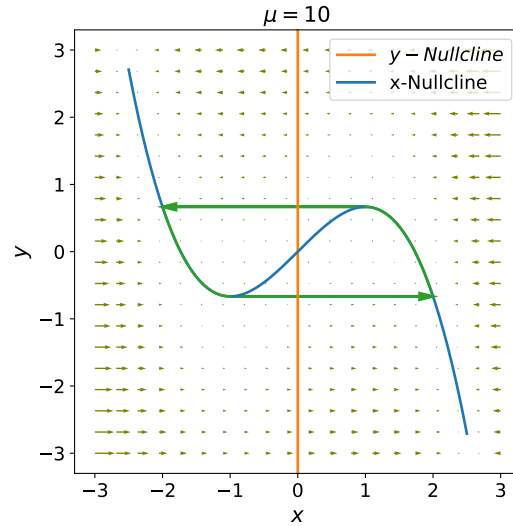


Fig. 19.3 Phase portrait for $\mu \gg 2$ illustrating relaxation oscillations. Thick blue lines trace a possible oscillation trajectory, rapidly switching between lateral branches (thin red lines) of the x -nullcline at local minima/maxima and slowly creeping along branches. Arrows indicate vector field flow.

19.6 Discussion

In this chapter, we have introduced and analyzed the dynamics of the van der Pol oscillator. This model, developed by Balthasar van der Pol in 1926, marked the first appearance of the concept of relaxation oscillations in physics and mathematics. By incorporating a nonlinear damping term into the harmonic oscillator equation, van der Pol was able to capture a peculiar oscillatory phenomenon characterized by alternating episodes of rapid change and slow progression between stable solutions.

The relaxation oscillations exhibited by the van der Pol system in the limit of large damping parameter μ distinguishes it fundamentally from conventional harmonic motion. This characteristic oscillatory behavior arises from the system's tendency to rapidly approach one lateral branch of the x -nullcline before abruptly switching to the other branch at local extremes.

Historically, the van der Pol oscillator played a pivotal role in conceptualizing relaxation oscillations and establishing them as a unique class of self-sustained oscillation distinct from sinusoidal waveforms. Beyond applications in electronics and engineering, van der Pol recognized the potential relevance of relaxation dynamics to biological oscillators underlying rhythmic processes in living organisms.

Indeed, relaxation-type oscillations provide insightful analogies for cyclic behaviors across disciplines. In neuroscience, they have helped quantify electrical spiking

patterns in excitable cells like neurons. In cardiovascular physiology, relaxation oscillations resemble pressure-volume loops associated with the heartbeat.

By deriving the first model exhibiting relaxation oscillations, van der Pol laid foundations not only for oscillator theory but also quantitative modeling applications to biological rhythms. The ubiquitous nature of relaxation phenomena continues motivating research at the intersections of physics, engineering, mathematics and the life sciences.

Chapter 20

The FitzHugh-Nagumo Model

Abstract This chapter introduces the FitzHugh-Nagumo model, a two-variable representation of excitable dynamics. We begin by reviewing the Hodgkin-Huxley model of the neuronal action potential, which provided the first quantitative description but was too complex for broader analysis. We then motivate the need for a simplified model that could capture key properties while facilitating mathematical insights. Next, we introduce the FitzHugh-Nagumo equations and analyze their fixed points and nullclines. Through linear stability analysis and examination of phase plane portraits, we demonstrate how the system can generate self-sustained oscillations via a stable limit cycle. We show that these oscillations qualitatively reproduce the spike-and-wave behavior of excitable systems through relaxation oscillations. Finally, we discuss how the FitzHugh-Nagumo model established an important conceptual and mathematical framework for investigating fundamental principles of excitability and excitation waves in a computationally simpler setting than previous approaches.

20.1 Introduction

Early models of cell excitability focused on reproducing the qualitative spiking behavior of the action potential. The van der Pol oscillator provided a simple representation of self-sustained oscillations in autoexcitable systems like the heart. However, it did not account for the distinct properties of neurons and other excitable cells that require an external stimulus to trigger an action potential.

A breakthrough came with the Hodgkin-Huxley model in the 1950s. Through pioneering experimental and theoretical work, Hodgkin and Huxley developed the first quantitatively accurate model of neuronal excitation. They showed that action potentials result from non-linear interactions between voltage-gated sodium and

potassium ion channels and membrane potential. This established the foundations of computational neuroscience and quantitative modeling of excitable cells.

However, the Hodgkin-Huxley model is complex, with four non-linear differential equations and multiple voltage-dependent gating variables. This complexity limited analytical insights and computation. A simpler explanatory model was needed to better understand the general principles governing excitability and oscillatory behavior in nerve and muscle fibers.

In the early 1960s, FitzHugh and Nagumo independently developed minimal two-variable models of neuronal excitability that captured the essence of excitable dynamics while removing biochemical details. These “reduced” models provided a mathematically tractable framework for analyzing properties like excitation thresholds and traveling waves.

The goal of this chapter is to introduce the FitzHugh-Nagumo model and analyze its dynamics. We will derive its equations, examine fixed points and oscillations, and discuss its applications to diverse excitable systems. The FitzHugh-Nagumo model established a new paradigm for conceptualizing excitability and remains influential for its insights into universal organizing principles of excitable media.

20.2 The Hodgkin-Huxley Model

The Hodgkin-Huxley model, developed in the 1950s, profoundly transformed the field of neuroscience. Prior to it, neuronal signaling was conceptualized in an oversimplified binary framework, with neurons considered to either fire an action potential or remain inactive. Hodgkin and Huxley shattered this notion by quantifying the ionic underpinnings of excitation. They established that the action potential results from finely coordinated ion movements, firmly establishing membrane biophysics as a quantitative discipline.

It is important to understand the historical context preceding this landmark achievement. In the 1930s, Cole and Curtis developed the voltage-clamp technique, permitting direct measurement of membrane ionic currents for the first time. This opened new insights into neural membrane properties. Further, Hodgkin made pioneering intracellular recordings of the action potential in squid giant axons in the late 1940s, providing new data but leaving the precise mechanisms unclear. Building on these foundations, Hodgkin joined efforts with Huxley at Cambridge University in the early 1950s. Through ingenious experimentation and quantitative modeling, they elucidated the molecular sequence of events underlying excitation. Their paired experimental and theoretical work effectively solved the mystery of how ions propagating an electrical signal across neural membranes.

Conceptually, Hodgkin and Huxley modeled the cell membrane as a capacitor separating two ionic solutions of differing concentration: the extracellular medium and the cytoplasm. To explain ion flux dynamics, they proposed the existence of transmembrane structures, now known as ion channels, that were selectively permeable to ions like sodium and potassium. critically, Hodgkin and Huxley hypoth-

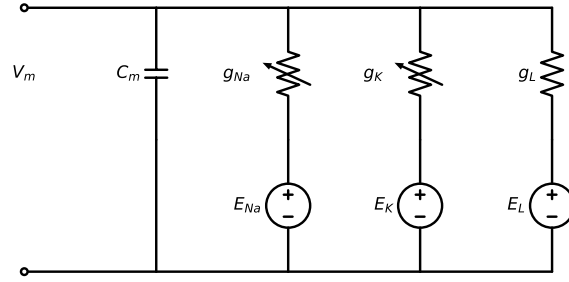


Fig. 20.1 Equivalent circuit diagram of the Hodgkin-Huxley model. The membrane is represented as a capacitor separating two ionic solutions of different concentration. Conductances for sodium (g_{Na}), potassium (g_K) and leak (g_L) currents are modeled as variable resistors in parallel with the membrane. Reversal potentials (V_{Na} , V_K , V_L) drive ion flow down electrochemical gradients.

esized that these channels acted as variable resistors in parallel with the membrane capacitor.

Based on this ionic hypothesis, they developed the equivalent circuit diagram shown in Fig. 20.2 to mathematically describe dynamic electric behavior in excitable cells. The governing equation for this circuit is:

$$I = C_M \frac{dV_M}{dt} + g_{Na}(V_M - V_{Na}) + g_K(V_M - V_K) + g_L(V_M - V_L),$$

where I represents the total membrane current per unit area, C_M is the membrane capacitance, g_{Na} and g_K are the sodium and potassium conductances, V_{Na} and V_K are the ion reversal potentials, and g_L and V_L characterize leak conductance and potential. The reversal potential is the membrane voltage at which net ion flow is zero. Ion flux results from electrochemical gradients comprising concentration differences and voltage potentials. At equilibrium, these counteracting forces balance and establish the reversal potential with no net ion movement. Leak currents, mediated by open leak channels permeable to ions like potassium, sodium and chloride, provide a small continuous current important for maintaining the resting potential.

In Figure 20.2, the sodium and potassium resistors are depicted as variable to model their voltage dependence. Hodgkin and Huxley postulated that each ion channel consists of several subunits that can individually transition between open and closed conformations. They proposed that the entire channel only conducts ions when all subunits adopt the open state. To mathematically represent this, Hodgkin and Huxley defined the sodium and potassium conductances as:

$$\begin{aligned} g_{Na} &= \bar{g}_{Na} m^3 h, \\ g_K &= \bar{g}_K n^4. \end{aligned}$$

where m , h , and n refer to the fraction of subunits in the open state for their respective channels. It was later discovered that voltage-gated sodium channels contain three

identical subunits plus one distinct subunit, while potassium channels contain four identical subunits.

Hodgkin and Huxley modeled the dynamics of subunit conformational changes with:

$$\begin{aligned}\frac{dm}{dt} &= \alpha_m(V_M)(1 - m) - \beta_m(V_M)m, \\ \frac{dn}{dt} &= \alpha_n(V_M)(1 - n) - \beta_n(V_M)n, \\ \frac{dh}{dt} &= \alpha_h(V_M)(1 - h) - \beta_h(V_M)h,\end{aligned}$$

where the transition rates α_i and β_i depend on membrane potential. For brevity, we omit Hodgkin and Huxley's specific functional forms for these rates.

20.3 Motivation for Simplification

While the Hodgkin-Huxley model provided the first successful quantitative description of neuronal action potentials, its complexity also limited its utility for analyzing broader dynamical properties. The model contains four nonlinear differential equations involving several voltage-dependent gating variables. This made analytical insights into its behavior difficult to obtain.

Furthermore, implementing the Hodgkin-Huxley model numerically was computationally untractable at that time due to the need to resolve fast timescales of gating variable kinetics. There was thus a need for simpler models that could retain the essential feature of excitability while facilitating mathematical analysis and simulations. The goal was to distill the Hodgkin-Huxley model down to its bare conceptual minimum in order to understand general principles governing oscillatory and excitable phenomena in nerve and muscle fibers.

This motivated FitzHugh and Nagumo in the early 1960s to independently develop simplified two-variable models of neuronal excitability that abstracted away biochemical details. While less biophysically detailed, these minimal models opened new opportunities to investigate fundamental properties like limit cycles, thresholds for excitation, and traveling wave behaviors through qualitative analysis and simulation—paving the way for novel insights into neural and cardiac dynamics.

20.4 Derivation of the FitzHugh-Nagumo Equations

The FitzHugh-Nagumo model was developed to capture the essential features of excitability in a simplified manner. FitzHugh drew inspiration from the van der Pol os-

cillator, which was known to reproduce properties of autoexcitable systems through a limit cycle behavior.

To mathematically represent neuronal excitability, FitzHugh modified the van der Pol framework such that the system's steady state could transition between stable and unstable regimes. He proposed a two-variable formulation involving a fast membrane potential variable V and slower recovery variable R .

There is some flexibility in how the FitzHugh-Nagumo model is expressed mathematically. A common formulation considers the equations:

$$\frac{dV}{dt} = f(V) - R + I, \quad (20.1)$$

$$\frac{dR}{dt} = \varepsilon(\gamma V - R). \quad (20.2)$$

The function $f(V)$ represents a cubic polynomial feedback for the variable V , which can take positive or negative values depending on the magnitude of V . This nonlinear feedback captures the regenerative dynamics underlying excitability. In this common formulation, the nonlinear feedback is defined as:

$$f(V) = V(a - V)(V - b),$$

with $a < b$. The small parameter $\varepsilon \ll 1$ establishes a time scale separation between the fast variable V and slower variable R . Physiologically, this reflects the separation between rapid membrane dynamics and slower cytoplasmic processes. Due to its slower time scale, R provides negative feedback to V , mimicking neural recovery mechanisms that return the membrane potential to its resting level following excitation. Finally, the parameter I acts as a constant input current, analogous to leak currents that determine the neuronal resting potential. Together, these features allow the FitzHugh-Nagumo model to reproduce the essential excitable spiking dynamics in a simplified mathematical framework.

20.5 Analysis of Steady States

To analyze the fixed points and their stability, we first find the nullclines of the system. For this system, the V -nullcline corresponds to points where $\dot{V} = 0$, and the R -nullcline corresponds to points where $\dot{R} = 0$. Through algebraic manipulation, these nullclines can be written as:

$$R = f(V) + I,$$

$$R = \gamma V.$$

These nullcline equations are plotted in Figure 20.2 for parameter values $a = 1$, $b = 3$, $\gamma = 2.2$, and three different values of the input current $I = 0, 1, 2$. We see that when $I = 0, 1$, the cubic V -nullcline and linear R -nullcline intersect in the left

branch of the cubic where $f'(V) < 0$. In contrast, when $I = 2$ the nullclines intersect in the middle portion where $f'(V) > 0$.

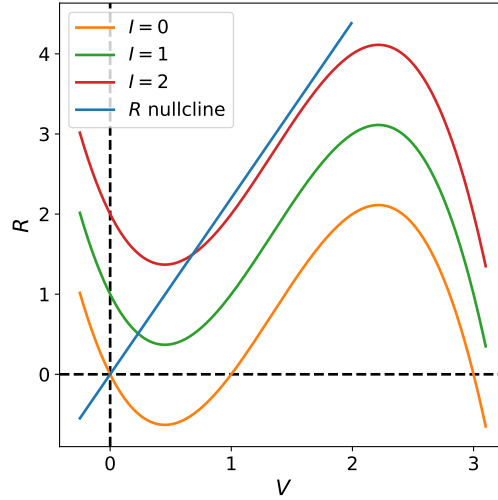


Fig. 20.2 Nullcline diagrams of the FitzHugh-Nagumo system for different values of the input current I . When $I = 0$ and $I = 1$, the cubic V -nullcline intersects the linear R -nullcline in the left branch where $f'(V) < 0$, yielding a stable fixed point. For $I = 2$, the intersection occurs in the middle branch where $f'(V) > 0$, producing an unstable fixed point.

Fixed points correspond to the intersections of the nullclines. To analyze their stability, we calculate the Jacobian matrix:

$$J = \begin{bmatrix} f'(V) & -1 \\ \varepsilon\gamma & -\varepsilon \end{bmatrix}.$$

All entries of the Jacobian are constant except for the term $f'(V)$, which changes sign depending on whether the nullcline intersection occurs in the left or middle branch of the cubic.

The trace (τ) and determinant (Δ) of the Jacobian are:

$$\tau = f'(V) - \varepsilon, \quad \Delta = \varepsilon(\gamma - f'(V))$$

The stability of the fixed points depends on the signs of the Jacobian trace, τ , and determinant, Δ . Specifically, if $f'(V) < 0$, the fixed point is stable with $\tau < 0$ and $\Delta > 0$. When the condition $\varepsilon < f'(V) < \gamma$ is satisfied instead, the fixed point becomes an unstable node or spiral, characterized by $\tau > 0$ and $\Delta > 0$. Physiologically, we expect the parameter ε governing the timescale of recovery variable R to

be much smaller than 1, since R represents a slower process than the membrane dynamics of V . This is consistent with the condition $\varepsilon < f'(V)$.

In the following section, we will conduct a phase plane analysis to show that when the fixed point is unstable, it lies within a stable limit cycle orbit. This limit cycle behavior underlies the oscillations exhibited by excitable systems modeled by the FitzHugh-Nagumo equations.

20.6 Phase Plane Analysis

When the fixed point of the FitzHugh-Nagumo system is unstable, its trajectory will not remain in the vicinity of the fixed point. In a small neighborhood of the unstable fixed point, the system is topologically equivalent to its linearization. Since both eigenvalues of the Jacobian have positive real parts, all trajectories will flow outward from the fixed point. We can also see in figure 20.6 that trajectories far from the origin converge to the V -nullcline to then approach the fixed point. We can apply the Poincaré-Bendixson theorem to show that all trajectory must converge to a limit cycle. The phase space of the FitzHugh-Nagumo system is the plane, which has no singular points. Furthermore, the vector field describing the system is continuous and smooth. Therefore, by the Poincaré-Bendixson theorem, any bounded non-wandering trajectory in the plane must asymptotically approach a fixed point or a limit cycle. However, the only fixed point is unstable, so trajectories cannot approach it. The bounded trajectories must therefore converge to a periodic orbit, namely a stable limit cycle.

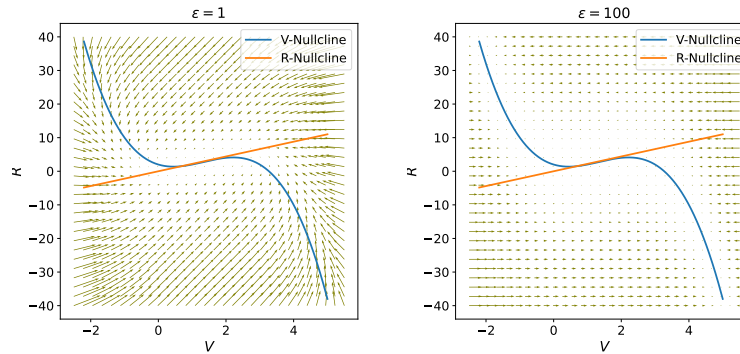


Fig. 20.3 Phase portraits of the FitzHugh-Nagumo oscillator for parameter values $a = 1$, $b = 3$, $\gamma = 2$, and 2 different values of parameter ε , overlaid with nullclines. Arrows indicate vector field flow.

20.7 Relaxation oscillator behavior

When the parameter γ governing the time scale of the recovery variable R is small ($\gamma \ll 1$), the FitzHugh-Nagumo model exhibits relaxation oscillation dynamics. In the phase plane portrait shown in Figure 20.4, the intersection of the nullclines occurs along the middle branch of the cubic curve, where the slope $f'(x) < 0$, rendering the fixed point unstable. This instability positions the system within the basin of attraction of a stable limit cycle.

To understand the trajectory of the limit cycle oscillation, we can examine the vector field flow. When the system is near the left cubic branch, the vector field points sharply to the right, rapidly driving the trajectory upward along the branch. This corresponds to the swift rise of the membrane potential toward its peak value during an action potential. Once the trajectory crosses the cubic branch at its local maximum, the vector field reverses direction, sharply pointing leftward. This causes a rapid decline in the membrane potential as it descends along the left branch. Meanwhile, the recovery variable R continues to move slowly leftward along its linear branch due to its longer timescale ($\gamma \ll 1$).

Eventually, R pulls the trajectory below the cubic branch at a local minimum. At this juncture, the vector field reverses again, and the membrane potential begins a slow ascent along the right cubic branch as R decreases. This gradual motion along the branch represents the extended falling phase and undershoot period of a relaxation oscillation. Consequently, the limit cycle trajectory alternates between rapid excursions along the lateral cubic branches, representing the spike phases, and slower movements along the branches during the falling and recovery phases. This oscillatory behavior closely mimics the characteristic relaxation oscillations observed in autoexcitable systems, such as the van der Pol oscillator and cardiac pacemaker cells.

20.8 Applications to Excitable Systems

While initially developed as a simplified model of neuronal action potentials, the FitzHugh-Nagumo model is universal in its ability to reproduce the core properties of excitable and autoexcitable systems. Through variations in its parameter values, it can replicate important behaviors observed experimentally across diverse excitable cell and medium types.

In neurons, changes in the applied current I allow the model to transition between quiescence at low I and repetitive spiking at higher I above a threshold, closely mimicking rheobase properties. Varying the recovery time scale ε alters spike frequencies, qualitative matching adaptation properties seen in neuronal firing patterns.

In cardiac tissue, decreasing ε slows oscillation periods, akin to effects of slowing heart rates via vagus nerve stimulation. Altering excitability parameters a, b reproduces changes in action potential shape seen with altered ion channel expression lev-

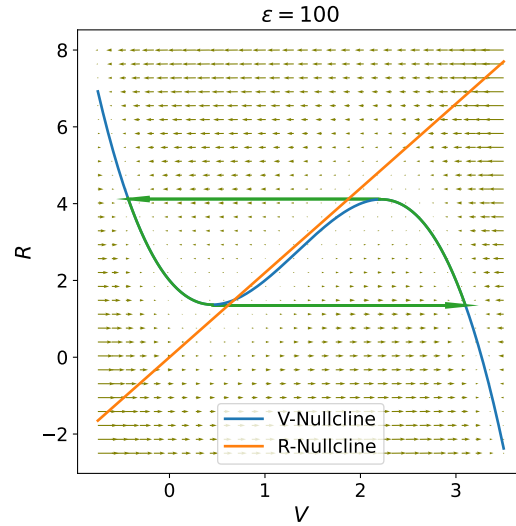


Fig. 20.4 Phase portrait for $\gamma \ll 1$ illustrating relaxation oscillations. Thick green lines trace the limit cycle trajectory, rapidly switching between lateral branches of the V -nullcline at local minima/maxima and slowly creeping along branches. Arrows indicate vector field flow. During rapid excursions, the membrane potential spikes, while the slower recovery variable R modulates the falling and rising phases.

els. Propagating wavefronts of activity in the two-dimensional FitzHugh-Nagumo model with spacial coupling emulate cardiac conduction.

Even in non-biological chemical and physical systems, the model applies. Light-sensitive Belousov-Zhabotinsky reactions and lipid bilayers are autoexcitable, supported by the phase plane framework through a supercritical Andronov-Hopf bifurcation as a control parameter is varied. Self-igniting flames and autocatalytic surface reactions behave as subexcitable media between quiescent and oscillatory phases.

Overall, the FitzHugh-Nagumo equations provide a versatile mathematical description illuminating universal organizing principles for excitability. Its canonical form enables reduced computational requirements compared to detailed biophysical models while still faithfully reproducing qualitative phenomena across media exhibiting rapid switching between stable steady states. This makes it a mainstay for investigating general properties of excitability and excitation wave propagation.

20.9 Discussion

In this chapter, we introduced the FitzHugh-Nagumo model as a simplified two-variable representation of neuronal excitability. While far more abstract than the

original Hodgkin-Huxley formulation, the FitzHugh-Nagumo model effectively distills the essential features of excitable dynamics down to their conceptual minimum.

Through its formulation as a fast-slow system with a cubic nonlinearity and recovery variable, the FitzHugh-Nagumo model can reproduce the hallmark electrical spiking behavior of neurons in a qualitatively accurate manner. Analysis of its nullclines and fixed point stability provided insight into how subthreshold oscillations arise via a supercritical Andronov-Hopf bifurcation.

Examination of the model's phase plane portraits and vector field flows demonstrated its ability to generate relaxation oscillations, closely mimicking the characteristic spike-and-wave profile of excitable membranes. This oscillatory behavior emerges from a stable limit cycle attracted to when the fixed point loses stability.

Importantly, simulations and applications to diverse excitable media indicated the FitzHugh-Nagumo model captures universal organizing principles, not just details specific to neurons. It provides a computationally simpler framework than biophysical models while still faithfully replicating qualitative excitable phenomena.

Overall, the FitzHugh-Nagumo equations established a new paradigm for conceptualizing and mathematically investigating excitability. Their development illuminated fundamental properties of excitable systems and excitation wave propagation in a more tractable setting than earlier approaches. This makes the FitzHugh-Nagumo model highly influential as a foundational tool for studying excitation across many fields.

Chapter 21

Quasisteady State Approximation

Abstract This chapter introduces the concept of quasi-steady state (QSS) approximations, which provide a means of dimensionality reduction for dynamical systems exhibiting separated timescales. Intuition is developed for timescale filtering effects through examination of a generalized system response equation and specific analytical solutions. A prototypical two-dimensional fast-slow system demonstrates how leveraging clear timescale separation via non-dimensionalization and a QSS approximation reduces the system dimensionality. Comparing the full and reduced systems verifies the approach by showing steady states and stability conditions match under the assumption of large timescale separation. Examining eigenstructure reveals trajectories relax to the slow subsystem, where dynamics are dominated, demonstrating how timescale separation enables analytical tractability. The example establishes the methodology and conceptual foundations for employing QSS approximations to analyze multi-timescale dynamics, which commonly arise across fields including physics, biology and chemistry.

21.1 Introduction

Many natural and engineered systems exhibit dynamics that evolve over time governed by underlying mathematical equations. An important class of these dynamical systems involve processes operating on separated timescales, known as multi-timescale systems. In such systems, different state variables respond on distinct fast and slow timescales.

Analyzing multi-timescale dynamics presents challenges due to their inherent complexity from multiple interacting processes. This chapter introduces a useful approach called the quasi-steady state (QSS) approximation. The QSS technique

leverages clear separations between fast and slow timescales to simplify multidimensional systems into reduced representations.

We begin by considering a simple electrical circuit example: an RC low-pass filter. Through circuit analysis, we derive a differential equation governing the output voltage over time. This equation takes a generalized form applicable to broader physical systems. Analyzing solutions for different input frequencies builds intuition on timescale filtering effects.

Next, we present a conceptual two-dimensional dynamical system with variables evolving on separated timescales. By rescaling time, the fast-slow nature becomes evident. Employing the QSS approximation then reduces the dimensionality.

Comparing steady states and stability of the full and reduced systems validates the approach. Examining eigenstructure reveals how trajectories rapidly relax to the slow subsystem, where long-term dynamics emerge. This demonstrates how timescale separation enables analytical insights through dimensionality reduction approaches like QSS approximations.

By working through examples, this chapter aims to develop conceptual and practical understanding of quasi-steady state analysis for multi-timescale dynamical systems. Such systems arise commonly, requiring techniques like QSS approximations to gain tractable descriptions of their behaviors.

21.2 RC Low-Pass Filter Circuit

We begin by considering an RC low-pass filter, whose circuit is illustrated in Fig. 21.1. The filter contains a resistor R and a capacitor C connected in series.

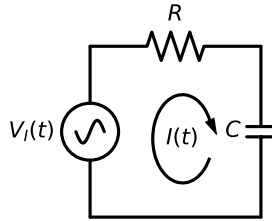


Fig. 21.1 Circuit diagram of an RC low-pass filter.

Let $V_I(t)$ denote the input voltage applied to the filter, $V_R(t)$ the voltage drop across the resistor, and $V_O(t)$ the output voltage, which is equal to the voltage drop across the capacitor. Using Kirchhoff's laws, we can write:

$$V_I(t) = V_R(t) + V_O(t).$$

Since the resistor and capacitor are in series, the current $I(t)$ through them must be the same. Applying Ohm's law to the resistor gives $V_R(t) = R \cdot I(t)$, and using the

capacitor equation gives $I(t) = C dV_O(t)/dt$. Substituting these into Kirchhoff's law equation yields:

$$V_I(t) = RC \frac{dV_O(t)}{dt} + V_O(t).$$

Rearranging this, we obtain a first-order differential equation for the output voltage:

$$\frac{dV_O(t)}{dt} = \frac{1}{RC} (V_I(t) - V_O(t)).$$

This differential equation has a general form that appears in other physical systems as well. In the next section, we rewrite it more abstractly to account for this versatility.

21.3 A Generalized Response Equation

The differential equation describing the output voltage of the RC filter circuit can be generalized to model a broader class of dynamic systems. To account for this versatility, we rewrite the equation more abstractly as:

$$\frac{dx}{dt} = \gamma(\bar{x}(t) - x(t)), \quad (21.1)$$

where $x(t)$ is a general time-varying quantity representing the state of the system, $\bar{x}(t)$ is a time-varying input or driving quantity for the system and γ is a system parameter that determines the response timescale. In the context of the RC filter, $x(t) = V_O(t)$, $\bar{x}(t) = V_I(t)$, and $\gamma = 1/RC$. More generally, this equation can model any physical system whose rate of change is proportional to the difference between its current state and the input/driving quantity.

The general solution to the above equation is:

$$x(t) = e^{-\gamma t} \left[x_0 + \gamma \int_0^t e^{\gamma t'} \bar{x}(t') dt' \right], \quad (21.2)$$

where x_0 is the initial condition. This solution encapsulates both the system's transient response and its behavior under different input conditions $\bar{x}(t)$.

In the next section, we examine some specific cases of interest, including the response to a constant input and a sine wave input. This builds intuition on how system response depends on input characteristics and timescale γ .

21.4 Solution Forms for Specific Input Cases

In this section, we examine the solution to the generalized response equation (21.1) for some important cases of the input $\bar{x}(t)$. This provides insight into how the system responds under different input conditions.

21.4.1 Constant Input

When the input is held at a constant value, the integral term in the solution (21.2) evaluates to simply $\bar{x}\exp(\gamma t) - 1$. Substituting this into the solution yields:

$$x(t) = \bar{x} + e^{-\gamma t} [x_0 - \bar{x}].$$

This solution describes an exponential relaxation process for the state variable $x(t)$. It relaxes from the initial condition x_0 towards the constant input value \bar{x} . The timescale for this relaxation is characterized by the rate parameter γ . Physically, γ represents how quickly the system responds to perturbations from equilibrium.

The larger the value of γ , the faster the relaxation occurs. In the limit of very large γ , the relaxation is essentially instantaneous and the state $x(t)$ remains fixed at the input value \bar{x} . For smaller γ , it takes a longer time approaching $1/\gamma$ for $x(t)$ to settle towards \bar{x} .

21.4.2 Sinusoidal input

When the driving input takes the form of a sinusoid, such that $\bar{x}(t) = e^{i\omega t}$, the solution to the generalized response equation yields additional insight. For this sinusoidal input case, the solution is:

$$x(t) = \left[x_0 - \frac{\gamma}{\gamma + i\omega} \right] e^{-\gamma t} + \frac{\gamma}{\gamma + i\omega} e^{i\omega t}.$$

This solution involves two competing time-dependent terms: an exponential decay governed by γ and an oscillatory term set by the input frequency ω . The relative balance of these terms depends strongly on the ratio of ω/γ .

In the limit of very low input frequencies ($\omega \ll \gamma$), the decaying term becomes negligible after a transient set by $1/\gamma$, compared to the oscillatory term. Hence, $x(t)$ closely follows the input behavior.

Conversely, for high frequencies ($\omega \gg \gamma$), it is now the oscillatory term that is negligible. In this regime, $x(t)$ rapidly decays to zero, showing almost no response to the rapidly fluctuating driving input.

Physically, this frequency-dependent damping behavior illustrates how the intrinsic system timescale γ acts as a low-pass filter, smoothing out input variations that are rapid relative to γ . Only fluctuations with periods much longer than $1/\gamma$ produce significant responses in $x(t)$.

21.4.3 General Time-Varying Input

Thus far we have considered relatively simple constant and oscillatory inputs. However, the generalized response equation is also applicable when the driving quantity $\bar{x}(t)$ exhibits more complex arbitrary time-variation.

Any continuous input defined over a finite time interval $([0, T])$ can be represented as a Fourier series, expressing it as a sum of sinusoidal components with angular frequencies $\omega_n = 2\pi n/T$. Applying the solution derived earlier for sinusoidal inputs, the response $x(t)$ to each Fourier component will take the appropriate sinusoidal-exponential form.

Crucially, the relative balance of decaying and oscillating terms again depends on the ratio ω_n/γ for each frequency component n . Higher frequencies satisfying $\omega_n \gg \gamma$ will see their oscillating terms strongly attenuated according to the low-pass filtering behavior uncovered previously.

Physically, this implies the system effectively smooths and filters out rapidly fluctuating fine structure in the driving input $\bar{x}(t)$. Only variations that are sufficiently slow, with periods much longer than the intrinsic relaxation time $1/\gamma$, produce substantive responses in the state $x(t)$.

Thus for a general time-dependent input, the output $x(t)$ reflects predominantly the large-scale low-frequency properties of the input signal, stripping away higher harmonics. The parameter γ characterizes a sharp cutoff in the frequency spectrum separating meaningful signal from imperceptible noise.

In particular, when the characteristic timescale of the input greatly exceeds the relaxation timescale $1/\gamma$, the system achieves rapid equilibrium with respect to the slowly-evolving driving conditions. This causes the time derivative term in the generalized response equation to become negligible for times past $1/\gamma$. Consequently, the output is able to closely track the input in a quasi-steady manner, with the mathematically simplified relationship of $x(t) \approx \bar{x}(t)$ emerging. This special case forms the theoretical basis for quasi-steady state approximations, whereby timescale separation between driving forces and system responses enables reduced representations of multi-timescale behavior through techniques leveraging the assumption of sluggish input dynamics relative to swift system adjustment.

21.5 Timescale Separation

Many natural and engineered systems exhibit dynamics governed by processes operating on separated timescales. To understand such multi-timescale systems, it is useful to employ approximations that leverage clear differences in timescale.

Consider the following prototypical 2-dimensional dynamical system:

$$\begin{aligned}\frac{dx}{dt} &= \alpha(f(y) - x), \\ \frac{dy}{dt} &= \beta(g(x) - y).\end{aligned}$$

We assume the parameter β governing the y dynamics is much larger than α for the x dynamics ($\beta \gg \alpha$). This implies that y evolves much more rapidly than x .

To make this timescale separation evident, we non-dimensionalize the system by rescaling time as $t' = \alpha t$. In the rescaled timescale, the system is:

$$\frac{dx}{dt'} = f(y) - x, \quad (21.3)$$

$$\frac{dy}{dt'} = \gamma(g(x) - y), \quad (21.4)$$

where $\gamma = \beta/\alpha \gg 1$ represents the large separation between y and x timescales.

This formulation, combined with the results of previous sections, suggests that y will rapidly achieve quasi-steady state balance with respect to changes in the slower-varying x . Specifically, for $\gamma \gg 1$, the rate of change of y (dy/dt') will become negligible on timescales where changes in x (dx/dt') are observable. This allows us to make the quasi-steady state approximation that $y \approx g(x)$, reducing the original 2D system to a simpler 1D form governed by

$$\frac{dx}{dt'} = f(g(x)) - x. \quad (21.5)$$

21.6 Comparing Steady States and Stability of the Full and Reduced Systems

In the previous section, we derived the quasi-steady state (QSS) approximation for a prototypical two-dimensional dynamical system exhibiting timescale separation between the variables. This approximation reduced the dimensionality by eliminating the faster subsystem under the assumption that it relaxes rapidly to quasi-equilibrium.

However, for the QSS approach to be valid, the full and reduced systems should exhibit comparable qualitative behavior on long timescales driven by the slow vari-

able(s). In this section, we test this assumption by directly comparing key properties of the full and approximated systems.

First, we analyze the reduced 1D quasi-steady state approximation given by Eq. (21.5). At steady state, the time derivative must equal zero, yielding the steady state condition $x^* = f(g(x^*))$.

To assess the stability of the system, we can perform a linear stability analysis. The Jacobian and its single eigenvalue are simply the partial derivative of the right-hand side of Eq. (21.5) with respect to x , evaluated at the equilibrium point. That is,

$$J = \lambda = f'(g(x^*))g'(x^*) - 1. \quad (21.6)$$

Then, if $\lambda < 0$, the steady state is locally asymptotically stable.

For the full 2D system, steady states satisfy both $dx/dt' = 0$ and $dy/dt' = 0$, yielding the equilibrium conditions $x^* = f(y^*)$ and $y^* = g(x^*)$. Hence, the steady state values of x^* are the same solutions to $x^* = f(g(x^*))$ as in the 1D reduced system.

To analyze stability, we compute the Jacobian matrix of the 2D system:

$$J = \begin{bmatrix} -1 & f'(y^*) \\ \gamma g'(x^*) & -\gamma \end{bmatrix}.$$

Its eigenvalues are given by:

$$\begin{aligned} \lambda_1 &= -\frac{\gamma+1}{2} + \frac{\sqrt{(\gamma+1)^2 - 4\gamma(1 - f'(y^*)g'(x^*))}}{2}, \\ \lambda_2 &= -\frac{\gamma+1}{2} - \frac{\sqrt{(\gamma+1)^2 - 4\gamma(1 - f'(y^*)g'(x^*))}}{2}. \end{aligned}$$

Using the large timescale separation assumption of $\gamma \gg 1$, we obtain the following simplified expressions for the eigenvalues—see Eq. (21.6):

$$\lambda_1 \approx f'(y^*)g'(x^*) - 1 = \lambda, \quad (21.7)$$

$$\lambda_2 \approx -\gamma. \quad (21.8)$$

Geometrically, this reveals that, initially, trajectories will evolve rapidly along the direction of the fast eigenvector v_2 , on a timescale of $1/\lambda_2 \approx 1/\gamma$. On this transient timescale, the system approaches the slow manifold aligned with the slow eigenvector v_1 . Thereafter, with $-\gamma \ll \lambda_1$, the system dynamics are dominated by the slower motion along v_1 , characterized by the velocity given by the eigenvalue $\lambda_1 = \lambda \approx f'(y^*)g'(x^*) - 1$.

Although the full system displays brief two-dimensional behavior, the presence of distinctly separated timescales facilitates rapid relaxation. This allows the one-dimensional reduced approximation, which focuses solely on the slow component v_1 , to accurately describe the system's behavior near steady states that are comparable to those of the full system. Consequently, the significant difference in timescales enables effective dimensionality reduction, justifying the analysis of the simplified

one-dimensional system for gaining insights into the long-term, multi-timescale dynamics.

21.7 Conclusions

In this chapter, we introduced and demonstrated the quasi-steady state (QSS) approximation technique for analyzing multi-timescale dynamical systems. By considering a generalized response equation, we developed intuition for how systems respond to different input conditions depending on their intrinsic timescale.

We then presented a prototypical two-dimensional dynamical system with separated timescales as a test case. Non-dimensionalizing time made the fast-slow behavior evident. Leveraging this timescale separation, we employed the QSS approximation to reduce the system dimensionality.

Comparing the full and reduced systems' steady states and stability validated the approximation approach. Exploiting the assumption of wide timescale gap, we showed the conditions for stable equilibrium match between the two descriptions.

Examining the eigenstructure revealed trajectories' initial rapid evolution along the fast eigenmode, before relaxing onto the slower manifold. Thereby, the long-term behavior reduces dimensionally to motion along this slow subsystem.

This example demonstrated how timescale separation enables analytical tractability for multi-timescale problems. By projecting dynamics onto slower variables after an initial transient, QSS approximations provide qualitative and sometimes quantitative insight into long-term behaviors of interest. Overall, this chapter established the intuition, concepts and methodology behind QSS analysis of multi-timescale dynamics.

Chapter 22

Hematopoiesis Regulation

Abstract This chapter reviews key concepts of hematopoiesis and develops a mathematical model of erythropoiesis regulation via negative feedback to gain insights into hematopoietic homeostasis. The model describes the dynamics of erythrocyte and erythropoietin levels over time using a system of ordinary differential equations that captures the essential feedback inhibition mechanism. It utilizes a quasi-steady state approximation to simplify the model formulation. Steady state and stability analyses reveal the equilibrium conditions and relaxation behavior, providing a quantitative framework to understand how modulating degradation rates, sensitivity thresholds, and other regulatory parameters impacts the system response time and red blood cell production requirements. While simplified, the model demonstrates how even basic representations can provide mechanistic insights. This introduces mathematical modeling as a tool to rigorously study the dynamics of complex physiological systems like blood cell generation.

22.1 Introduction

Hematopoiesis precisely regulates blood cell production through negative feedback control. In this chapter we develop a mathematical model of erythropoiesis dynamics using ordinary differential equations. The model represents interactions between circulating erythrocytes and erythropoietin levels, which provides a framework to explore homeostasis.

A key feature is applying a quasi-steady state approximation. This leverages the large difference in erythrocyte and erythropoietin degradation timescales, allowing elimination of the fast erythropoietin variable. This simplification produces a reduced model focusing on long-term erythrocyte behavior while retaining feedback dynamics.

Analyzing the reduced model yields insights into steady states, stability, and response time properties of negative feedback regulation. Comparisons with literature validate the model's biological relevance.

This chapter demonstrates how even simple mathematical models augmented with techniques like quasi-steady state approximations can generate mechanistic understanding of physiological regulation beyond observation alone.

22.2 Hematopoiesis Physiology

Hematopoiesis is the process of blood cell production that continuously replenishes various circulating cell types. This ensures a healthy supply of erythrocytes, leukocytes, and platelets, which all play crucial roles in oxygen transport, immune defense, and hemostasis. The most common site of blood cell production is the spongy tissue inside bones called bone marrow. Hematopoiesis that occurs in the bone marrow is called medullary hematopoiesis. Less often, hematopoiesis takes place in other parts of the body, like the liver and spleen. Hematopoiesis that occurs outside of the bone marrow is called extramedullary hematopoiesis (Jaffe et al., 2024).

Red blood cells, also called erythrocytes, carry oxygen from the lungs to tissues and carbon dioxide back to the lungs. They are the most abundant cell type in blood. The production of red blood cells is termed erythropoiesis. White blood cells, or leukocytes, fight infection and protect the body from pathogens. They also destroy abnormal cells. Leukocyte production is termed leukopoiesis. Platelets, or thrombocytes, are cell fragments that clump to form clots after injury and create seals in damaged tissue to prevent blood loss. Their production is called thrombopoiesis.

Hematopoiesis begins with an originator cell common to all blood cell types. It's called a hematopoietic stem cell (HSC). An HSC develops into a precursor cell, or "blast" cell. A precursor cell is on track to become a specific type of blood cell, but it's still in the early stages. A precursor cell goes through several cell divisions and changes before it becomes a fully mature blood cell.

Hematopoiesis is tightly regulated through negative feedback loops that help maintain optimal blood cell levels. When cell concentrations rise in circulation, signals are sent to slow or inhibit further hematopoietic production. This prevents overabundance of cells.

Specifically for erythropoiesis, elevated red blood cell counts or hemoglobin trigger the kidneys to decrease secretion of erythropoietin (EPO). Since EPO stimulates proliferation and differentiation of red blood cell precursors in the bone marrow, lowered EPO then downregulates these processes. This negative feedback mechanism helps stabilize red blood cell production.

A similar process occurs for thrombopoiesis. Higher platelet counts inhibit thrombopoietin secretion by the liver, which dampens megakaryocyte development and thrombopoiesis in the bone marrow.

Meanwhile, leukocyte regulation involves feedback suppression via certain cytokines. Immune cells secrete less of growth factors like G-CSF and GM-CSF when

higher leukocyte levels are detected. This decreased cytokine stimulation, in turn, curbs further leukopoiesis.

Mature circulating blood cells provide another level of negative feedback regulation. As their numbers increase systemically, fully differentiated cells secrete signaling molecules that act to inhibit further proliferation and self-renewal of hematopoietic stem cells (HSCs) in the bone marrow niche. This feedback mechanism helps balance the production of new cells from the HSC pools with the clearance of older senescent cells from circulation.

As new blood cells are generated, aging cells are cleared through specialized elimination pathways. Mature red blood cells, with their biconcave disc morphology, are superbly adapted for oxygen transport as they flexibly navigate narrow vasculature. However, after approximately 120 days in circulation, they become increasingly fragile. Macrophages in the spleen and liver then break down senescent erythrocytes.

Upon fulfilling their immune duties, white blood cells undergo programmed cell death, or apoptosis. Lifespans vary considerably by subtype, from roughly one day for granulocytes like neutrophils, eosinophils and basophils, to months for B cells, and even decades for memory T cells.

Platelets, as small cytoplasmic fragments released from megakaryocytes, play a vital role in initiating clot formation. Yet due to their inherent fragility, platelets are removed from circulation after about 10 days as they become progressively less sturdy.

Precise coordination between ongoing production and timely degradation of aging cells through specialized pathways ensures the balanced homeostasis of distinct blood cell populations essential for normal physiological functioning. Close regulation at both stages is critical for maintaining healthy hematopoiesis.

22.3 Mathematical modeling of erythropoiesis

We propose the following mathematical model to capture the dynamics of erythropoiesis regulation via negative feedback:

$$\frac{dE}{dt} = k_E P - \gamma_E E, \quad (22.1)$$

$$\frac{dP}{dt} = k_P \frac{K_E}{K_E + E} - \gamma_P P. \quad (22.2)$$

This mathematical model of erythropoiesis regulation via negative feedback captures the essential dynamics governing the process in a simplified yet biologically meaningful way. It describes the time-evolution of two key variables—circulating erythrocyte levels (E) and erythropoietin concentration (P)—using a system of ordinary differential equations under reasonable assumptions.

The underlying model assumptions include a stationary hematopoietic stem cell population, which focuses the model on erythrocyte production and turnover dynamics without explicitly modeling upstream hematopoiesis. Linear degradation terms represent natural removal of erythrocytes and erythropoietin from circulation at rates γ_E and γ_P , respectively.

A key component is the negative feedback Michaelis-Menten function $K_E/(K_E + E)$, where the half-saturation constant K_E determines the erythrocyte level at which erythropoietin production is reduced by half. This formalizes the process by which increased E signals lower P , stabilizing erythropoiesis. See Chapter 24 for more detail.

The production rates k_E and k_P provide a quantitative description of erythrocyte generation and erythropoietin secretion. Together with the other terms and parameters, this framework can be analyzed mathematically and simulations run to examine behaviors like equilibrium states and responsiveness.

22.4 Quasi-steady state approximation

We observe that erythrocytes have a mean half-life on the order of 120 days, while erythropoietin's half-life is only a few hours (Bélair et al., 1995). This implies that the degradation rate of EPO, γ_P , greatly exceeds that of red blood cells, γ_E . Mathematically, we can assume that $dP/dt \approx 0$, representing a quasi-steady state where EPO concentration adjusts much more rapidly than erythrocyte levels change.

With this approximation, the EPO dynamics can be reduced to:

$$P \approx \frac{k_P}{\gamma_P} \frac{K_E}{K_E + E}.$$

Substituting back into the original equation for dE/dt yields:

$$\frac{dE}{dt} = k_e \frac{K_E}{K_E + E} - \gamma_E, \quad (22.3)$$

where the effective erythrocyte production rate is $k_e = k_E k_P / \gamma_P$.

This quasi-steady state approximation produces a simpler reduced model by eliminating the fast EPO timescale. While an idealization, it retains the negative feedback dynamics and steady states of the full system for analytically exploring long-term erythrocyte behavior.

22.5 Steady State Analysis

The steady state condition for the reduced dynamical system (22.3) is $dE/dt = 0$, which transforms into

$$\frac{k_e}{\gamma_E} \frac{K_E}{K_E + E^*} = E^*,$$

where E^* represents the steady state value of E . The left-hand side of the above equation is a decreasing function of E , while the right-hand side is increasing. Thus, the dynamical system has a single positive steady state.

Solving the last equation for k_e gives:

$$k_e = \gamma_E E^* \left(1 + \frac{E^*}{K_E} \right). \quad (22.4)$$

Notice that, if E^* remains constant, k_e is an increasing function of γ_E and a decreasing function of K_E .

22.6 Stability Analysis

Define the function corresponding to the right-hand side of the reduced model as

$$f(E) = k_e \frac{K_E}{K_E + E} - \gamma_E.$$

The stability of the steady state is determined by the sign of $f'(E^*)$. After taking the derivative, we obtain

$$f'(E^*) = -\gamma_E \left(\frac{k_e}{\gamma_E} \frac{K_E}{(K_E + E^*)^2} + 1 \right).$$

Observe that $f'(E^*)$ is negative, implying that the steady state is stable.

Substituting the expression for k_e in (22.4) yields:

$$f'(E^*) = -\gamma_E \left(\frac{E^*}{E^* + K_E} \right).$$

The value of $f'(E^*)$ determines the relaxation time of the dynamical system; the more negative it is, the faster the system returns to steady state after a perturbation. Interestingly, increasing γ and/or decreasing K_E under constant E^* accelerates this relaxation dynamics.

The regulatory mechanisms governing hematopoiesis appear designed to restore basal blood cell levels as quickly as possible following a perturbation such as hemorrhage. As shown in the stability analysis, decreasing the half-saturation constant K_E or increasing the degradation rate γ_E serves to accelerate the dynamical system's relaxation back to the erythrocyte steady state E^* . However, holding E^* constant requires compensating through higher erythrocyte production rate k_E —see (22.4). Therefore, while modulating parameters like K_E and γ_E can minimize the system's

response time, this comes at the cost of increased red blood cell generation via elevated k_E under homeostasis.

It is remarkable that adult humans have the capacity to regenerate their entire complement of blood cells every 7 years through hematopoiesis (Mackey, 2001). This estimated production of an individual's body weight in red blood cells, white blood cells, and platelets over such a short timeframe indicates the exquisitely optimized nature of blood cell generation and regulation in humans.

Overall, the model analysis suggests that hematopoietic regulatory mechanisms have evolved to prioritize rapid restoration of baseline blood cell populations through adjustable response kinetics. This analysis illustrates how quantitative mechanistic understanding of human blood cell dynamics and how perturbations impact the highly integrated negative feedback system sustaining blood homeostasis.

22.7 Discussion

This chapter developed a mathematical model of erythropoiesis regulation via negative feedback that provided insights into hematopoietic homeostasis. Steady state, stability, and response time analyses revealed key properties of the negative feedback system. However, opportunities remain to enhance the model's scope and realism.

While the model illustrated how feedback control stabilizes erythron levels, a primary limitation was the omission of precursor cell dynamics. Explicitly modeling erythroid progenitor proliferation, differentiation, and apoptosis could provide a more mechanistic representation of how feedback cues impact red blood cell output over time.

Additionally, simplifying assumptions around exponential decay kinetics for cells and EPO ignored spatial and temporal variations inherent in biological systems. Incorporating distributed or age-structured terms may better represent the time-delayed responses between changes in populations, signaling factors, and feedback regulation.

The model also considered erythropoiesis independently from cross-talk with other cell lineages. In reality, erythropoiesis is integrated within broader networks regulating hematopoietic production. Accounting for cross-regulation could alter predictions, particularly regarding system recovery following pan-lineage perturbations.

Parameter values were estimated from literature rather than calibrated to experimental data, neglecting biological variability. Tailored calibration approaches may enhance the model's clinical and predictive applicability.

Despite these limitations, the model provided a useful foundation for quantitative exploration of erythropoietic control mechanisms. Future efforts expanding on precursor dynamics, spatiotemporal details, and inter-lineage interactions have potential to deepen understanding of normal and dysregulated hematopoietic regula-

tion. Mathematical modeling serves as a valuable tool complementing experimental investigation of complex biological systems like hematopoiesis. Overall, this work demonstrated how even simple models can provide mechanistic insights into negative feedback regulation sustaining blood cell homeostasis.

Chapter 23

A.V. Hill and the Origins of Modern Biophysics

Abstract Archibald Vivian Hill was a pioneering British physiological scientist in the early 20th century. Through his meticulous and rigorous experimental work combined with quantitative modeling approaches, A.V. Hill made seminal discoveries that laid the foundations of the field now known as biophysics. His most groundbreaking contributions were pioneering studies on two key physiological systems: muscle function and the cooperative binding of oxygen to the respiratory protein hemoglobin. This chapter will provide historical context by outlining Hill's education and early career development. It will then highlight his landmark discoveries on muscle physiology and hemoglobin cooperativity, which led to the derivation of the eponymous "Hill equation." By examining Hill's career and key discoveries, this chapter aims to convey his enduring scientific legacy and rigorous quantitative experimental approach.

23.1 Education and Early Career

Archibald Vivian Hill was born in Bristol, England on September 26, 1886. He attended Blundell's School in Tiverton, where he demonstrated academic promise and was awarded scholarships to Trinity College, Cambridge. At Cambridge, Hill studied mathematics and achieved Third Wrangler status on the prestigious Mathematical Tripos examination in 1907.

Upon graduation, Hill was encouraged by his professor Walter Morley Fletcher to pursue physiology. While still an undergraduate, Hill published his first paper deriving what became known as the Langmuir equation. Under the supervision of John Newport Langley, Hill's 1909 publication derived both equilibrium and exponential association forms of the Langmuir isotherm to model nicotine and curare binding at neuromuscular junctions. This work represented an important early application of receptor theory.

In 1910, Hill was awarded a fellowship at Trinity College. He spent the following winter of 1910-1911 in Germany conducting research. From 1911-1914 at Cam-

bridge, Hill continued his investigations of muscle contraction physiology while also studying nerve impulse transmission, hemoglobin binding properties, and animal calorimetry—collaborating with eminent scientists including Gaskell, Barcroft and Adrian.

By 1914, Hill had been appointed University Lecturer in Physical Chemistry at Cambridge, showing early interdisciplinary interests. During World War I, he served as an artillery officer in the Royal Garrison Artillery, rising to the rank of Major and directing experimental research sections. Hill's distinguished early career foreshadowed his later contributions to quantitative physiology.

23.2 Studies on Muscle Physiology

Hill made significant contributions to understanding muscle physiology through rigorous experimentation and quantitative analysis. After the war, Hill returned to Cambridge before accepting a faculty chair at Manchester University (Bassett, 2002).

Using calorimetry techniques, Hill measured the heat produced during different phases of muscle contraction. This allowed him to correlate metabolic heat with biochemical and cellular events underlying muscle function. For this work elucidating muscle energetics, Hill received the 1922 Nobel Prize in Physiology or Medicine.

Through force measurements and biochemical analysis, Hill identified distinct phases of the muscle contraction-relaxation cycle. He discovered the dependence of muscle power output on velocity of shortening.

In 1923, Hill accepted a professorship at University College London where he continued research on muscle biomechanics and energetics.

In 1938, Hill proposed his influential three-element muscle model to account for experimental observations of contraction force, velocity relationships, and heat production dynamics. The model conceptualized the muscle as consisting of contractile, parallel elastic and series elastic elements. The contractile element, comprising actin and myosin filaments, generates force during activation and is responsible for shortening. The parallel and series elements represent passive connective tissue forces and intrinsic fiber elasticity, respectively.

Hill's model integrated biomechanical, biochemical and energetic aspects of muscle function into a unified quantitative framework. It proved highly influential and was verified by later experimental studies. Throughout the 1950s, Hill continued multidisciplinary muscle investigations using techniques such as calorimetry, biochemistry and force measurements. His work established foundations for modern structural and molecular models of muscle contraction.

23.3 Hemoglobin saturation and the Hill equation

In the early 1900s, Hill began investigating factors influencing oxygen delivery and transport. In a 1910 paper (Hill, 1910), he studied the saturation curve of hemoglobin binding oxygen. Hill introduced an empirical equation to describe the saturation fraction as a function of oxygen concentration. This equation, now known as the Hill equation, assumed that hemoglobin exists in different aggregation states. It takes the form:

$$sf = \frac{x^{n_H}}{x^{n_H} + K_H^{n_H}},$$

where sf is the saturation fraction, x is the oxygen concentration, K_H is the half-saturation constant, and n_H represents the average degree of hemoglobin aggregation, as interpreted by Hill.

In 1913, Hill further studied this empirical equation, modeling stepwise oxygen binding to hemoglobin aggregates Hill1913. He discovered that the equation could be derived from the assumption that binding one oxygen molecule increases affinity for the next. This established the fundamental concept of “cooperativity” that would be formally introduced into science somewhat later.

Hill’s remarkable insight provided the first quantitative framework describing cooperativity using what is now known as the Hill equation. This unified mathematical model of multi-site cooperative binding revolutionized the field and remains widely used over a century later.

23.4 Discussion

Through meticulous experimentation and quantitative modeling, Hill established key concepts still central to biochemistry today. His derivation of the empirical Hill equation revolutionized descriptions of cooperative systems, setting a mathematical framework still widely applied over a century later.

Hill integrated studies of muscle contraction mechanistics, energetics and biochemistry integrated disciplines and advanced quantitative rigor in the field. His three-element muscle model conceptualized the contractile ensemble stimulating molecular-level investigations.

While refined over decades, Hill established foundations for modern biophysics. His achievements and intellectual legacy continue enabling advances at interfaces of physics, chemistry and biology. Hill exemplified how experiment and theory synergistically advance life sciences research.

Chapter 24

Ligand-Receptor Dynamics

Abstract In this chapter we introduce a mathematical modeling framework based on chemical kinetics to quantitatively analyze ligand-receptor binding dynamics. Receptor-ligand interactions are represented as reversible chemical reactions, and rate equations are derived from the law of mass action for receptors with single and multiple independent binding sites. The models are expanded to incorporate cooperative binding. The equilibrium saturation fraction relating receptor binding-site occupancy to concentration, affinity, and cooperativity parameters is derived for the general cooperative case. The model provides insights into ligand binding profiles and how factors like cooperativity influence equilibrium behavior. This kinetic modeling approach offers a rigorous foundation for systematically incorporating molecular complexity to quantitatively analyze receptor-mediated cellular signaling through ligand-receptor interactions.

24.1 Introduction

Ligand-receptor interactions play a crucial role in many biological processes. Receptors act as signalling molecules that initiate intracellular responses upon binding to extracellular ligands. Some examples of important ligand-receptor systems include hormone-receptor interactions regulating metabolic functions, immunological reactions mediated via antigen-antibody binding, and neurotransmission via neurotransmitter receptors in the nervous system. Proper understanding of the dynamics of ligand-receptor binding is fundamental to elucidating the mechanisms of various physiological and pathological processes.

Chemical kinetics provides a powerful framework to mathematically model and analyze ligand-receptor interactions. In this chapter, we develop a kinetic framework to describe the dynamics of ligand binding to cell surface receptors. We start from the simplest case of a single ligand binding to a receptor with a single binding site. We then extend this model to account for receptors with an arbitrary number of

independent binding sites. Finally, we incorporate the phenomenon of cooperativity in ligand binding to model more complex receptor systems.

In this chapter we discuss the basic concepts of chemical reactions relevant to ligand-receptor binding, introduce chemical kinetics and derive the rate equations based on mass-action law, present kinetic models for single-site and multi-site binding and extend these models to cooperative binding.

24.2 Chemical Reactions

Chemical reactions describe the process of interconversion between reactants and products. Ligand-receptor binding can be regarded as a chemical reaction between the reactants, ligand (L) and free receptor (R), converting to products bound ligand-receptor complex (R_L).

Based on their molecular steps, chemical reactions can be categorized as elementary or non-elementary. Elementary reactions involve a single concerted reaction step where all reactants are transformed to products simultaneously. Ligand-receptor binding often approximates an elementary reaction process where the ligand directly binds to the receptor in a single step without forming any intermediate complexes.

In addition, chemical reactions can either be reversible or irreversible. The binding of ligand to receptor is generally reversible in nature, which allows the complex to dissociate back to free entities. The reaction representing ligand-receptor binding can thus be written as:



Here, the forward reaction represents ligand binding to receptor to form the complex R_L , while the reverse reaction denotes dissociation of the complex back to free ligand and receptor. The double arrows indicate that this is a reversible process, in contrast to an irreversible reaction which only proceeds in one direction. Given these basic properties of chemical reactions, we now introduce the kinetic theory to quantitatively model ligand-receptor binding dynamics.

24.3 Chemical Kinetics Approach

Chemical kinetics provides a quantitative framework to study the rates of chemical reactions based on experimental observations. For elementary reactions involving single reaction steps like ligand-receptor binding, kinetics theory relies on the law of mass action.

The law of mass action states that the rate of a reaction is directly proportional to the active collision frequency of reactants. This is because for the reaction to occur, the reactant molecules must collide with sufficient energy and correct orientation for the reaction to take place. The frequency of successful collisions is directly pro-

portional to the chance of reactants meeting. This chance is given by the product of their concentrations at the reaction site. Therefore, the reaction rate is proportional to the product of reactant concentrations.

We use square brackets ($[\cdot]$) to represent the molar concentrations of species in a solution. The concentrations as opposed to amounts or numbers give an indication of how dense or dilute the reactants and products are in the reaction volume. This is important because reaction rates depend on the volume as well as amounts of substances present.

For the reversible binding reaction in Eq. 24.1, application of the law of mass action gives:

$$v_{\text{forward}} = k_{\text{on}}[\text{L}][\text{R}], \quad (24.2)$$

$$v_{\text{reverse}} = k_{\text{off}}[\text{R}_L]. \quad (24.3)$$

A reaction is said to be at chemical equilibrium when the forward and reverse reaction rates become equal, such that there is no further change in concentrations with time. At equilibrium, $v_{\text{forward}} = v_{\text{reverse}}$, which upon substitution from above leads to the relation:

$$K_D = \frac{k_{\text{off}}}{k_{\text{on}}} = \frac{[\text{L}][\text{R}]}{[\text{R}_L]} \quad (24.4)$$

Parameter K_D is known as the equilibrium or dissociation constant, and characterizes the equilibrium of the reversible binding reaction.

24.4 Modeling Ligand Binding to a Receptor with Single Binding Site

We consider the case where the receptor R has a single binding site for ligand L. The reversible binding reaction is given by Eq. 24.1.

Here we make two assumptions: (1) the free ligand concentration $[\text{L}]$ is kept constant, and (2) the total receptor concentration $[\text{R}_T] = [\text{R}] + [\text{R}_L]$ remains constant.

From the law of mass action, the rate equations are:

$$v_{\text{forward}} = k_{\text{on}}[\text{L}][\text{R}],$$

$$v_{\text{reverse}} = k_{\text{off}}[\text{R}_L].$$

From this, we can write the rate of change of complex concentration $[\text{R}_L]$ as:

$$\frac{d[\text{R}_L]}{dt} = k_{\text{on}}[\text{L}][\text{R}_T] - k_{\text{off}}[\text{R}_L].$$

This differential equation can be solved analytically to obtain:

$$[\text{R}_L] = \frac{k_{\text{on}}[\text{L}][\text{R}_T]}{k_{\text{off}} + k_{\text{on}}[\text{L}]} \left(1 - e^{-(k_{\text{off}} + k_{\text{on}}[\text{L}])t} \right). \quad (24.5)$$

This solution gives the time-dependent concentration of ligand-receptor complex under the stated assumptions. The concentration of free receptors can be computed at any time as $[R] = [R_T] - [R_L]$.

At steady state, the concentration $[R_L]$ becomes time-independent. Taking the time derivative to be zero gives the steady state solution:

$$\overline{[R_L]} = \frac{k_{\text{on}}[L][R_T]}{k_{\text{off}} + k_{\text{on}}[L]}. \quad (24.6)$$

This represents an equilibrium condition where the forward and reverse reaction rates balance each other. The fraction of receptors bound at equilibrium is given by:

$$f_{\text{bound}} = \frac{\overline{[R_L]}}{[R_T]} = \frac{k_{\text{on}}[L]}{k_{\text{off}} + k_{\text{on}}[L]} = \frac{[L]}{K_D + [L]}.$$

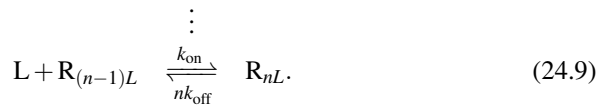
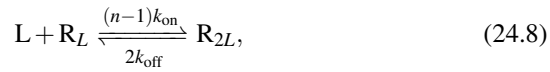
The fraction of free receptors is given by

$$f_{\text{free}} = \frac{K_D}{K_D + [L]}.$$

We thus obtain simple analytical expressions relating the steady state complex concentration and fraction of free and bound receptors to the system parameters like ligand concentration and kinetic rate constants.

24.5 Modeling Ligand Binding to Receptors with Multiple Independent Binding Sites

We extend the previous model to allow binding of multiple ligands independently to a receptor with n equivalent binding sites. Let R represent free receptors and R_{mL} the concentration of receptors with m ligands bound. The general reaction scheme can be written as:



We assume the ligand can bind to any of the n available sites with the same rate constants k_{on} and k_{off} . The factors multiplying k_{on} and k_{off} respectively stand for the number of empty binding sites and the number of bound ligands in each reaction.

According to the law of mass action, the net rate of R_{mL} formation is:

$$v_m = (n - m + 1)k_{\text{on}}[L][R_{(m-1)L}] - mk_{\text{off}}[R_{mL}] \quad \forall m = 1 \text{ to } n.$$

From this, the equilibrium binding equation in terms of total ligand $[L]$ is:

$$K_D = n \frac{[L][R]}{[R_L]} = \frac{n-1}{2} \frac{[L][R_L]}{[R_{2L}]} = \dots = \frac{1}{n} \frac{[L][R_{(n-1)L}]}{[R_{nL}]}.$$

This represents a system of n equations with $n+1$ unknowns. When completed with the conservation equation,

$$[R] + [R_L] + \dots + [R_{nL}] = [R_T],$$

it can be solved to obtain steady state concentrations of all receptor states:

$$[R_{mL}] = [R_T] \frac{m!}{(n-m)!n!} \frac{([L]/K_D)^m}{(1 + [L]/K_D)^n} \quad \forall m = 1 \text{ to } n.$$

In particular, the fraction of free and full receptors are given by:

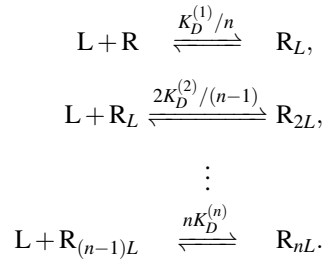
$$f_{\text{free}} = \left(\frac{1}{1 + [L]/K_D} \right)^n,$$

$$f_{\text{full}} = \left(\frac{[L]/K_D}{1 + [L]/K_D} \right)^n.$$

24.6 Extension to Cooperatively Binding Ligands

So far we have assumed independent, non-interacting binding of ligands to receptor sites. However, many receptor-ligand systems exhibit cooperative binding where ligand affinity increases with the occupancy of neighboring sites.

To incorporate cooperativity, we modify the binding scheme in previous section such that the dissociation constant, $K_D^{(m)}$, of the m th binding site depends on the number of ligands $m-1$ already bound:



The dissociation constants are defined as:

$$K_D^{(m)} = \frac{K_D}{K_A^{m-1}},$$

where $K_A \leq 1$ is the cooperativity factor and K_D is the affinity of first site.

In terms of total ligand $[L]$, the equilibrium binding equations for the above reaction set are:

$$K_D = n \frac{[L][R]}{[R_L]} = \frac{n-1}{2} K_A \frac{[L][R_L]}{[R_{2L}]} = \dots = \frac{1}{n} K_A^{n(n-1)/2} \frac{[L][R_{(n-1)L}]}{[R_{nL}]}.$$

This represents a system of n equations with $n+1$ unknowns. When completed with the conservation equation,

$$[R] + [R_L] + \dots + [R_{nL}] = [R_T],$$

it can be solved to obtain steady state concentrations of all receptor states:

$$[R_{mL}] = [R_T] \frac{\binom{n}{m} \left[\frac{K_A^{(m-1)/2} [L]}{K_D} \right]^m}{\sum_{i=0}^n \binom{n}{i} \left[\frac{K_A^{(i-1)/2} [L]}{K_D} \right]^i}.$$

By defining $K_H = K_D / K_A^{(n-1)/2}$ the above solutions can be rewritten as

$$[R_{mL}] = [R_T] \frac{\binom{n}{m} \left[\frac{[L]}{K_A^{(n-m)/2} K_H} \right]^m}{\sum_{i=0}^n \binom{n}{i} \left[\frac{[L]}{K_A^{(n-i)/2} K_H} \right]^i}. \quad (24.10)$$

Consider the term

$$\binom{n}{i} \left[\frac{[L]}{K_A^{(n-i)/2} K_H} \right]^i.$$

Notice that it is independent of K_A when $i = 1, n$; it equals one when $i = 1$ and is equal to $([L]/K_H)^n$ when $i = n$. For all other intermediate values of i , the given term is a decreasing function of K_A that tends to zero as $K_A \rightarrow \infty$. From this, we can prove that

$$\lim_{K_A \rightarrow \infty} [R] = \frac{1}{1 + ([L]/K_H)^n}, \quad (24.11)$$

$$\lim_{K_A \rightarrow \infty} [R_{mL}] = 0, \quad m = 1 \dots n-1, \quad (24.12)$$

$$\lim_{K_A \rightarrow \infty} [R_{nL}] = \frac{([L]/K_H)^n}{1 + ([L]/K_H)^n}. \quad (24.13)$$

This means that, in the limit of very high cooperativity, ligand binding occurs in an “all-or-none” fashion instead of progressively as in the independent case.

24.7 Saturation Fraction, Cooperativity and the Hill Function

In ligand-binding experiments, the saturation fraction (σ) is typically measured. This represents the fraction of receptor binding sites that are bound ligands. Specifically, σ is calculated as the ratio of total ligand-occupied binding sites to the total number of binding sites across all receptors. For receptors with n binding sites that bind ligand cooperatively, σ can be expressed as—see Eq. (24.10):

$$\sigma = \frac{\sum_{m=0}^n m[R_{mL}]}{n[R_T]} = \frac{\sum_{m=0}^n \binom{n}{m} m \left[\frac{[L]}{K_A^{(n-m)/2} K_H} \right]^m}{\sum_{m=0}^n \binom{n}{m} n \left[\frac{[L]}{K_A^{(n-m)/2} K_H} \right]^m} \quad (24.14)$$

When the cooperativity factor K_A equals 1, indicating no cooperativity, Eq. (24.14) simplifies to:

$$\sigma = \frac{[L]}{[L] + K_H}. \quad (24.15)$$

Moreover, we have from its definition that $K_H = K_D$. In other words, in this case of no cooperativity we can equivalently think of there being a concentration of $n[R_T]$ single-site receptors instead of $[R_T]$ multi-site receptors. Eq. (24.15) then takes the well-known Michaelis-Menten form, with the property that σ is 0 when $[L]$ is 0, increases linearly at low $[L]$, equals 1/2 when $[L] = K_H$, and saturates to 1 as $[L]$ becomes very large.

In the limit of very high cooperativity ($K_A \rightarrow \infty$), $[R_{mL}]$ approaches 0 for $m = 1$ to $n - 1$ —see Eq. (24.13). Therefore, Eq. (24.14) reduces to the equation:

$$\sigma = \frac{0[R] + n[R_{nL}]}{n[R] + n[R_{nL}]} = \frac{[L]^n}{K_H^n + [L]^n}. \quad (24.16)$$

This equation resembles the Michaelis-Menten equation but has an initial zero slope and a sigmoidal shape. The steepness at $[L] = K_H$, where $\sigma = 1/2$, depends on n . Large n values give nearly switch-like sigmoidal behavior—see the bottom panel of Fig. 24.1.

For finite cooperativity factors K_A , the saturation fraction σ given by Eq. (24.14) also exhibits sigmoidal behavior as a function of ligand concentration $[L]$ —top panel of Fig. 24.1. The sigmoid curve starts at the origin, reaches half-saturation where $\sigma = 1/2$ at $[L] = K_H$, and approaches full saturation with $\sigma \rightarrow 1$ as $[L]$ becomes very large. The steepness of the sigmoid curve at the half-saturation point $[L] = K_H$ is determined by the magnitude of K_A . Specifically, higher K_A values produce steeper sigmoidal curves, indicating that ligand binding occurs in a more cooperative or con-

certed fashion. Thus, K_A not only influences whether ligand binding is cooperative versus independent, but also modulates the degree of cooperativity as characterized by the steepness of the saturation fraction curve at K_H . In summary, both the number of binding sites n and the cooperativity factor K_A help determine the switching behavior of the system in its transition from the unbound to fully bound state.

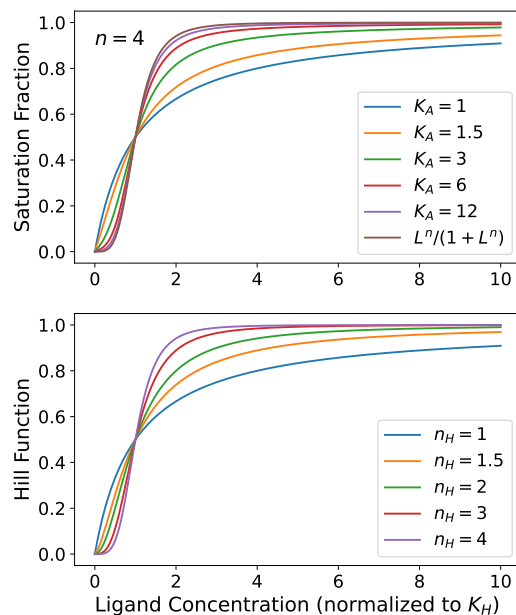


Fig. 24.1

The British physiologist A.V. Hill recognized that varying a single parameter in his equation could qualitatively replicate the effects of changing the cooperativity factor K_A from one to infinity. Specifically, he proposed the equation (now bearing his name):

$$\sigma = \frac{[L]^{n_H}}{[L]^{n_H} + K_H^{n_H}},$$

where n_H is a new parameter that can be continuously varied between 0 and the maximum number of binding sites per receptor, n . Just as increasing K_A made the binding curve steeper, larger n_H values also produce a sharper sigmoidal shape. Therefore, the Hill equation captures the essence of cooperative binding through a single tunable exponent rather than two separate parameters (K_A and n).

This elegantly simplified description proved invaluable for analyzing ligand-binding data. By fitting experimental saturation fractions to the Hill equation, the

degree of cooperativity could be estimated from a single parameter, n_H . Since its introduction, the Hill equation has become widely adopted for modeling systems exhibiting sigmoidal saturation behavior, including cooperative ligand-receptor interactions and many other biological switch-like responses. Its popularity stems from providing a tractable phenomenological description of cooperativity using a single cooperativity index.

24.8 Discussion

In this chapter, we developed a kinetic framework to quantitatively model the binding dynamics of ligands to cell surface receptors. Starting from the basic concepts of chemical reactions and kinetics, we derived reaction-rate equations based on the law of mass action.

We first considered a single ligand binding reversibly to receptors with one or multiple independent binding sites. The corresponding reaction schemes led to systems of ordinary differential equations describing changes in species concentrations over time. Analytical solutions were obtained for the single site case under specific assumptions. We then extended the independent binding model to incorporate cooperativity between ligand-binding sites. The affinity of subsequent binding was made dependent on the number of sites already occupied.

The saturation fraction was derived for the general cooperative case in terms of system parameters like ligand concentration, affinity constants and cooperativity factor. This quantity characterizes the fraction of receptors that are fully ligand-bound at equilibrium. The obtained results provided quantitative insights into how ligand occupancy is influenced by biochemical parameters like cooperativity.

In summary, chemical kinetics provides a rigorous mathematical framework for analyzing ligand-receptor interactions, which form the basis of many cellular signaling pathways. Future work could involve applying these models to specific biological systems and experimentally validating model assumptions and parameters. Extensions may also account for ligand depletion, receptor heterogeneity and conformational changes.

Chapter 25

The Interdisciplinary Origins of Molecular Biology

Abstract This chapter traces the intellectual roots and early scientific developments that established molecular biology as a distinct field through cross-disciplinary contributions from 1900-1950s. Pioneering genetics experiments suggested genes reside on chromosomes and have a physical nature, while subsequent discoveries identified DNA as the hereditary material and elucidated its double-helical structure. French scientists also made important independent findings in areas like gene regulation and restriction enzymes. Though initially dominated by separate structural and informational schools applying techniques like X-ray crystallography and quantum genetics, collaboration between thinkers such as Pauling, Astbury, Bernal, Morgan, Muller, Avery, Delbrück, Lwoff, Monod, Jacob, Watson, Crick, Wilkins and Franklin gradually decoded life's processes at the intricately coded molecular level. Their diverse lines of investigation across disciplines ultimately culminated in Watson and Crick's 1953 determination of DNA's double-helical architecture, unifying molecular genetics through physical principles and launching the independent field of modern molecular biology.

25.1 Introduction

The origins of molecular biology can be traced back to the rediscovery and synthesis of Gregor Mendel's work on inheritance at the turn of the 20th century. In 1900, nearly 40 years after Mendel's experiments with pea plants, his work was independently rediscovered by three European botanists: Hugo de Vries in the Netherlands, Carl Correns in Germany, and Erich von Tschermak in Austria. They confirmed Mendel's laws of inheritance through experiments with other plant species.

This sparked a revival of interest in genetic research. In 1902, the American zoologist Walter Sutton suggested that chromosomes may be the physical supports of Mendel's hypothetical units of inheritance, which he called "genes". Then in 1910, Thomas Hunt Morgan began using the fruit fly *Drosophila melanogaster* as a model organism to study genetics at Columbia University. Through analyzing the

inheritance of different traits in crossbred flies over many generations, Morgan and his colleagues were able to show that genes have a fixed position on chromosomes. They eventually created the first genetic map locating genes in a linear order on the chromosomes.

A major breakthrough occurred in 1928 when German botanist and geneticist Friedrich Miescher discovered that chromosomes contain a nucleic acid, which he called “nuclein”. Later investigations in the 1930s determined that there were two main types of nucleic acids: DNA and RNA. However, the physical nature and function of genes remained unclear, though it was increasingly believed they must have a molecular basis. Then in 1944, Oswald Avery’s experiments at Rockefeller University provided the decisive evidence that DNA is the genetic material of life, able to replicate itself and determine inheritance of traits.

This set the stage for the great discoveries to follow in the post-World War 2 era that would establish molecular biology as a distinct field, cracking open the secrets of heredity and life at the level of macromolecules and unraveling the molecular mechanisms of genetics.

Readers seeking a deeper understanding of the topics covered in this chapter are encouraged to consult the following sources: (Watson, 1968; Stent, 1968; Perutz, 1987; Weiner, 1999; Burian and Gayon, 1999; Moore, 2015).

25.2 Early Steps Towards a Physical and Molecular View of Genes

While Avery’s experiments cemented DNA as the genetic material, understanding how it specified traits required further elucidation of genes’ physical nature. Early insights came through Morgan’s studies of *Drosophila* genetics at Columbia in the early 1900s. Examining inheritance patterns of traits like eye color in fruit fly offspring, Morgan and his “fly room” colleagues discovered that genes appear to be located on chromosomes and pass from parents to offspring in specific arrangements during cell division. They were able to construct the first genetic maps ordering genes along the fly’s four chromosomes.

Other key advances included Herman Muller’s discovery in 1926 that X-rays could sharply increase mutation rates in *Drosophila*, providing evidence that genes correspond to discrete chromosomal locations that can be damaged. Meanwhile, in the 1930s at Rockefeller Institute, Avery along with Colin MacLeod and Maclyn McCarty identified DNA as the active component of the transforming principle—the substance enabling bacteria to change identity—in a series of classic experiments on pneumococcal bacteria.

This work established DNA as the chemical support of inheritance and genes. However, the exact physical nature of genes as material units within DNA was still unknown. Answers began emerging from the so-called “Morgan School” of genetics centered at Columbia. Through painstaking analysis of inheritance patterns in many fruit fly generations, Morgan’s students were able to demonstrate that genes

are arranged linearly along chromosomes like beads on a string. This supported the concrete view of genes as real, localized molecular entities rather than abstract concepts. Their efforts led to the first linkage maps of the *Drosophila* genome ordering many fruit fly genes.

25.3 The Structural School in Molecular Biology

With genetics increasingly focused on genes' material basis, researchers sought techniques to elucidate molecules' three-dimensional structures. Pioneering this area known as molecular structuralism was the field of X-ray crystallography, launched in 1912 through the work of British physicists William and Lawrence Bragg at the University of Leeds. Using X-rays to analyze regular crystal structures, they devised the Bragg equation allowing precise calculations of inter-atomic distances based on diffraction pattern measurements.

The Bragg father and son established Cambridge University's renowned crystallographic laboratory in 1915. There, scientists like William Astbury and John Desmond Bernal applied X-ray crystallography to analyze larger biological molecules. In the late 1930s, they obtained the first low-resolution structures of proteins like keratin and DNA. Around this time, Astbury also discovered the common structural motif of stacked nucleotide bases running perpendicular to DNA molecules' long axes.

Meanwhile, Linus Pauling at the California Institute of Technology used both crystallography and modeling to propose alpha helices as the dominant secondary structure within proteins. Published in 1951, this successfully explained experimental X-ray patterns and represented a breakthrough for structural biology. Pauling's innovative approach earned him the 1954 Nobel Prize in Chemistry. Back at Cambridge, Max Perutz and John Kendrew were deciphering hemoglobin and myoglobin's complex three-dimensional atomic architectures through X-ray crystallography of protein crystals, validated by electron microscopy. Their accomplishments gained the 1962 Chemistry Nobel.

This "Cambridge school" and Pauling exemplified the emerging structuralist approach, seeking to understand biology through high-resolution visualization of molecules' physical forms. Their work convincingly demonstrated genes' material basis as nucleic acid and protein structures amenable to physical-chemical analyses. This set the stage for molecular insights into biological functions like oxygen transport and storage of genetic information.

25.4 The Informational School and its Origins in Quantum Physics

While structuralism dominated early molecular biology, an alternative “informational” view developed stressing genetic function over form. Pioneering this school was Danish physicist Niels Bohr, a founding father of quantum mechanics. In the 1930s, Bohr explored biology’s interface with physics and proposed that life’s phenomena may not be fully explained by classical concepts alone. He advocated considering organisms as unique, indivisible entities subject to an analog of Heisenberg’s uncertainty principle.

Bohr’s ideas greatly influenced German biophysicist Max Delbrück. Delbrück pursued interests in mutation and inheritance through collaboration with geneticist Nikolai Timofeeff-Ressovsky in 1930s Berlin. Their 1935 paper proposing ionizing radiation causes mutations by interacting quantally with genes inspired Erwin Schrödinger’s later writings.

In 1943-44, as WW2 raged in Europe, Schrödinger delivered a notable series of lectures in Dublin that served as origin for his influential book *What is Life?*. Building on Delbrück and Timofeeff-Ressovsky’s work, Schrödinger emphasized genetics as transmission and execution of an “aperiodic crystal” storing coded instructions, which he presciently suggested could be a large molecule like DNA.

Schrödinger’s text exposed the problem of genetics to a wide scientific audience and helped attract young physicists into exploring life’s molecular basis. Foremost among them was Delbrück himself, who fled Nazi Germany for research with bacteriophage viruses at Vanderbilt University and the California Institute of Technology. Collaborating with Italian-born Salvador Luria from 1939-40, Delbrück made seminal discoveries validating statistical laws of bacterial mutation proposed by experimental genetics. Their combined efforts established phage as model systems and laid foundations for molecular genetics.

25.5 The Emergence of Molecular Biology in France

While the structural and informational schools initially developed largely in Britain, Germany, and the United States, France too contributed importantly to early molecular biology. Several pioneers worked largely independently in French institutions during and after World War II.

André Lwoff studied microbiology at the Pasteur Institute in Paris, where in 1950 he discovered lysogeny—how some viruses can insert their genes into bacterial chromosomes without killing the host. This opened perspectives on gene regulation. Meanwhile, at the Collège de France and CNRS, François Jacob and Jacques Monod began investigating how *E. coli* switches between metabolizing lactose and glucose.

In 1961 at the Pasteur Institute, they revealed a genetic control system where the *lac* repressor protein prevents lactose operon expression unless lactose or its isomer allolactose is present. This constituted the first detailed example of gene regulation, demonstrating precisely how environmental inputs control transcriptional activity. The same year, Jacob, Monod, and Lwoff received the 1965 Nobel Prize in Physiology or Medicine for discovering genetic regulatory mechanisms in bacteria.

Another Pasteur scientist, François Gros, made independent contributions around this period through isolating the first restriction enzymes in the 1950s. Restriction enzymes can cut DNA at specific recognition sequences, enabling their use as molecular tools. Later, in the 1960s, genomic research was advanced through genome mapping methods like membrane hybridization developed by French biologist Jean Weil.

These efforts exemplified productive collaboration even during wartime, as French researchers established their nation as a global center for molecular genetics through basic discoveries in gene regulation, enzyme technology, and genomic analysis foreshadowing the post-DNA era's explosion of knowledge.

25.6 The Discovery of the Double Helix

Building on earlier advances, the stage was set in the 1950s for determining DNA's structure, the keystone achievement that would truly launch the era of molecular biology. Inspired by the Schrödinger's ideas, a new generation of young scientists embraced biological problems with fresh physical perspectives. At the University of Cambridge, American biologist James Watson joined British biophysicist Francis Crick aiming to elucidate DNA's architecture based on existing legacies of nucleic acid research.

Across town at King's College London, Australian biophysicist Maurice Wilkins and post-doc Raymond Gosling were conducting X-ray crystallography experiments on DNA fibres using new techniques like fiber diffraction. Simultaneously, Rosalind Franklin—a British biophysicist at King's—was photographing exquisitely clear X-ray patterns showing DNA adopted a regular twisted, helical form while in the lattice.

After Franklin "Photo 51" was shown to Crick, he and Watson were galvanized with inspiration. Borrowing insights from colleagues like Erwin Chargaff on DNA composition and Linus Pauling on triple-stranded helices, within two years they correctly unveiled B-DNA's now-iconic twisted ladder structure with pairs of nucleotide bases. Published in 1953, their model instantly explained genes' replication and immediately took the scientific world by storm.

Though Wilkins, Franklin, and others contributed crucially, Watson and Crick received most acclaim for their intuitive theoretical leap. Their triumph solved biology's greatest riddle—the basis for heredity—in one stroke by decoding DNA's symbolic language of life in structural terms. It also marked the true emergence of

molecular biology, kickstarting an explosive growth era for genetics as fields like biochemistry integrated with other sciences at life's most intimate chemical level.

25.7 Discussion

This chapter has outlined some of the key early developments that established the foundations of molecular biology as an independent field of research. It began with classical genetics experiments in the early 20th century suggesting genes have a physical-chromosomal basis. Subsequent discoveries then firmly identified DNA as the carrier of genetic information and driving further investigation into its molecular structure.

The origins of molecular biology showcase the power of cross-disciplinary thinking and dialogue between different scientific fields. Marrying diverse experimental and conceptual approaches from physics, chemistry and genetics paid immense dividends in cracking open life's code recorded in the language of molecules. This laid the foundation for today's data-rich biomedical revolution transforming human health.

Chapter 26

Gene Regulation

Abstract Gene regulation is a fundamental process that allows cells to control when and to what extent genes are expressed. This chapter explores the central principles and mechanisms involved, including the central dogma of molecular biology, gene regulatory networks, feedback loops, and specific examples like the tryptophan and tryptophanase operons in bacteria. These operons illustrate how complex regulatory circuits integrate multiple signals like metabolite levels and environmental cues to precisely modulate gene expression. Negative feedback mediated by repressors and attenuators allows metabolic homeostasis, while additional layers of control are achieved through mechanisms like enzyme inhibition and post-translational regulation. Understanding such natural gene regulation systems is crucial for fields like medicine, biotechnology, and evolutionary biology. It provides inspiration for rational design of synthetic genetic circuits and holistic insights into how intricate molecular networks facilitate the robust, adaptive behavior of living systems.

26.1 Introduction

Gene regulation is a fundamental process that allows cells to control the expression of their genes in response to various internal and external signals. The ability to precisely regulate when, where, and to what extent genes are expressed is essential for the proper functioning, development, and survival of all living organisms.

At the most basic level, gene regulation determines which genes are transcribed into messenger RNA (mRNA) molecules and subsequently translated into proteins. However, the regulatory mechanisms that govern gene expression are highly complex and involve intricate networks of interactions between DNA, RNA, proteins, and various small molecules.

Gene regulation is crucial for many biological processes, including cellular differentiation, developmental patterning, metabolic control, and the response to environmental stimuli. Failure to properly regulate gene expression can lead to a wide range of diseases, such as cancer, developmental disorders, and metabolic disorders.

This chapter will explore the fundamental principles and mechanisms of gene regulation, including the central dogma of molecular biology, gene regulatory networks, and feedback loops. We will examine several well-studied examples of gene regulation systems in bacteria, such as the tryptophan and tryptophanase operons. These examples illustrate the remarkable complexity and precision with which cells can control gene expression, often involving intricate interplay between transcription factors, regulatory DNA sequences, and small molecules.

Understanding the mechanisms of gene regulation is not only essential for our comprehension of fundamental biological processes but also has profound implications for fields such as biotechnology, medicine, and evolutionary biology. By elucidating the intricate regulatory networks that govern gene expression, we can gain insights into the development of new therapeutic strategies, the engineering of biological systems, and the evolution of complex traits.

26.2 The Central Dogma of Molecular Biology

The central dogma of molecular biology is a hypothesis proposed by Francis Crick in 1958 that describes the flow of genetic information within a cell from deoxyribonucleic acid (DNA) to proteins. It can be summarized in two fundamental principles: Replication and Transcription and translation.

In general terms, the central dogma establishes that the flow of genetic information follows the pattern: $\text{DNA} \rightarrow \text{RNA} \rightarrow \text{Protein}$. This flow of information can be described in three main stages:

1. **DNA replication:** DNA replicates itself through a semi-conservative process, in which each strand of the double helix serves as a template for the synthesis of a new complementary strand.
2. **Transcription:** In this stage, the genetic information contained in a specific region of DNA (a gene) is transcribed into a messenger RNA (mRNA) molecule. This process is carried out by the RNA polymerase enzyme, which reads the nucleotide sequence of the DNA and synthesizes a complementary strand of mRNA.
3. **Translation:** The resulting mRNA is translated into a sequence of amino acids that form a protein. This process occurs in ribosomes, where the mRNA is read, and the corresponding proteins are synthesized according to the genetic code.

It is important to note that, although the central dogma establishes that information cannot flow from proteins to nucleic acids, some exceptions to this rule have been discovered in certain viruses and unicellular organisms. However, in the vast majority of organisms, the central dogma remains an accurate description of the flow of genetic information.

26.3 Gene Regulatory Networks

Gene regulation is a fundamental process in living organisms that allows controlling when, where, and to what extent genes are expressed. This regulation is essential to ensure that proteins are produced in the appropriate amounts and at the right time and place. One of the key mechanisms of gene regulation involves feedback loops, which generally involve metabolites interacting with transcription factors.

Feedback loops are regulatory circuits in which the final product of a metabolic pathway or biological process influences its own synthesis or degradation. These loops can be negative or positive and play a crucial role in maintaining homeostasis and responding appropriately to environmental changes.

In the case of gene regulation, negative feedback loops are the most common and aim to maintain the levels of certain proteins or metabolites within an optimal range. In these loops, the final product of a metabolic pathway (a metabolite) interacts with a repressor, which is a protein that regulates gene expression by binding to specific regions of DNA.

The negative feedback loop works as follows.

In the absence of the metabolite, the repressor cannot bind to the regulatory region of the corresponding gene, allowing its transcription and, consequently, the synthesis of the associated protein.

As the protein is synthesized, the corresponding metabolite is also produced as a result of its enzymatic activity or its participation in a metabolic pathway. When the levels of the metabolite reach a specific threshold, it binds to the repressor, causing a conformational change that slows it to bind to the regulatory region of the gene.

As a result, the transcription of the gene stops, halting further production of the protein and, therefore, reducing the synthesis of the metabolite.

This negative feedback loop allows maintaining the levels of the metabolite within an optimal range, avoiding excessive accumulation or scarcity of the same.

Positive feedback loops can also be involved in gene regulation, although they are less common. In these loops, the final product of a metabolic pathway or biological process stimulates its own synthesis, leading to an amplification or reinforcement of the process. These loops are important in processes such as cell differentiation, apoptosis (programmed cell death), and the inflammatory response.

In summary, feedback loops involving metabolites that interact with transcription factors are key mechanisms in gene regulation, allowing precise adjustment of protein and metabolite levels in response to environmental conditions and cellular needs.

26.4 The Amino Acid Tryptophan

Tryptophan is an essential amino acid that plays a crucial role in various biological processes. It is one of the 20 standard amino acids used in protein synthesis and is encoded by the UGG codon in the genetic code. Tryptophan is considered an

essential amino acid because it cannot be synthesized by humans and other animals, and therefore must be obtained from dietary sources.

Tryptophan has several important functions in the body:

1. **Protein synthesis:** Like other amino acids, tryptophan is a building block for proteins. It is incorporated into polypeptide chains during translation and is found in a wide range of proteins with diverse functions.
2. **Precursor for metabolic pathways:** Tryptophan is the precursor for several important metabolic pathways. It is involved in the synthesis of the neurotransmitters serotonin and melatonin, as well as the vitamin niacin (nicotinic acid).
3. **Regulation of biological processes:** Tryptophan and its metabolites play a role in regulating various biological processes, including sleep, mood, appetite, and immune function. For example, serotonin, derived from tryptophan, is involved in regulating mood, sleep, and appetite.
4. **Structural and functional roles in proteins:** The unique structure of tryptophan, with its aromatic indole ring, allows it to participate in various structural and functional roles within proteins. It can be involved in protein folding, stability, and interactions with other molecules.

Tryptophan is found in a variety of dietary sources, including meat, dairy products, nuts, seeds, and some vegetables. However, it is generally present in relatively low quantities compared to other amino acids. Adequate intake of tryptophan is essential for maintaining proper protein synthesis, neurotransmitter balance, and overall health.

Due to its importance in various biological processes, the regulation of tryptophan metabolism is tightly controlled in living organisms. The tryptophan operon, discussed in the next section, is a well-studied example of how bacteria regulate the biosynthesis of this essential amino acid through a complex gene regulatory network.

26.5 The Tryptophan Operon

The tryptophan operon is one of the best-studied gene regulation systems in bacteria and serves as a classic example of how negative feedback loops control gene expression in response to the levels of a specific metabolite.

The tryptophan operon is involved in the biosynthesis of the tryptophan amino acid in bacteria such as *Escherichia coli* and *Salmonella typhimurium*. This operon contains five structural genes (*trpE*, *trpD*, *trpC*, *trpB*, and *trpA*) that encode the enzymes necessary for the synthesis of tryptophan from a precursor called chorismate.

The regulation of the tryptophan operon is based on a negative feedback mechanism mediated by the TrpR transcriptional repressor and the tryptophan coactivator. Additionally, supplementary mechanisms such as enzyme inhibition and transcriptional attenuation are employed to regulate tryptophan synthesis more precisely.

Regulation by the TrpR repressor: in the absence of tryptophan, TrpR is in its inactive conformation and cannot bind to the tryptophan operon, allowing transcription. When tryptophan levels are high, some molecules bind to TrpR, causing a conformational change that allows it to bind to the *trp* operator, blocking transcription.

Enzyme inhibition: the anthranilate synthase enzyme (encoded by the *trpE* gene) is allosterically inhibited by tryptophan. When tryptophan levels are high, it binds to the anthranilate synthase enzyme, inhibiting its catalytic activity. This reduces the production of anthranilate, a key precursor in the tryptophan synthesis pathway, thereby decreasing tryptophan synthesis.

Transcriptional attenuation: the leader region of the tryptophan operon mRNA contains a specific sequence that can form alternative secondary structures. In the presence of high levels of tryptophan, a transcriptional termination structure is formed, prematurely stopping transcription. In the absence of tryptophan, an antiterminator structure is formed, allowing complete transcription of the operon. This attenuation mechanism regulates the expression of the structural genes in response to tryptophan levels.

These complementary regulation mechanisms allow precise and coordinated control of tryptophan synthesis in bacteria. Enzyme inhibition by tryptophan reduces the activity of a key enzyme in the biosynthetic pathway. Transcriptional attenuation allows adjusting the transcription rate of the operon based on tryptophan levels. Regulation by the TrpR repressor controls transcription at the level of the entire operon.

This multi-level regulation prevents excessive accumulation of tryptophan and ensures efficient allocation of cellular resources for the synthesis of this essential amino acid.

26.6 The Tryptophanase Operon

The tryptophanase (*tna*) operon in *Escherichia coli* encodes the proteins necessary for uptake and metabolism of the amino acid tryptophan as a carbon source in the absence of glucose. The *tna* operon consists of two structural genes: *tnaA* and *tnaB*.

The *tnaA* gene codes for the enzyme tryptophanase (TnaA), which metabolizes tryptophan to allow it to be used as a carbon source. The *tnaB* gene codes for the tryptophan-specific permease TnaB, which transports tryptophan from the extracellular environment into the bacterial cell.

The expression of the *tna* operon genes is regulated by 3 different mechanisms:

1. **Catabolite Repression** - This mechanism depends on the intracellular glucose level. High glucose leads to low levels of cAMP, which prevents the cAMP-CAP complex from binding to the *tna* promoter and activating transcription. Low glucose allows cAMP-CAP to bind and activate *tna* operon expression.
2. **Rho (ρ)-mediated Transcription Termination** - The rho protein can bind to the *tnaC* leader sequence and prematurely terminate transcription of *tnaA* and

tnaB. However, this termination is suppressed when tryptophan is present in the cytoplasm due to ribosome stalling on the *tnaC* transcript.

3. **Post-translational Regulation of TnaA** - The TnaA enzyme is initially produced in an inactive form clustered into foci. In the stationary phase, these foci disperse and TnaA becomes an active tetrameric enzyme that can metabolize tryptophan. This activation is regulated by an unknown cAMP-CAP independent mechanism related to glucose levels.

As more TnaB permease is produced from the *tna* operon, it imports more tryptophan into the cell. This increased tryptophan pool further enhances suppression of the transcription terminator, creating a positive feedback loop that reinforces *tna* operon expression. The positive feedback from *tnaB* expression, combined with the multiple regulatory inputs (glucose, tryptophan levels, growth phase), suggests the *tna* operon could exhibit bistable expression dynamics. At certain inducing conditions, the regulatory circuit may permit two distinct stable states of operon expression.

The sophisticated regulation of the *tna* operon exemplifies how bacteria have evolved intricate gene circuits to precisely control metabolism of non-preferred nutrient sources. By integrating various signals, *E. coli* activates tryptophan utilization only when it is advantageous, while allocating resources preferentially to glucose metabolism when available. The potential for bistable dynamics may further enhance the operon's responsiveness while preventing futile oscillations.

This regulatory strategy highlights the remarkable ability of even simple organisms to deploy complex decision-making at the molecular level, optimizing survival and growth through efficient resource allocation. Uncovering such regulatory principles informs both our understanding of microbial ecology and provides inspiration for synthetic biology efforts to engineer analogous gene circuits.

26.7 Discussion

The examples of gene regulation systems covered in this chapter—the tryptophan and tryptophanase operons—highlight the remarkable complexity and precision with which cells regulate gene expression. While the specific mechanisms and components vary, some common principles emerge.

Negative feedback loops involving metabolites and transcription factors are a recurring motif in gene regulation. These loops allow cells to maintain optimal levels of enzymes, metabolites, and proteins by repressing expression when concentrations become too high. The tryptophan operon exemplifies this through attenuation and repression by TrpR.

Gene regulation frequently integrates multiple signals and inputs, allowing cells to make sophisticated decisions. The tryptophanase operon is regulated by both tryptophan and glucose levels, prioritizing the most efficient carbon source.

Regulatory systems often employ multiple layered mechanisms like transcriptional, translational, and metabolic control for finer-tuned expression. The tryptophan operon uses repression, attenuation, and enzyme inhibition in concert.

The intricate interplay between regulatory DNA sequences, transcription factors, small molecules, and cooperative binding enables cells to deploy complex regulatory strategies tailored to their specific needs. However, many questions remain about how these systems evolved, how they adapt to changing environments, and how dysregulation contributes to disease.

As synthetic biology and genome engineering advance, understanding natural gene regulation will be invaluable for rationally designing novel genetic circuits, metabolic pathways, and cellular behaviors. Additionally, comprehensive mapping of regulatory networks will shed light on systems-level properties governing cellular decision-making.

Ultimately, gene regulation represents a central layer of control that allows the remarkably robust and adaptive behavior of living systems to emerge from a finite set of genetic instructions. Continued research in this area will be crucial for furthering our understanding of life's molecular logic.

Chapter 27

Mathematical Modelling of Simple Bacterial Gene Regulatory Networks

Abstract This chapter explores the mathematical modeling of gene regulatory networks, focusing on both negative and positive feedback mechanisms through the lens of the tryptophan and tryptophanase operons. We develop ordinary differential equations to capture the dynamics of gene expression, enzyme activity, and metabolite synthesis, revealing the underlying feedback mechanisms that govern these processes. The tryptophan operon exemplifies a system characterized by redundant negative feedback regulation, highlighting the roles of transcriptional attenuation and repression in maintaining homeostasis and enabling rapid responses to environmental changes. In contrast, the tryptophanase operon showcases positive feedback regulation, demonstrating how such mechanisms can lead to bistability under specific conditions. This bistable behavior allows for toggling between distinct expression states, enhancing the operon's adaptability in fluctuating environments. Overall, our findings underscore the intricate interplay between feedback regulation and gene expression, emphasizing their critical roles in bacterial survival and resilience.

27.1 Introduction

27.2 General Model Development

Gene expression is a complex process involving numerous chemical reactions at each step of transcription and translation. However, we can build a simple model based on the central dogma of molecular biology.

Consider a basic operon whose genes code for an enzyme E that catalyzes the synthesis of a metabolite P . The synthesis of the operon's mRNA, M , via transcription is feedback-regulated by P . Additionally, the activity of the E enzymes may also be feedback-regulated by P . With these considerations, the dynamics of M , E , and P are governed by the following ordinary differential equations (ODEs):

$$\dot{M} = k_M f(P) - \gamma_M M, \quad (27.1)$$

$$\dot{E} = k_E M - \gamma_E E, \quad (27.2)$$

$$\dot{P} = k_P g(P) E - \gamma_P P, \quad (27.3)$$

Here, k_M represents the maximum transcription initiation rate, γ_M is the rate constant for mRNA degradation, k_E denotes the translation initiation rate, γ_E is the rate constant for enzyme degradation, k_P is the maximum metabolite synthesis rate per enzyme molecule, and γ_P is the rate constant for metabolite degradation. The functions $f(P)$ and $g(P)$ denote feedback regulation in terms of metabolite concentration. $f(P)$ can be interpreted as the probability that the promoter is not repressed, while $g(P)$ represents the fraction of un-inhibited enzyme molecules. These functions are decreasing (increasing) functions of P in case of negative (positive) feedback regulation.

The functions $f(P)$ and $g(P)$ take values in the interval $[0, 1]$ as they can be understood as probabilities. $f(P)$ is the probability that the mRNA polymerase binding site is not blocked by a repressor molecule, which depends on the amount of active repressor molecules. Depending on the system, repressor molecules are active when they are free from or bound by specific metabolites. In summary, transcriptional repression can be reduced to a, more or less intricate, ligand-receptor interaction. Thus, based on the results in Chapter 24, the function $f(P)$ can be approximated by a growing or decreasing Hill function, depending on whether it accounts for positive or negative feedback regulation:

$$f(P) = \frac{1}{2} \frac{(K_f^{n_f} + P^{n_f}) \pm (K_f^{n_f} - P^{n_f})}{K_f^{n_f} + P^{n_f}}.$$

In the equation above, K_f is the half-saturation constant ($f(K_f) = 1/2$), and $n_f \geq 1$ is the so-called Hill exponent. It measures the sigmoidicity of the Hill function. When $n_f = 1$, the function $f(P)$ becomes a Michaelis-Menten equation, whereas it approaches a step function when $n_f \rightarrow \infty$. The sign $+$ ($-$) is chosen to account for negative (positive) regulation.

Enzymes are often inhibited or activated when they are bound by specific metabolites. Thus, enzyme inhibition can also be reduced to a ligand-receptor problem, and the function $g(P)$ can be approximated by a Hill function:

$$g(P) = \frac{1}{2} \frac{(K_g^{n_g} + P^{n_g}) \pm (K_g^{n_g} - P^{n_g})}{K_g^{n_g} + P^{n_g}}.$$

27.3 The Tryptophan Operon

A specific model for the tryptophan operon, discussed in the previous chapter, can be derived from our general model as follows:

$$\dot{M} = k_M f(W) - \gamma_M M, \quad (27.4)$$

$$\dot{E} = k_E M - \gamma_E E, \quad (27.5)$$

$$\dot{W} = k_W g(W) E - \gamma_W W, \quad (27.6)$$

with

$$f(W) = \frac{K_M^{n_M}}{K_M^{n_M} + W^{n_M}},$$

$$g(W) = \frac{K_W^{n_W}}{K_E^{n_W} + E^{n_W}}.$$

In these equations, T represents the intracellular concentration of tryptophan, the amino acid produced by the tryptophan operon. E denotes the concentration of the enzyme anthranilate synthase, a tetrameric protein composed of two peptides resulting from the expression of the first gene (*trpE*) and two peptides from the second gene (*trpD*) of the tryptophan operon. Anthranilate synthase catalyzes the rate-limiting step in tryptophan biosynthesis, and its activity is feedback-regulated by the end product, tryptophan.

The first equation describes the dynamics of mRNA concentration, where k_M is the maximum rate of mRNA synthesis, K_M is the half-saturation constant for tryptophan's negative feedback on gene transcription, and n_M is the Hill coefficient governing the cooperativity of this feedback regulation.

The second equation models anthranilate synthase dynamics. k_E is the enzyme synthesis rate per mRNA molecule and γ_M is the rate constant for enzyme degradation.

The third equation models the dynamics of tryptophan concentration, where k_T is the maximum rate of tryptophan synthesis, K_T is the half-saturation constant for tryptophan's negative feedback on its own synthesis, n_T is the corresponding Hill coefficient, and γ_T is the rate constant for tryptophan degradation or consumption.

This model captures the essential features of the tryptophan operon, including the multi-layered negative feedback regulation mechanisms employed to control tryptophan biosynthesis. Firstly, the transcription of the operon is negatively regulated by tryptophan through two distinct mechanisms: repression and transcriptional attenuation, both of which are accounted for by a single regulatory function. Secondly, the activity of the key enzyme anthranilate synthase is directly inhibited by tryptophan through allosteric regulation.

One of the first questions that arises is the reason for redundant negative feedback mechanisms in the tryptophan operon system. We address this question by analyzing the stability of the system's steady states. But first, it is convenient to simplify the model.

According to Santillán and Zeron (2004), the half-life of mRNA is about one minute, while that of anthranilate synthase is a few hours, and that of tryptophan is a few seconds. This suggests that mRNA and tryptophan have much faster dynamics than anthranilate synthase. Therefore, we can make quasi-steady-state approximations for M and T .

From the condition $\dot{M} = 0$, we get:

$$M = \frac{k_M}{\gamma_M} f(T), \quad (27.7)$$

On the other hand, the condition $\dot{T} = 0$ implies:

$$E = h(T) = \frac{\gamma_T}{k_T} \frac{T}{g(T)}.$$

Since $g(T)$ is a continuous decreasing function of T , representing the negative feedback regulation of enzyme activity by tryptophan, $h(T)$ is a continuous growing function that can be inverted to give:

$$T = h^{-1}(E). \quad (27.8)$$

Substituting Eqs. (27.7) and (27.8) into the equation for \dot{E} (Eq. (27.5)), we obtain a reduced model that ignores the rapid transients of M and T and focuses on the slow dynamics of E :

$$\dot{E} = \frac{k_M k_E}{\gamma_M} f(h^{-1}(E)) - \gamma_E E. \quad (27.9)$$

The value of E at the steady states can be computed from the condition $\dot{E} = 0$, which yields:

$$E = \frac{k_M k_E}{\gamma_M \gamma_E} f(h^{-1}(E)). \quad (27.10)$$

The left-hand side of this equation is the 45-degree diagonal straight line, while the right-hand side is a continuously decreasing function of E that is greater than zero at $E = 0$. It can be proven from these facts that the two curves intersect at a single point, implying that our model has only one steady state given by the solution of Eq. (27.10). The steady-state values of M and T can then be obtained by substituting the stationary value of E into Eqs. (27.7) and (27.8), respectively.

The stability of the steady state is determined by the derivative of the right-hand side of Eq. (27.9). After some algebraic manipulation, it can be shown that this derivative is given by the following expression:

$$\rho = \gamma_E \left(T_{max} \frac{f'(T^*) g^2(T^*)}{g(T^*) - T^* g'(T^*)} - 1 \right), \quad (27.11)$$

where

$$T_{max} = \frac{k_M k_E k_T}{\gamma_M \gamma_E \gamma_T}$$

is the theoretical upper bound for the intracellular tryptophan concentration.

Note that $\rho < 0$ since $f'(T^*), g'(T^*) < 0$, implying that the steady state is locally stable. On the other hand, $-\gamma_E$ is the upper bound of ρ , which is achieved when $f'(T^*) = 0$. This indicates that transcriptional regulation plays a fundamental role in accelerating the system's response after a perturbation from the steady state. No-

tably, repression and transcriptional attenuation achieve maximal sensitivity at quite different tryptophan levels; repression at about T^* and transcriptional attenuation one order of magnitude below T^* (Santillán and Zeron, 2004). This may ensure a rapid response over a wide range of tryptophan concentrations.

Regarding enzyme inhibition, observe in Eq. (27.11) that ρ increases (becomes less negative) as $g(T^*)$ decreases. Thus, this regulatory mechanism slows down the system's response instead of accelerating it. Interestingly, the dissociation constant for the binding of tryptophan to anthranilate synthase is one order of magnitude smaller than T^* , implying that $g(T^*) \approx 0$ because enzyme inhibition is in the saturation regime at the steady state (Santillán and Zeron, 2004). This indicates that enzyme inhibition plays an energetic rather than a dynamical role. By releasing inhibited enzymes, it ensures an efficient response when tryptophan levels are very low, without having to wait for more enzymes to be synthesized.

27.4 The Tryptophanase Operon

A simple mathematical model that captures the key regulatory features of the tryptophanase operon can be written as follows:

$$\begin{aligned}\dot{P} &= k_P(G_E) \frac{W^n}{W^n + K_P^n} - \mu_P P, \\ \dot{W} &= k_W(W_E)P - \gamma_W PW - \mu_W W.\end{aligned}$$

In these equations, P denotes the level of the tryptophanase operon proteins (TnaA and TnaB), while W represents the intracellular tryptophan concentration. The parameter $k_P(G_E)$ is the maximum transcription rate of the operon, which is negatively regulated by external glucose G_E via catabolite repression. The Hill function $\frac{W^n}{W^n + K_P^n}$ accounts for the positive regulation of transcription by intracellular tryptophan W (mediated by inactivation of the ρ terminator). The term $\mu_P P$ represents protein degradation and dilution due to cell growth. The rate of tryptophan uptake is given by $k_W(W_E)P$, where $k_W(W_E)$ is an increasing function of the external tryptophan level W_E , reflecting the role of TnaB as a tryptophan permease. The term $\gamma_W PW$ is the rate at which intracellular tryptophan is metabolized by the TnaA enzyme. Finally, $\mu_W W$ accounts for tryptophan consumption by other processes like protein synthesis and dilution by growth.

To simplify the analysis, we assume the tryptophan metabolism flux $\gamma_W PW$ is much smaller than the other tryptophan consumption terms ($\mu_W W$). This yields the reduced model:

$$\begin{aligned}\dot{P} &= k_P(G_E) \frac{W^n}{W^n + K_P^n} - \mu_P P, \\ \dot{W} &= k_W(W_E)P - \mu_W W.\end{aligned}$$

By introducing the dimensionless variables $p = P / (k_P(G_E) / \mu_P)$, $w = W / (k_P k_W / (\mu_P \mu_W))$, $t' = \mu_P t$, and defining $\mu = \mu_W / \mu_P$, $K(G_E, W_E) = K_P(G_E) \mu_P \mu_W / (k_P(G_E) k_W(W_E))$, the model becomes:

$$\dot{p} = \frac{w^n}{w^n + K^n(G_E, W_E)} - p, \quad (27.12)$$

$$\dot{w} = \mu(p - w). \quad (27.13)$$

Note that $K(G_E, W_E)$ increases with G_E (repressing operon expression) and decreases with W_E (enhancing expression).

To find steady states, we set $\dot{p} = \dot{w} = 0$, yielding:

$$p = \frac{w^n}{w^n + K^n(G_E, W_E)},$$

$$w = p.$$

Thus, the steady-state value of p satisfy:

$$p = \frac{p^n}{p^n + K^n(G_E, W_E)}.$$

Graphical analysis (Fig. 27.1) reveals that for large K , this equation has a single solution $p = 0$ (no expression). As K decreases, two additional steady states emerge via a saddle-node bifurcation: an intermediate state and a high expression state near $p = 1$.

Fig. 27.1 .

To study stability, we compute the Jacobian matrix:

$$J = \begin{bmatrix} -1 & H'(w) \\ \mu & -\mu \end{bmatrix},$$

where $H'(w) = d/dw (w^n / (w^n + K^n))$ is the derivative of the Hill function. The trace $\tau = -(1 + \mu)$ is negative, while the determinant is $\Delta = \mu(1 - H'(w))$. A steady state is stable if $\Delta > 0$, i.e. $H'(w^*) < 1$ at the steady state w^* . Since the sigmoidal curve $w(p)$ has a slope less than 1 at the low and high stable states, these are stable nodes. However, the intermediate state has $H'(w^*) > 1$, making it an unstable saddle point.

In summary, the tryptophanase operon can exhibit bistable expression dynamics when tryptophan and glucose levels permit it. In bacterial populations, gene expression is not uniform; instead, it exhibits a phenomenon known as biochemical noise. In the presence of bistability, this variability can lead to some individual bacteria expressing genes at low rates (corresponding to the low-expression steady state) while others express them at high rates (corresponding to the high expression steady state). This heterogeneity can be particularly advantageous for bacterial populations fac-

ing rapidly changing environments as it can facilitate a form of bet-hedging, where the population as a whole can respond more flexibly to environmental shifts. For instance, if a sudden change in the environment favors a particular metabolic pathway, those bacteria with higher expression levels of the relevant genes are more likely to thrive. At the same time, the presence of low-expressing cells ensures that not all members are similarly affected by deleterious environmental changes, thereby providing a reservoir of potential adaptability. This dynamic interplay of expression levels, driven by biochemical noise, underscores the importance of gene regulatory networks, such as the tryptophanase operon, in enabling bacterial populations to swiftly adapt to their surroundings.

27.5 Discussion

In this chapter, we have delved into the mathematical modeling of gene regulatory networks, particularly focusing on two key feedback regulatory motifs: negative and positive feedback regulation, using the tryptophan and tryptophanase operons as representative examples.

Through the development of ordinary differential equations, we have captured the dynamics of gene expression, enzyme activity, and metabolite synthesis, shedding light on the origins of the feedback mechanisms that govern these processes.

The tryptophan operon serves as a prototypical example of gene networks characterized by redundant negative feedback regulation. Our analysis revealed the critical roles of transcriptional attenuation and repression in maintaining homeostasis while facilitating rapid responses to environmental changes. Interestingly, while allosteric enzyme inhibition does not accelerate system responses, it enhances the energetic efficiency of tryptophan biosynthesis.

In contrast, we examined the tryptophanase operon as an example of gene expression influenced by positive feedback regulation. We demonstrated that this positive regulation can lead to the emergence of bistability under certain conditions. This bistable behavior underscores the operon's capacity to toggle between distinct expression states, providing a robust mechanism for adaptation in fluctuating environments.

Overall, our exploration of these operons highlights the intricate interplay between feedback mechanisms and gene expression, emphasizing their significance in bacterial adaptation and resilience.

References

- Bacaër N (2011) *A Short History of Mathematical Population Dynamics*. Springer London, DOI 10.1007/978-0-85729-115-8, URL <http://dx.doi.org/10.1007/978-0-85729-115-8>
- Baigrie B (2006) *Electricity and magnetism*. Greenwood Guides to Great Ideas in Science, Greenwood Press, Westport, CT
- Bassett DR (2002) Scientific contributions of a. v. hill: exercise physiology pioneer. *Journal of Applied Physiology* 93(5):1567–1582, DOI 10.1152/japplphysiol.01246.2001, URL <http://dx.doi.org/10.1152/japplphysiol.01246.2001>
- Borges J (1982) *El hacedor*, 16th edn, Emecé Editores SA, chap Del rigor en la ciencia
- Box E (1976) Science and statistics. *Journal of the American Statistical Association* 71(356):791–799
- Bremmer H, Bouwkamp C, Pol, van der B (eds) (1960) *Selected scientific papers Balthasar van der Pol*. North-Holland Publishing Company, Netherlands
- Brown A (2020) *A companion guide to the Hodgkin-Huxley papers*. Physiological Society
- Burian R, Gayon J (1999) The french school of genetics: From physiological and population genetics to regulatory molecular genetics. *Annual Review of Genetics* 33(1):313–349, DOI 10.1146/annurev.genet.33.1.313, URL <http://dx.doi.org/10.1146/annurev.genet.33.1.313>
- Bélair J, Mackey MC, Mahaffy JM (1995) Age-structured and two-delay models for erythropoiesis. *Mathematical Biosciences* 128(1–2):317–346, DOI 10.1016/0025-5564(94)00078-e, URL [http://dx.doi.org/10.1016/0025-5564\(94\)00078-E](http://dx.doi.org/10.1016/0025-5564(94)00078-E)
- Cajori F (1913a) History of the exponential and logarithmic concepts. *The American Mathematical Monthly* 20(5):148–151, DOI 10.1080/00029890.1913.11997942, URL <http://dx.doi.org/10.1080/00029890.1913.11997942>
- Cajori F (1913b) History of the exponential and logarithmic concepts. *The American Mathematical Monthly* 20(1):5–14, DOI 10.1080/00029890.1913.11997909, URL <http://dx.doi.org/10.1080/00029890.1913.11997909>
- Cajori F (1913c) History of the exponential and logarithmic concepts. *The American Mathematical Monthly* 20(2):35–47, DOI 10.1080/00029890.1913.11997915, URL <http://dx.doi.org/10.1080/00029890.1913.11997915>
- Cajori F (1913d) History of the exponential and logarithmic concepts. *The American Mathematical Monthly* 20(3):75, DOI 10.2307/2973441, URL <http://dx.doi.org/10.2307/2973441>
- Cajori F (1913e) History of the exponential and logarithmic concepts. *The American Mathematical Monthly* 20(4):107–117, DOI 10.1080/00029890.1913.11997933, URL <http://dx.doi.org/10.1080/00029890.1913.11997933>

- Cajori F (1913f) History of the exponential and logarithmic concepts. *The American Mathematical Monthly* 20(6):173–182, DOI 10.1080/00029890.1913.11997951, URL <http://dx.doi.org/10.1080/00029890.1913.11997951>
- Cajori F (1913g) History of the exponential and logarithmic concepts. *The American Mathematical Monthly* 20(7):205–210, DOI 10.1080/00029890.1913.11997960, URL <http://dx.doi.org/10.1080/00029890.1913.11997960>
- Cipolla CM (2003) *Clocks and Culture*. WW Norton, New York, NY
- Clarke AC (2011) *How the world was one*. Hachette UK
- Goodstein J (2007) *The Volterra Chronicles: The Life and Times of an Extraordinary Mathematician, 1860-1940*. History of mathematics, American Mathematical Society
- Hill AV (1910) The possible effects of the aggregation of the molecules of haemoglobin on its dissociation curves. *The Journal of Physiology* 40(suppl):1–7, DOI 10.1113/jphysiol.1910.sp001386, URL <http://dx.doi.org/10.1113/jphysiol.1910.sp001386>
- Hodgson MGS (1977) *The venture of Islam: The classical age of Islam v.1*. University of Chicago Press, Chicago, IL
- Izhikevich E, FitzHugh R (2006) FitzHugh-nagumo model. *Scholarpedia* 1(9):1349, DOI 10.4249/scholarpedia.1349, URL <https://doi.org/10.4249/scholarpedia.1349>
- Jaffe ES, Arber DA, Campo E, Quintanilla-Fend L, Orazi A, Rimsza LM, Swerdlow SH (2024) *Hematopathology*. Elsevier
- Kingsland S (1995) *Modeling Nature. Science and Its Conceptual Foundations* series, University of Chicago Press
- Kreager P (1991) Early modern population theory: A reassessment. *Population and Development Review* 17(2):207, DOI 10.2307/1973729, URL <http://dx.doi.org/10.2307/1973729>
- Mackey MC (2001) Cell kinetic status of haematopoietic stem cells. *Cell Proliferation* 34(2):71–83, DOI 10.1046/j.1365-2184.2001.00195.x, URL <http://dx.doi.org/10.1046/j.1365-2184.2001.00195.x>
- Maxwell J (2011a) *A Cambridge library collection - physical sciences A treatise on electricity and magnetism: Volume 1*. Cambridge University Press, Cambridge, England
- Maxwell J (2011b) *A Cambridge library collection - physical sciences A treatise on electricity and magnetism: Volume 2*. Cambridge University Press, Cambridge, England
- Mira C (1997) Some historical aspects of nonlinear dynamics—possible trends for the future. *Journal of the Franklin Institute* 334(5–6):1075–1113, DOI 10.1016/s0016-0032(97)00030-6, URL [http://dx.doi.org/10.1016/s0016-0032\(97\)00030-6](http://dx.doi.org/10.1016/s0016-0032(97)00030-6)
- Moore W (2015) *Schrödinger life and thought*. Canto classics, Cambridge University Press, Cambridge, England
- Parry JH (1992) *The discovery of the sea*. University of California Press, Berkeley, CA

- Perutz MF (1987) Physics and the riddle of life. *Nature* 326(6113):555–558, DOI 10.1038/326555a0, URL <http://dx.doi.org/10.1038/326555a0>
- van der Pol B (1926) Lxxxviii.on “relaxation-oscillations”. *The London, Edinburgh, and Dublin Philosophical Magazine and Journal of Science* 2(11):978–992, DOI 10.1080/14786442608564127, URL <http://dx.doi.org/10.1080/14786442608564127>
- van der Pol B, van der Mark J (1928) Lxxii.the heartbeat considered as a relaxation oscillation, and an electrical model of the heart. *The London, Edinburgh, and Dublin Philosophical Magazine and Journal of Science* 6(38):763–775, DOI 10.1080/14786441108564652, URL <http://dx.doi.org/10.1080/14786441108564652>
- Rosenblueth A, Wiener N (1945) The role of models in science. *Philosophy of Science* 12(4):316–321
- Santillán M, Zeron ES (2004) Dynamic influence of feedback enzyme inhibition and transcription attenuation on the tryptophan operon response to nutritional shifts. *Journal of Theoretical Biology* 231(2):287–298, DOI 10.1016/j.jtbi.2004.06.023
- Shamos MH (1987) *Great Experiments in Physics*. Dover Publications, Mineola, NY
- Sobel D (2007) *Longitude*. Walker, New York, NY
- Stent GS (1968) That was the molecular biology that was. *Science* 160(3826):390–395, DOI 10.1126/science.160.3826.390, URL <http://dx.doi.org/10.1126/science.160.3826.390>
- Watson JD (1968) *The double helix*. The new American library, New York
- Weiner J (1999) *Time, love, memory: a great biologist and his quest for the origins of behavior*. Alfred A. Knopf, New York